Genetic analysis of the FLRT family of proteins during early mouse embryonic development

Dissertation

Der Fakultät für Biologie der Ludwig-Maximilians-Universität München

Eingereicht am 17. Februar 2009 von Christian Erlacher

1. Gutachter: Prof. Dr. Rüdiger Klein
2. Gutachter: PD Dr. Angelika Böttger

Tag der mündlichen Prüfung: 24.04.2009

Work presented in this dissertation was performed in the laboratory of Prof. Dr. Rüdiger Klein, Department of Molecular Neurobiology, Max Planck Institute of Neurobiology, Martinsried, Germany.
Work was performed under the supervision of Prof. Dr. Rüdiger Klein and Dr. Joaquim Egea

Ehrenwörtliche Versicherung

Ich versichere hiermit ehrenwörtlich, dass die vorgelegte Dissertation von mir selbständig und ohne unerlaubte Beihilfe angefertigt ist.

München, den _____ _____

(Unterschrift)

Erklärung

Hiermit erkläre ich, dass ich mich anderweitig einer Doktorprüfung ohne Erfolg nicht unterzogen habe.

München, den _____ _____

(Unterschrift)

Publication from the work presented in this dissertation

Joaquim Egea*#, Christian Erlacher*, Eloi Montanez, Ingo Burtscher, Satoru Yamagishi, Martin Heß, Falko Hampel, Rodrigo Sanchez, Maria Teresa Rodriguez-Manzaneque, Michael R. Bösl, Reinhard Fässler, Heiko Lickert, and Rüdiger Klein#

„Genetic ablation of FLRT3 reveals a novel morphogenetic function for the anterior visceral endoderm in suppressing mesoderm differentiation."

Genes & Development 22, Nr. 23 (Dec 2008): 3349-3362.

* and #: These authors contributed equally to this work.

Für Margareta und Hans

Table of contents

Abbreviations

°C	degree celsius
AER	apical ectodermal ridge
AIP	anterior intestinal portal
AP	anterior posterior
AVE	anterior visceral endoderm
BCIP	5-bromo-4-chloro-3-indolylphosphat
ß-gal	ß-galactosidase
BM	basement membrane
BMP4	bone morphogenetic protein 4
Bra/T	brachyury T-box transcription factor
Cer1	cerberus like 1
CHAPS	3-[(3-Cholamidopropyl)dimethylammonio]-1-propanesulfonate
col I	collagen type I
col IV	collagen type IV
DAB	DiAminoBenzidine
DAPI	4' ,6-Diamidino-2-phenylindol
DE	definitive endoderm
DIG	digoxygenin
Dkk1	dickkopf 1
DMEM	Dulbecco's Modified Eagle's Medium
DMSO	Dimethylsulfoxide
DNA	DeoxyriboNucleic Acid
dNTP	deoxyribonucleoside triphosphate
DTT	1,4-Dithio-DL-threitol
DV	dorsal ventral
DVE	distal visceral endoderm
E	embryonic day
EB	embryoid body
ECL	enhanced chemoluminescence
ECM	extracellular matrix
EDTA	ethylendiamine-tetra acetic acid
EHF	early head fold stage

EMT	epithelial-mesenchymal transition
emVE	embryonic VE
ERK	extracelluar signal regulated kinase
ES	early streak stage
EtOH	ethanol
ExE	extraemrbyonic ectoderm
exVE	extraembryonic VE
FCS	fetal calf serum
FGF	fibroblast growth factor
FLRT	fibroectin leucine rich transmembrane protein
FN3	fibronectin type 3
GATA4/6	GATA binding factor 4/6
GFP	green fluorescent protein
Gsc	goosecoid
h	hours
HeLa	Henrietta Lacks
hf	head fold stage
HPSF	High Purity Salt Free
HRP	horse radish peroxidase
ht	heart
ICM	inner cell mass
ISH	*in situ* hybridisation
LB	Luria-Bertani
LHF	late head fold stage
Lim1	lim domain only transcription factor 1
LN	laminin
LPD	lectin pull down
LR	left right
LRR	leucine rich repeats
LS	late streak stage
MDCK	madin darby canin kidney cells
MEM	Modified Eagle's Medium
mes	mesoderm
MetOH	methanol
min	minutes
mRNA	messenger RNA
MS	midstreak stage
n.s.	not significant
NBT	nitroblue tetrazolium
neo	neomycin
Otx2	orthodenticle homologue 2

PAGE	polyacrylamide-gel-electrophoresis
PBS	phosphate buffered saline
PBT	PBS with Tween
PCR	polymerase chain reaction
PD	proximal distal
PE	parietal endoderm
pH	potentium hydrogenii
PrE	primitive endoderm
PS	primitive streak
RNA	ribonucleic acid
RNAi	RNA interference
RT	room temperature
SDS	sodium dodecyl sulfate
sec	second
SEM	scanning electron microscopy
shh	sonic hedgehog
shRNA	short hairpin RNA
SPC4	Subtilisin-like proprotein convertase 4
TAE	Tris-acetate EDTA
TCL	total cell lysate
TE	Tris-EDTA
TE	Trophectoderm
TEMED	N,N,N´,N´-Tetremethylethylenediamine
TGF-ß	transforming growth factor beta
VE	visceral endoderm
WISH	whole mount in situ hybridisation
Wnt	wingless like
wt	wild type
µ	micro
α	alpha

List of Figures

Abstract

During early postimplantation development of mice, two major events are crucial for the establishment of the embryonic body plan: the formation of the anterior posterior (AP) axis and the formation of the three germ layers during gastrulation. The mouse anterior visceral endoderm (AVE) is a central structure required for the establishment of the AP axis and the positioning of the primitive streak (PS) – the site of gastrulation. Several gene products, mainly transcription factors, have been implicated in the function of the AVE.

In this study, evidence for the involvement of FLRT3 in AVE function will be presented. FLRT3 is a member of a family of leucine rich repeat containing proteins comprising FLRT1, FLRT2 and FLRT3. While the expression of *FLRT1* and *FLRT2* begins at early head fold to late bud stages, *FLRT3* expression commences at pre- to early streak stages and is confined to the visceral endoderm. Later during gastrulation, *FLRT3* is present in the embryonic endoderm as well. The genetic targeting of *FLRT3* in mice shows early embryonic lethality and severe malformations in embryos up to 10 days of gestation. Malformations, such as asymmetric and unfused head folds, cardia bifida, impairment of embryonic turning and the development of embryos outside the visceral yolk sac; are restricted to the anterior region of the embryo. The analysis of typical patterning marker genes showed no apparent defects.

Further analysis of head fold stage embryos by in situ hybridization and scanning electron microscopy revealed a discontinuous endoderm layer on the outside of the mutant embryos. Instead, the underlying ectoderm protruded through the endoderm layer and populated the outside of the embryo. Interestingly, the ectopic ectoderm showed expression of mesodermal genes such a *Bra/T*, *FGF8* and *Eomes*. Nevertheless, the signaling function of the AVE, judged by the expression of key signaling factors such as *Cer1*, *Lefty1* and *Nodal*, are unperturbed. Together, this demonstrates that the loss of FLRT3 in mouse embryos leads to a breakage in the endoderm and the upregulation of mesoderm maker genes. This is reminiscent of events occurring in the PS region during gastrulation, when mesoderm is specified.

To understand the cell biological function of FLRT3, in vitro studies using heterologous cell systems were employed. In attempts to investigate a potential role for FLRT3 in

cell-cell or cell-matrix adhesion, HeLa and MDCK cells were used. Both gain-of-function and loss-of-function approaches were applied in either cell-matrix adhesion or scatter assays. Unfortunately, no conclusive data on the involvement of FLRT3 in either cell-cell or cell-matrix adhesion could be obtained.

This dissertation shows that FLRT3 is the first transmembrane protein to be shown to have an important function in the AVE during early postimplantation development of mouse embryos. Unfortunately the question of the cellular function of FLRT3 could not be answered and remains for further studies.

Zusammenfassung

Zwei Prozesse sind kennzeichnend für die frühe Entwicklung des Embryos nach der Implantation: die Bildung der Anterior Posterior (AP) Achse und die Bildung der drei Keimschichten während der Gastrulation. Das anteriore viszerale Entoderm (AVE) der Maus ist eine zentrale Struktur in der Axenbildung und der Positionierung des Primitiv Streifens (PS) - dem Ort der Gastrulation. Diverse Genprodukte, vorwiegend Transkriptionsfaktoren, sind mit der Funktion des AVE in Verbindung gebracht worden.

In der vorliegenden Arbeit wird gezeigt, dass FLRT3 an der Funktion des AVE während der Mausentwicklung beteiligt ist. FLRT3 gehört zu einer Familie von Proteinen die Leuzin reiche Repeats enthalten und aus FLRT1, FLRT2 und FLRT3 besteht. Während die Expression von FLRT1 und FLRT2 erst um E8.0 bzw. E7.5 erkennbar wird, ist FLRT3 schon vor oder während der frühen Primitiv Streifen Stadien exprimiert und auf das viszerale Entoderm beschränkt. Zu späteren Zeitpunkten während der Gastrulation wird FLRT3 jedoch auch im embryonalen Entoderm exprimiert.

Das genetische Targeting von FLRT3 führt zu frühembryonaler Letalität und schweren Fehlbildungen bei bis zu 10 Tage alten Embryonen. Die Fehlbildungen, zu denen unter anderem asymmetrische und nicht geschlossenen Kopfhälften, *Cardia Bifida*, Fehler bei der Drehung der Embryonen und die teilweise oder vollständige Entwicklung außerhalb des Dottersackes gehören, beschränken sich auf den anterioren Bereich des Embryos. Die Analyse typischer Marker Gene hat keine offensichtlichen Musterbildungs Defekte offenbart.

Eine weitergehende Analyse von Embryonen um E7.5 mit *in-situ*-Hybridisierung und Raster-Elektronenmikroskopie hat gezeigt, dass das außenliegende Entoderm in mutanten Embryonen unterbrochen war. Stattdessen hat in diesen Embryonen das darunterliegende Ectoderm nach außen gedrückt und ist nun auf der Oberfläche der Embryonen zu finden. Intersannterweise konnte in diesem ectopisch lokalisierten Ektoderm die Expression von typischen mesodermalen Genen wie *Bra/T*, *FGF8* oder *Eomes* nachgewiesen werden. Nichtsdestotrotz bleibt die Funktion des AVE als Signalzentrum, gemessen an der normalen Expression von wichtiger Signalmoleküle wie *Cer1*, *Lefty1* oder *Nodal*, unberührt. Zusammengenommen zeigt dies, dass das Fehlen von FLRT3 in Mausembryonen zu einem Bruch im Entoderm und der

Expression von mesodermalen Genen im anterioren Bereich der Embryonen führt. Diese Beobachtungen weisen parallelen zur Bildung von Mesoderm in der PS Region während der Gastrulation auf.

Um die zellbiologische Funktion von FLRT3 verstehen zu lernen, wurden *in vitro* Studien mit heterologen Zelllinen durchgeführt. In diesen Versuchen mit HeLa und MDCK Zellen wurde vor allem der mögliche Einfluss von FLRT3 auf die Zell-Zell- oder die Zell-Matrix Adhesion untersucht. Leider konnte weder in „Gain-of-Function" noch in „Loss-of Function" Experimenten ein eindeutiger Effekt von FLRT3 festgestellt werden.

In dieser Dissertation wird gezeigt, dass FLRT3 das erste bekannte Transmembranprotein ist, dass mit einer wichtigen Funktion im AVE während der frühen Embryonalentwicklung der Maus assoziiert ist. Leider konnte die zelluläre Funktion nicht ermittelt werden und bleibt somit Gegenstand für zukünftige Studien.

1. Introduction

In 2009, we celebrate the 200th anniversary of the founder of the modern theory of evolution, Charles Darwin. His groundbreaking work boosted the understanding of many observations made concerning evolution in the animal kingdom. It is fascinating to consider how complex organisms such as mammals, have been shaped to survive and thrive in their respective ecological niches. It is even more exciting that these basic principles needed for the development of higher animals were found in single cell organisms. These simpler organisms represented the major population on the planet for a long time, and persist until today.

For example, the amoeba slime mold *Dictyostelium discoideum*, naturally occurs in soil, spending most of its life time as a single cell organism. However, when its survival is threatened, for instance when nutrition conditions become worse, a fascinating process of differentiation can be observed. Many individual amoebae join together and form a simple organism, the so called slug (Newell, et al. 1969). Under certain circumstances, the slug transforms into a fruiting body, which differentiates into a stalk region and one or more balls of spores, which will be dispersed, and therefore guarantee the continued existence of the amoeba. This process must be strictly regulated and must involve communication between the individual cells. In *Dictyostelium*, this is achieved via waves of cyclic AMP (cAMP) secretion.

In multicellular organisms, the regulation of a number of processes, such as growth, tissue organization and metabolism is crucial. To establish a defined body plan, spatially and temporally precise signals are required. This applies to simple multicellular organisms such as *Hydra*, as well as to much more complex animals like mice. Interestingly, many signals that have been proven to be important for mammalian development are also employed by simple metazoans. Even the establishment of a very simple body plan with only a single body axis, the oral aboral axis; like cell differentiation through secreted signals, such as the canonical wnt signalling pathway (Hobmayer, et al. 2000; Steele 2002). *Hydra*, with its simple body plan comprised of two germ layers, the endoderm and ectoderm is a representative of the diploblastic organisms. But rather early in the evolution of metazoans, a third germ layer, the mesoderm has emerged. These tribloblastic animals, such as insects, amphibians and mammals, are founded on three germ layers, namely the ectoderm, the (new) mesoderm and the endoderm (Technau 2001). The formation of these germ layers occurs in the initial phases of embryonic development and will later give rise to diverse tissues and organ systems. Germ

layers are created in a process termed gastrulation, which is a central process in the ontogeny of triploblastic organisms. Although differences in the process of gastrulation are obvious between classes and even species, for instance comparing protostomes and deuterostomes, basic routines concerning the regulation of this process seem to be conserved during evolution (Technau and Scholz 2003). Nevertheless, systems have adapted to the spatial and temporal needs of different animals, and new signals have been adopted when necessary.

In mice, research during the last two decades has enhanced the understanding of gastrulation and early embryonic development in general. Although considerable efforts have been invested in recent years to unravel mechanisms that control and guide the establishment of the mammalian body plan, many gaps in knowledge still remain and are waiting to be filled.

1.1. Preimplantation development

Mammalian embryos, unlike other embryos, need to establish a permanent connection to maternal tissues in order to grant nutrient- and oxygen supply. This physical connection is established in a period of development called implantation. Timing of implantation is dependent on the species and takes place in the mouse at around 4.5 days of embryonic development (E4.5). Thus, the early phases of embryonic development are often referred to as preimplantation, peri-implantation and postimplantation development. At the blastula stage (E3.5), two cell lineages are apparent. The trophectoderm (TE) cells, which will connect the embryo to the placenta, and the inner cell mass (ICM), composed of pluripotent stem cells (reviewed in Arnold and Robertson 2009). Trophoblast cells, which differentiate from the TE, penetrate the endometrium of the uterus and initiate implantation of the conceptus. To ensure the supply of the conceptus with nutrients, the trophoblast cells establish a connection to the maternal blood stream (reviewed Lee and DeMayo 2004). This is crucial for mammalian embryos since they are not equipped with nutrients, which is the case in other classes in the animal kingdom, such as the yolk rich avian embryos. Already by implantation, the ICM cells have differentiated into the primitive endoderm (PrE) and the epiblast lineage, the major cell lineages important for gastrulation (Srinivas 2006).

1.2. Postimplantation development

Soon after implantation, at around E5.0, early postimplantation mouse embryos are divided into two regions and display a proximal distal (PD) body axis (Figure 1 A). Located at the proximal end of the embryo, close to the placental contact, is the so-called extraembryonic region. The tissues formed in this region, the ectoplacental cone that establishes the contact to the maternal tissues and the extraembryonic ectoderm (ExE), will not contribute to later embryonic structures but are involved in nurturing the embryo (reviewed in Arnold and Robertson 2009). The embryonic region, located distal to the ExE, consists mainly of the ICM derived epiblast. The descendents of the PrE lineage, namely the parietal endoderm (PE) and the visceral endoderm (VE) belong to the extraembryonic lineage, since they will not contribute extensively to embryonic structures (Rossant, et al. 2003). While the PE forms the parietal yolk sac, the VE lines the embryo both at the extraembryonic and the embryonic regions and therefore is subdivided into extraembryonic VE (ExVE) and embryonic VE (EmVE) (Arnold and Robertson 2009). The VE cells form a cuboidal epithelium, separated by a basement membrane (BM) from the pseudostratified epiblast epithelia. The epiblast forms the proamniotic cavity that reaches distally into the ExE. At this stage of development, a peculiar detail of rodent embryos becomes evident. In contrast to human or avian embryos, which develop as a flattened disc, the mouse embryo develops as a cup shaped structure. Therefore, embryos at this stage are referred to as egg-cylinders.

Figure 1 Early post implantation development in the mouse
The early post implantation development involves dynamic processes resulting in dramatic rearrangements in the embryo. (A) At PrS/egg cylinder stage, the embryo consists of two cell layers, the epiblast (blue) and the surrounding VE (green) and is characterized by a proximal distal (PD) axis. The differentiation of VE cells at the distal tip of the embryo into DVE (bright green) marks the first visible sign of the forming asymmetry. (B) Just prior to the beginning of gastrulation, the DVE has migrated in anterior direction (now termed AVE) and marked the future anterior pole of the embryo. At the opposing posterior side, at the very proximal end of the embryonic region; the primitive streak (PS) forms. Mesoderm (yellow) and DE (orange) are formed at the PS. (C) The PS progresses further distally and the produced DE and mesoderm migrate laterally, and in the case of mesoderm, also into the extraembryonic region, to form the visceral yolk sac (VYS) mesoderm. (D) At the EHF stage, almost the entire VE has been replaced by DE and displaced towards the extraembryonic region. The ectoderm in the anterior is specified to become neuroectoderm and the head folds start to extrude. At the anterior end of the PS, the node, an embryonic organizer region, has formed. (E) At E8.5, the head folds have formed and the ventral body side of the embryo begins to close and thereby the embryo will be incorporated into the VYS. The mesodermal derived allantois establishes a contact to the chorion.
Abbreviations: al, allantois; AVE, anterior visceral endoderm; DE, definitive endoderm; DVE, distal visceral endoderm; EHF, early head fold stage, emb, embryonic region; epc, ectoplacental cone; ES, early streak stage; ExE, extraembryonic ectoderm; exemb, extraembryonic region; hf, head fold; ht, heart; MS, mid streak stage; nd, node; PrS, pre streak stage; PS, primitive streak; VE, visceral endoderm; VYS, visceral yolk sack.

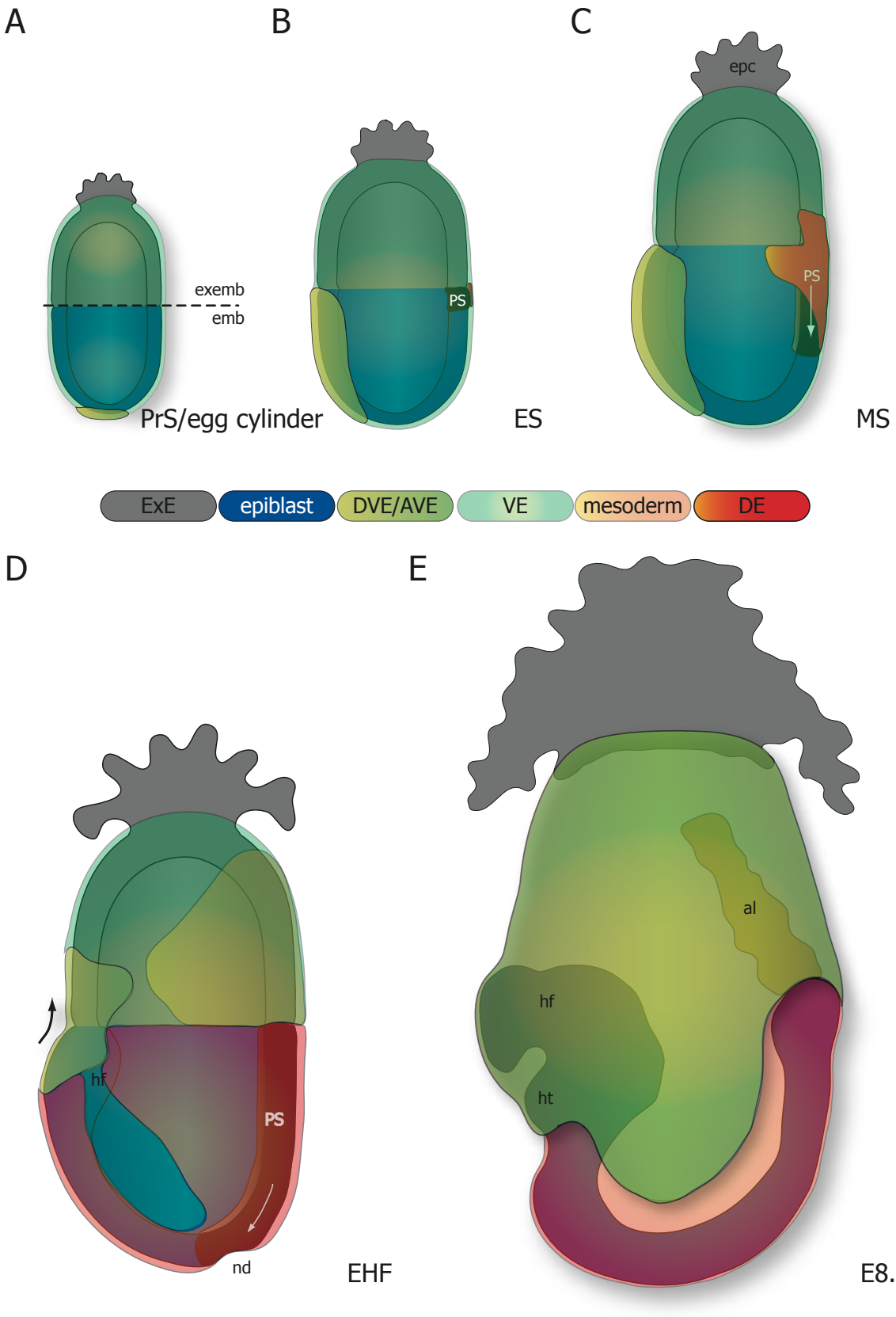
A
B
C
exemb
emb
PS
epc
PS
PrS/egg cylinder
ES
MS
ExE
epiblast
DVE/AVE
VE
mesoderm
DE
D
E
hf
PS
nd
al
hf
ht
EHF
E8.5

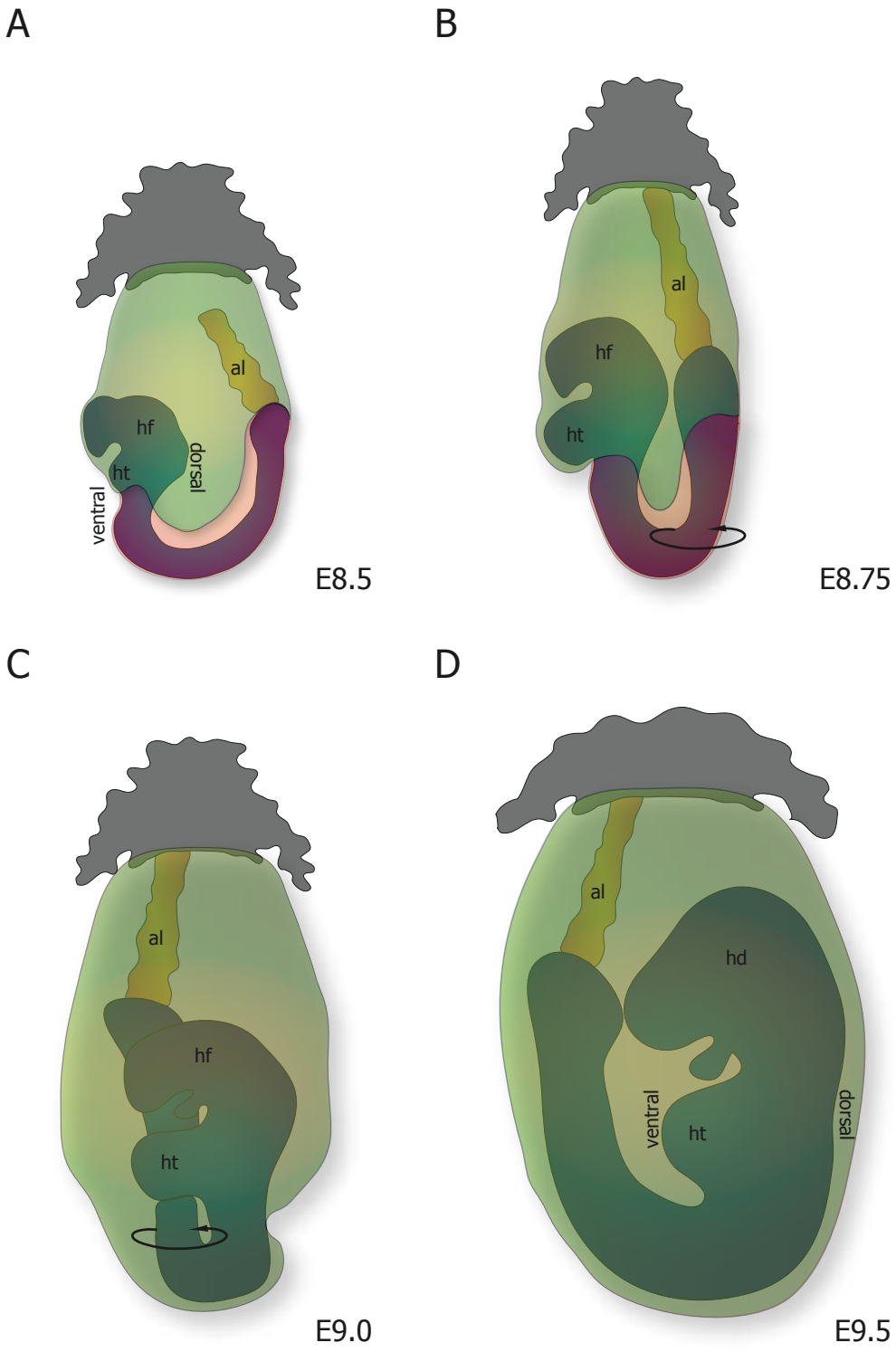

Figure 2 Embryonic turning occurs at E8.5 to E9.5
During early post-implantation development, the mouse embryo exhibits an inversion of germ layers. This special feature of mouse development requires the turning of the embryo in order to establish the embryonic body plan. (A) At E8.5, the embryo exposes its ventral body side consisting of endoderm to the outside and starts to be enclosed in the VYS. (B) While the enclosure in the VYS proceeds, the caudal end begins to "roll" in an anticlockwise motion around the rostral part of the embryo. (C) At E9.0, the embryo is almost entirely enclosed within the VYS. (D) The turning process is completed at around E9.5, and the embryo has achieved the fetal position, which is typical in chordate embryos.
Abbreviations: al, allantois; hd, head; hf, head fold; ht, heart; VYS visceral yolk sac
(Cartoon modified from Kaufman 1992)

About 20 to 24 hrs later, at early streak (ES; ~E6.5) stage, the body axis has shifted from a proximal distal to an anterior posterior (AP) axis and the embryonic germ layers begin to form; this is the process of gastrulation (Figure 1 B, C). In the posterior of the embryonic region, a transient structure, called the primitive streak (PS) forms, through which epiblast cells ingress and form mesoderm and definitive endoderm (DE). These cells then migrate to their respective destinations in the embryonic, and in the case of early-generated mesoderm, also into the extraembryonic region (Parameswaran and Tam 1995) (Figure 1 D, E). Interstingly, as a consequence of the cylindrical shape of rodent embryos, the early postimplantation mouse embryo exhibits an inversion of the germ layers, namely the endoderm forms the outermost and the ectoderm the innermost cell layer (Kaufman 1992). This particular detail makes it necessary to invert the embryonic germ layers for further development. The inversion occurs in concert with the closure of the ventral and parts of the dorsal body walls in order to form a closed primitive gut or neural tube, respectively, and is referred to as embryonic turning (Kaufman 1992). This turning occurs between E8.5 and E9.5 and together with the ventral closure leads to the folding of the midline endoderm and thereby forms the primitive gut tube (Figure 2). This also causes the fusion of the two lateral heart primordia, which have already formed by E7.5, and the complete enclosure of the embryo by the visceral yolk sac (VYS), which is composed of cells of the extraembryonic region, namely the ExVE and the extraembryonic mesoderm (Kaufman 1992).

Already with the commencement of gastrulation, the basis for proper development of neural and head structures is laid down. The anterior ectoderm is patterned to form the prospective brain structures. At head fold stage (HF; E8.0), the neuroectoderm can already be distinguished from neighbouring surface ectoderm and elevates into clearly visible head folds (hence the name). Between E8.0 and E9.5, the time of embryonic turning, the head folds and the more caudal neuroepithelium fold up and fuse in a precisely regulated fashion, starting at the hindbrain level and proceeding both rostrally and caudally to form the prospective fore- mid- and hindbrain regions and the neural tube, which will give rise to the spinal cord (Kaufman 1992).

During further development, many different cell types, structures and organs are specified at their designated location. All events that were briefly described so far are subject to precise regulatory machineries, consisting of a large number of different gene products that are present at a given time in a certain environment. In the following sections, some key events during early embryonic development and important regulatory pathways will be described.

1.3. Axis specification

The establishment of body axes is important for the development of multicellular organisms. The mouse for instance, like all vertebrates, possesses three body axes, the AP axis, the dorsal ventral (DV) axis and the left right axis (LR). Failures in the establishment of these axes can have severe consequences. Disturbances in the LR axis for instance can lead to situs inversus, a syndrome known in mice and man. Human patients suffer from either reversed or in more severe cases randomized positioning of inner organs (Hackett 2002). The first and most important body axis however, is the AP axis. Both the DV and LR axes are defined in relation to the AP axis. Hence the establishment of the AP axis is crucial for proper postimplantation development.

After implantation, around E5.0, no clear AP axis is noticeable. Rather, the conceptus is characterized by a PD axis, where proximal is defined as the point closest to the site of implantation (see Figure 1). The extraembryonic region is located proximal, whereas the embryonic region distal in the embryo. At E5.5, the PD axis begins to be transformed into an AP axis that will be established just before gastrulation commences at E6.5 (Srinivas 2006). What are the morphogenetic and molecular processes underlying this axis transformation?

A group of cells of the EmVE at the distal tip of the embryonic region differentiates at E5.5 into a morphologically distinct structure, the so-called distal visceral endoderm (DVE) (Rivera-Perez, et al. 2003; Srinivas, et al. 2004). The cells at the distal tip change their morphology to a more columnar appearance and create a thickening of

Figure 3 Axis formation in the mouse embryo
The formation of the embryonic axes is crucial for the ontogeny of the mouse embryo. (A) At the pre-streak/egg cylinder stage, the embryo is characterized by a PD axis. The epiblast expresses Nodal, a TGF-beta signalling molecule, throughout the epiblast, whereas the ExE shows expression of PACE and Furin, required for nodal maturation and activation. BMP4, another TGF-beta signalling molecule required for proper localization of the embryonic region and a target of nodal signalling, is also expressed in the ExE. At the distal tip of the embryo in the DVE, asymmetric expression of nodal inhibitors *Lefty1* and *Cer1* is visible. (B) As the AVE migrates anteriorly, the expression of nodal inhibitors shifts from its distal location to a more proximal location in the future anterior of the embryo. Additionally, the expression and activity of nodal concomitantly shifts from a uniform distribution in the epiblast to a more restricted pattern in the proximal posterior region. At the same time, BMP-4 induces wnt3 expression in the epiblast, which is restricted to the proximal posterior region by the expression of *Dkk1*, a Wnt inhibitor in the anterior proximal VE. (C) The expression of *Wnt3* and *Nodal* is locally confined to the posterior proximal region of the epiblast and induces the formation of the primitive streak. By now, the new anterior posterior axis (AP) is apparent and forms the foundation for the further development and asymmetry (D). At the mid streak stage, the expression of Wnt and Nodal inhibitors by the AVE persists and creates the position of the anterior and posterior poles of the embryo.

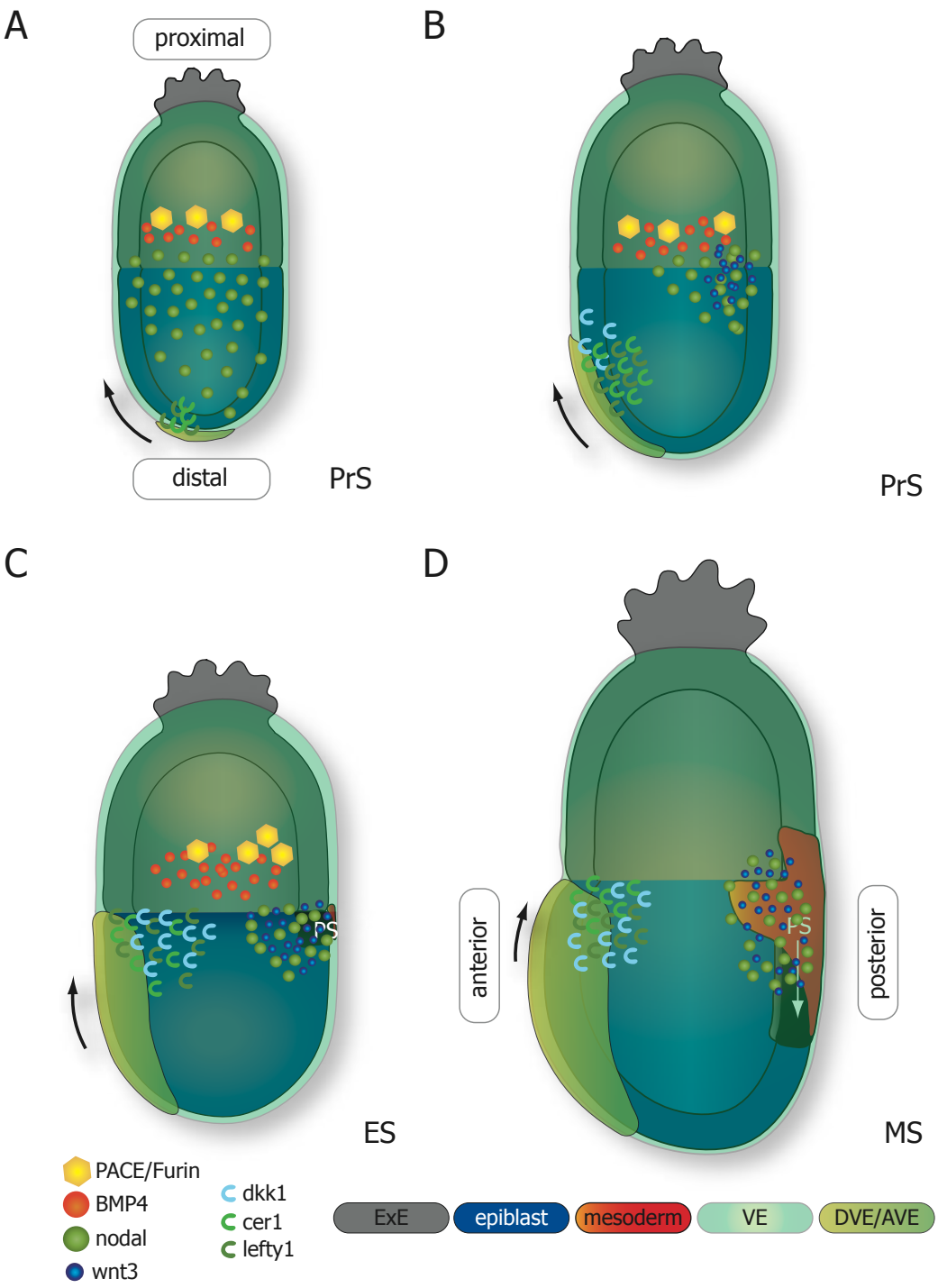
A
proximal
distal
PrS
B
PrS
C
PS
ES
D
anterior
posterior
PS
MS
PACE/Furin
BMP4
nodal
wnt3
dkk1
cer1
lefty1
ExE
epiblast
mesoderm
VE
DVE/AVE

the VE (Kimura, et al. 2000, Rivera-Perez, et al. 2003, Srinivas, et al. 2004). Hensin, a component of the BM, which is located at the distal tip of E5.5 embryos, is believed to influence these cell shape changes (Takito and Al-Awqati 2004). DVE differentiation is accompanied by the asymmetric expression of genes like *Hex*, *Lefty1* or *Cer1* in the DVE (Thomas, et al. 1998; Meno, et al. 2001; Perea-Gómez, et al. 1999; Belo, et al. 1997) (Figure 3). The migration of DVE cells subsequently begins in a unidirectional movement towards the proximal region of the conceptus and stops when the DVE arrives at the embryonic-extraembryonic border (Thomas, et al. 1998; Rivera-Perez, et al. 2003; Srinivas, et al. 2004). DVE cells then spread laterally and mark the future anterior pole of the embryo. Upon migration, the cells are called anterior visceral endoderm (AVE) cells as they determine the future anterior of the embryo (Figure 3).

In a classical experiment, Hilde Mangold and Hans Spemann made a very interesting discovery. By transplanting a region of a gastrulating amphibian embryo into a heterotypic location, they were able to induce a second site of gastrulation and thereby a second body axis. This so called Spemann Organizer has the ability to induce a second body axis autonomously (Spemann and Mangold 1923/2001). This was a new and exciting concept in embryology. In the last two decades extensive work has attempted to further characterize this organizer region and understand the molecular cues that underlie this inducing potential. In the mouse, it is believed, that a structure called the node is comparable to this previously discovered organizer region (Beddington 1994). The node is a derivative of the anterior primitive streak and showed, when transplanted, the ability to induce a second body axis. However, only posterior structures have formed and ectopic body axes showed severe anterior truncations (reviewed in Perea-Gomez, et al. 2001).It became clear, that unlike the Spemann organizer, the mouse node is not sufficient to fully induce a second body axis. Hence, it was postulated that a second, anterior organizer might exist. In loss of function experiments, where genes coding for *Lim1* (lhx1; lim domain transcription factor) or *Otx2* (orthodenticle homologue 2) were ablated, both of which are expressed in the AVE before and at the time of gastrulation, a complete loss of structures anterior to the developing hindbrain was evident (Shawlot and Behringer, 1995; Ang, Jin, et al. 1996). According to these findings, the AVE was thought to be the anterior organizer. However, transplantation of the AVE alone did not result in induction of anterior structures, whereas cotransplantation of the early gastrula organizer (EGO) and the AVE together with the anterior epiblast resulted in a complete ectopic body axis (Tam and Steiner 1999). This suggests that the AVE alone does not possess organizer functions. Consequently, the idea of the role of the AVE in early development changed. Further analysis made clear that a major function of the AVE lies in its signalling properties, which are important for embryonic axis formation. The next paragraph explains some of the signalling functions of the AVE and its involvement in the establishment of the AP axis.

1.4. Molecular basis of axis formation

Asymmetric expression of genes is important for the definition of cell lineages and embryonic axes. Already at the blastula stage, different lineages are determined by the expression of specific marker genes. The expression of GATA6 for instance, determines the PrE lineage, while the expression of Nanog characterizes the pluripotent epiblast lineage (Arnold and Robertson 2009). For subsequent processes during early postimplantation development, three signalling systems have been shown to be particularly important; the TGF-beta, the Wnt and the FGF signalling systems.

To establish a proper embryonic region of the conceptus and to pattern the epiblast and the EmVE, signals emerging from the ExE are essential. At the PrS stage, the TGF-beta like factor nodal is expressed throughout the epiblast and the ExE (Figure 4). To activate Nodal, which is expressed as an inactive pro-form, it needs to be cleaved

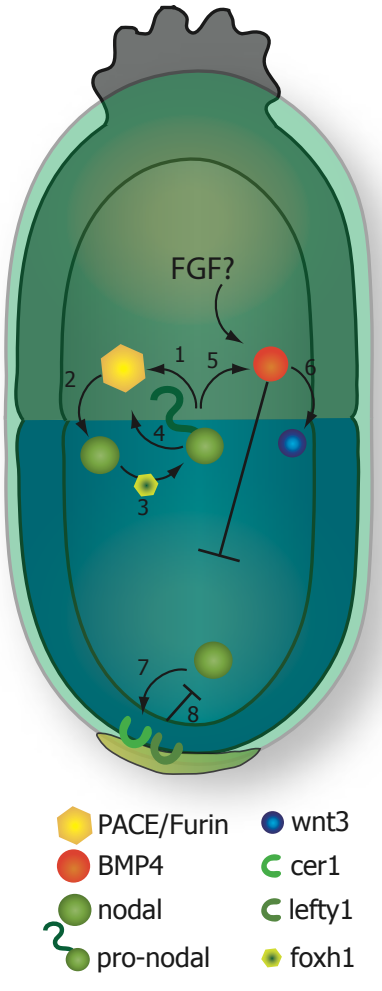

Figure 4 Signalling pathways during axis formation
Nodal signalling is a crucial determinant in the formation of the embryonic body axis. (1) Nodal is expressed as a pro-protein and needs to be activated by converting enzymes. (2) Furin and PACE, two convertases, are both expressed in the ExE and are necessary for Nodal maturation. (3) Mature Nodal can, in turn, regulate the expression of pro-nodal via a SMAD2/Foxh1 dependent pathway. (4) Also, pro-nodal is able to maintain the expression of PACE and Furin. (5) Furthermore, BMP4 expression is regulated by pro-nodal and probably by FGF signalling in the ExE. (6) BMP4 can also induce the expression of Wnt3 and is required for the restriction of gene expression in the embryonic region. (7) The signalling activity of nodal at the distal tip is important for the induction of the nodal inhibitors Cer1 and Lefty1. Both inhibitors get activated by Nodal and in turn repress the activity of Nodal (8).

by proprotein convertases. In the ExE, the expression of the convertase enzymes, Furin and SPC4 (PACE), has been proven to be necessary in order to activate nodal (Constam and Robertson 2000a; Roebroek, et al. 1998). Nodal can, in turn, through an autoinductive feedback loop by its downstream effectors SMAD2/3 and FoxH1, increase the production of its pro-form (Norris, et al. 2002) Saijoh, et al. 2000). Also the expression of Furin and PACE is positively regulated by Nodal in a feedback loop. Pro-nodal can, amongst other factors, induce the expression of bone morphogenetic protein 4 (BMP4), another TGF-beta factor in the ExE (Ben-Haim, et al. 2006). BMP4 is important in restricting the EmVE to the distal region of the conceptus and can induce the expression of Wnt3. The loss of BMP4 leads to mislocalization of genes expressed in the embryonic region that are involved in Nodal signalling (Soares, et al. 2005). Comparably, in experiments ablating the ExE, or components of the FGFR signalling such as FRS2 or Elf5, an expansion of genes that are normally expressed in the DVE, such as *Hex*, into the ExVE region was evident (Rodriguez, et al. 2005). It is hypothesized that FGF signalling is able to regulate BMP4 signalling (Gotoh, et al. 2005). The differentiation of DVE cells is mainly governed by Nodal signalling activity. The size of the embryo and therefore the activity of Nodal at the distal tip is believed to play an important role in the activation of DVE specific genes. The expression of Hex, a classical DVE/AVE marker, is Nodal dependent. Similarly, Nodal signalling positively regulates *Lefty 1* and *Cer1*, inhibitors of TGF-beta signalling expressed by the DVE and AVE (Perea-Gómez, et al. 1999).

The anterior migration of the DVE in order to form the AVE has been shown to be an active process (Srinivas, et al. 2004; Rakeman and Anderson 2006). Several lines of evidence support this idea. AVE cells migrate within a period of four to five hours from the distal tip to the future anterior of the embryo. It has been shown that AVE cells extend filopodia while migrating and additionally, the ablation of NAP1, a component of the actin modulating WAVE complex, blocks the migration of AVE cells (Srinivas, et al. 2004; Rakeman and Anderson 2006). Nevertheless, also a passive mechanism of differential proliferation rates appears to be involved in AVE positioning. Recent publications have shown that the expression of lefty1 and cer1 does not fully overlap with the expression of Hex in the DVE but is rather shifted towards the future anterior pole. Therefore, a slight gradient in the activity of nodal signalling is produced, with higher nodal activity posterior to the DVE (Takaoka 2006, Yamamoto 2004). Inhibition of Nodal signalling through Lefty1 has a negative effect on cell proliferation and therefore might "kick start" the initial directed migration of the AVE (Yamamoto, et al. 2004) (Figure 5 A). Asymmetric cell proliferation seems to cooperate with the active migration of cells in order to position the AVE (Srinivas et al. 2004). Interestingly, AVE migration seems to be directed, as only unidirectional movement is observed. It appears that wnt signalling activity serves as a directional cue for AVE migration (Figure

5 B). In embryos deficient for *Otx2*, the migration of the AVE cells towards anterior was found to be impaired (Perea-Gomez, Lawson, et al. 2001). *Otx2* is important for the positioning of the secreted Wnt signalling inhibitor *Dkk1*. Therefore *Dkk1* expression is lost in *Otx2*$^{-/-}$ embryos. Interestingly *Otx2*$^{-/-}$ defects could be rescued either by the ectopic expression of *Dkk1*, which is usually expressed in the proximal EmVE and the AVE under the Otx2 promoter, or at least partially by the reduction of beta-Catenin levels in *Otx2*$^{-/-}$ embryos. Notably, in both cases, Wnt activity at the proximal EmVE was reduced. In conjunction with Dkk1 soaked bead experiments, it was shown that Dkk1, by inhibiting Wnt signalling in the anterior, acts as an attractive guidance cue for AVE cells (Kimura-Yoshida, et al. 2005). Hence, low Wnt signalling activity serves as an attractive cue, whereas high level of Wnt activity is a repellent cue for AVE migration. Altogether, this shows that the combination of active migration, Nodal induced asymmetric cell proliferation and Dkk1 mediated Wnt signalling reduction is required for proper AVE migration and positioning.

How does the AVE guide the AP axis formation? The answer to that question was found already several years ago. Experiments, preventing the AVE migration showed severe anterior truncations (Perea-Gomez, et al. 2001; Ding, et al. 1998). At E5.5, *Nodal* and *Cripto*, a coreceptor for Nodal, expression was found throughout the epiblast (Ding, et al. 1998). Local expression of the Nodal inhibitors *Lefty1* and *Cer1* by DVE cells, was found to lower the activity of Nodal signalling at the distal tip of the epiblast. When the AVE migrates towards the future anterior, the distribution of *Nodal* expression is changed as well (see Figure 3). Concomitantly, *Nodal* expression is restricted through *Lefty1* and *Cer1* to the proximal posterior region of the epiblast. This is the region where the PS will form. In addition to Nodal, a second pathway, the Wnt pathway has been found to be important in AP specification (see Figure 3). BMP4, regulated by nodal expression in the ExE induces the transcription of *Wnt3*, a secreted ligand of the Wnt pathway. The expression and activity of Wnt3 is restricted to the posterior epiblast by the aforementioned expression of *Dkk1* in the proximal EmVE. Dkk1 is a secreted Wnt signalling inhibitor and is sufficient to reduce Wnt activity (Glinka, et al. 1998). Wnt3 however, is able to induce primitive streak markers by TCF/Lef, downstream targets of the so-called canonical Wnt signalling through Lrp5/6 and beta-Catenin (Mohamed, et al. 2004; Kelly, Pinson und Skarnes 2004) and can maintain the level of nodal in the epiblast (Ben-Haim, et al. 2006). Hence the combined expression of Wnt and TGF-beta/Nodal inhibitors in the AVE allows the restriction of Nodal and Wnt signalling to the posterior of the embryo (Perea-Gomez, et al. 2004). This asymmetric expression is crucial for proper gastrulation (Liu, et al. 1999; Robertson, et al. 2003), as will be discussed in the next section.

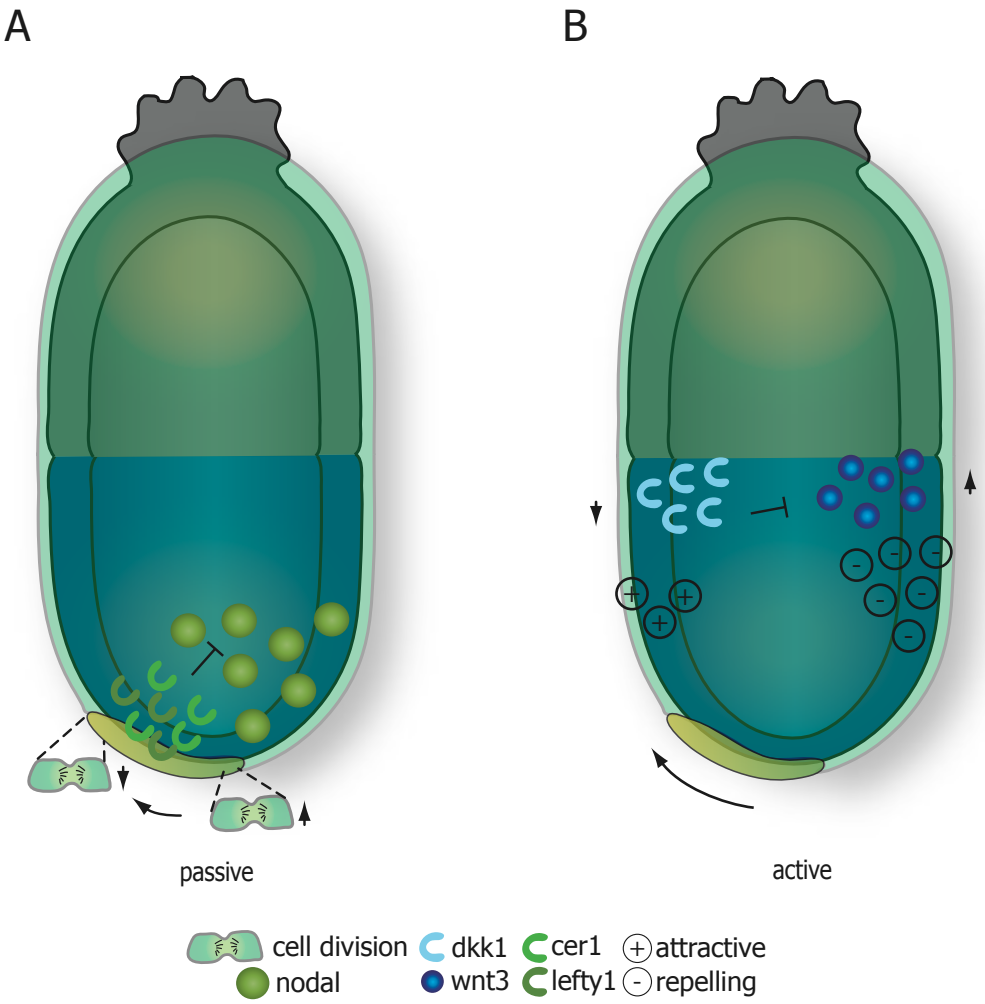

Figure 5 Active migration of the AVE requires molecular cues
AVE migration is essential during axis formation and driven by molecular cues. (A) Although AVE migration is an active process, asymmetric cell division seems to influence AVE migration. The asymmetric expression of *Lefty* and *Nodal* creates a gradient of Nodal activity in the DVE. Regions of high Nodal activity show higher cell division rates, that regions of lowerNodal activity, regulated by Cer1 and Lefty1. The resulting asymmetric cell division may give a directional kick-start to DVE cells. (B) Wnt signalling was shown to act as attractive or repulsive cue on DVE cells. The reduced level of Wnt signalling in the future anterior region, established by *Dkk1* expression, acts as attractive signal and drives directed active migration of DVE cells.

Some questions however remain. Expression of *Lefty1* was detected as early as in preimplantation embryos, in response to FoxH1 mediated Nodal signalling. Already at E4.5, expression was restricted in the PrE (Takaoka, et al. 2006). What determines this asymmetry is unclear. It is known, that axis formation is independent of implantation and therefore of maternal influence. This was shown in mouse embryos in culture and is known in other mammalian embryos, where axis formation occurs prior to implantation (Eakin and Behringer 2004). It is yet unclear which initial events spark asymmetry in the early mouse conceptus.

1.5. Gastrulation

In all vertebrates, including the mouse, tissues originate from three germ layers, the ectoderm, the mesoderm and the endoderm. However, during early phases of mouse development, the conceptus is composed of two cell layers, the VE and the epiblast. To convert this two-layered structure into a three-germ layer embryo, the process of gastrulation needs to take place. During gastrulation the epiblast will give rise to all three embryonic germ layers. In mouse and similarly in chicken embryos, epiblast cells are recruited to a transient structure formed in the posterior epiblast, the primitive streak (PS). Epiblast cells committed to become mesoderm or endoderm, migrate through this conduit and lose their epithelial morphology while acquiring a mesodermal cell fate (Technau, et al. 2003). Cells will migrate away from the PS until they reach their designated destination (Tam, et al. 2007). The PS itself extends in anterior direction until it reaches the distal region of the embryo. According to the position and time the mesoderm or endoderm cells are formed, their fate is determined (Tam, et al. 2007). Lineage allocation studies have helped to understand the fate of these cells. It seems that in early streak (ES) stage embryos, mesoderm cells first formed in the PS will mainly contribute to the extraembryoic mesoderm (Parameswaran and Tam 1995). The extraembryonic mesoderm forms the VYS mesoderm and the blood islands, which are important for haematopoesis (Winnier, et al. 1995). In midstreak (MS) stage embryos, the PS progresses and is located further distal. Mesoderm cells originating in this region will mainly contribute to the lateral plate, the paraxial and the cardiac mesoderm (Kinder, et al. 1999). Similarly, the endoderm cells produced at this stage of gastrulation will mainly contribute to more lateral endoderm structures such as the ventral lining of the primitive gut tube (Tam, et al. 2007). At late streak (LS) stage, the contribution of mesoderm and endoderm cells is more restricted to the midline structures of the embryo, such as the dorsal gut endoderm or the axial mesoderm and its decedents, the prechordal plate and notochord (Tam, et al. 2007). At its final position, the PS forms the node, the organizer structure important for midline structure formation. The node is also involved in the generation of the LR axis by creating a leftwards-directed fluid flow by cilia motion (Nonaka, et al. 1998).

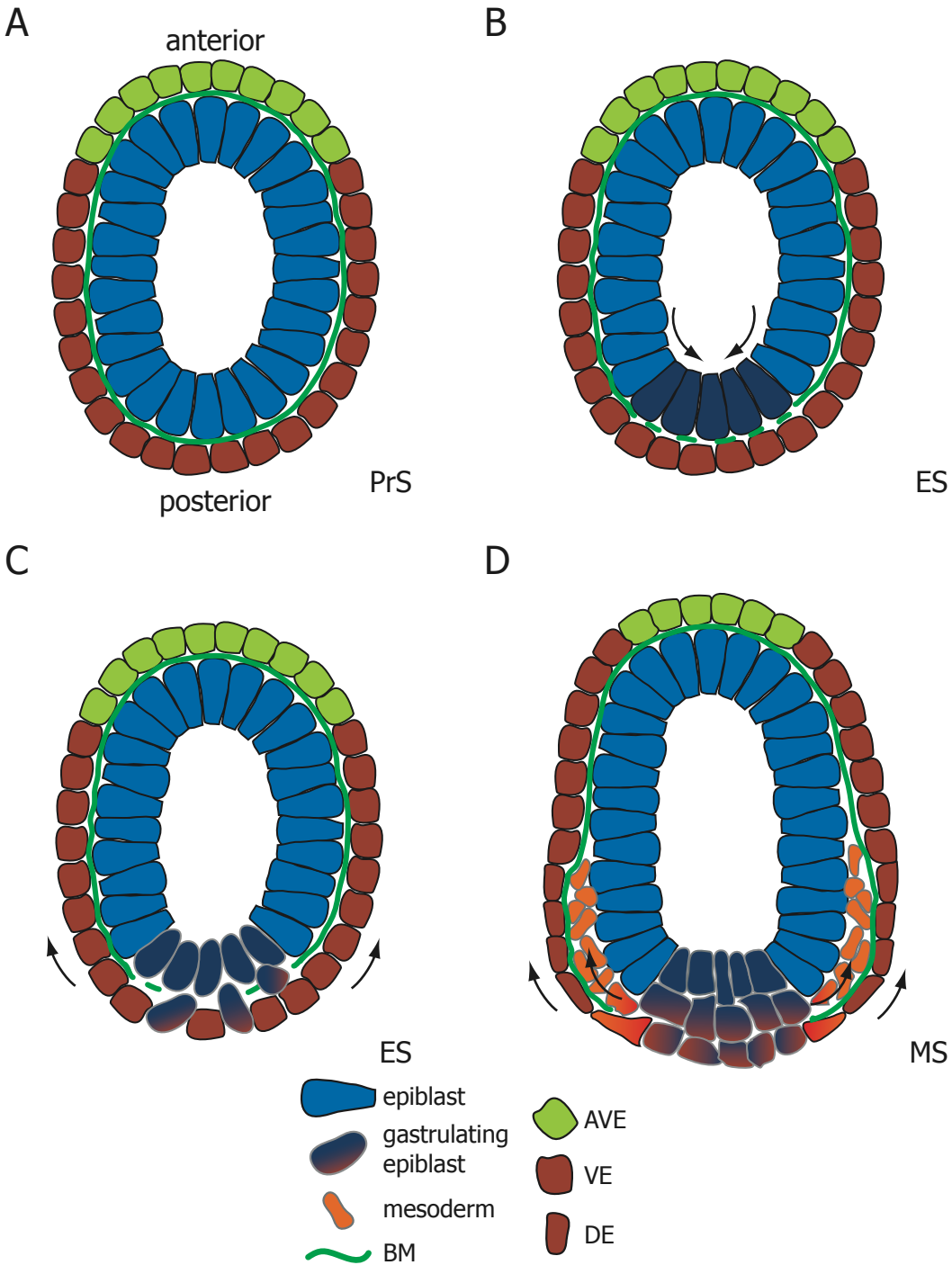

Figure 6 Cellular movements during mouse gastrulation
Gastrulation is the process of embryonic germ layer formation, a process that involves dynamic cellular changes. (A) At PrS, the embryo consists of two cell layers that are separated by a basement membrane (BM). (B) The PS, a transient conduit for epiblast cells, forms in the proximal posterior region and the BM in this region disintegrates. Epiblast cells migrate towards this transient structure and upregulate certain genes, such as *Bra/T* (dark blue cells). (C) Epiblast cells in the PS undergo an epithelial to mesenchyme transition (EMT) and acquire mesenchymal characteristics. (D) Newly formed mesoderm and DE cells migrate towards the anterior and, in the case of DE, intermingle with and displace most of the present VE cells.

While only epiblast cells that will become mesoderm or endoderm have to migrate through the primitive streak, the remaining epiblast cells will form the embryonic ectoderm. Newly generated mesoderm cells will migrate between the ectoderm/epiblast and the VE/DE (Figure 6). The VE cells overlying the embryonic region will be mostly displaced into the extraembryonic region by DE cells that have migrated away from the PS and intermingled with the VE cells. In the extraembryonic region, these cells will give rise to the VYS. Nevertheless, a significant population of VE cells persist in the embryonic region and contribute to embryonic structures (Eakin, et al. 2005; Kwon, et al. 2008). This is in contrast to the former view of the VE as a purely extraembryonic tissue that does not extensively contribute to the embryonic gut structures.

1.6. Molecular mechanisms guiding gastrulation

The molecular determinants of gastrulation have been heavily studied. Nodal/TGF-beta and Wnt signalling pathways are very important for the initiation of gastrulation and for the determination of mesodermal and DE cell fate. In addition, the FGF signalling pathway has been found to play an important role in proper germ layer formation (Arnold and Robertson 2009). As mentioned earlier, the expression of Nodal and Wnt3 is restricted to the proximal posterior epiblast at PrS to ES stages (~E6.0- E6.5; just prior to, or at the onset of gastrulation). In addition, as discussed earlier, BMP4 signalling in the ExE is important to induce the expression of *Wnt3* in the posterior region of the epiblast (see Figure 3). The two T-box transcription factors eomesodermin (*Eomes*) and brachyury (*Bra/T*) are known to be early "marker" genes in mesoderm and DE induction. Both genes are expressed in epiblast cells close to the forming primitive streak (Figure 6). Whereas *Eomes* is a target of Nodal signalling, *Bra/T* has been shown to be a direct target of canonical Wnt signalling through beta-Catenin activation (Arnold et al. 2000; Yamaguchi et al. 1999). *Eomes* expression is lost soon after cells have passed through the PS region. *Bra/T* expression, however, persists in nascent migrating mesoderm cells. The decision of whether a cell belongs to the mesoderm or DE lineage seems to depend to a large extent on Nodal signalling. In loss of function experiments using target genes of Nodal signalling, no DE production was evident (reviewed in Tam, et al. 2003). For example, interfering with Nodal signalling by deletion of *FoxH1*, a transcription factor necessary for Nodal function, results in the absence of DE (Hoodless, et al. 2001). The expression of goosecoid (*Gsc*) in response to Nodal signalling leads to a repression of *Bra/T* expression and therefore to the formation of DE. Accordingly, dependent on the dose of Nodal signalling, the lineage choice will be directed towards either mesoderm (low Nodal signalling) or DE (high Nodal signalling) (Tam, et al. 2003; Arnold and Robertson 2009). While Wnt and Nodal signalling are required for the initiation of gastrulation, the FGF pathway is more involved in the progression of gastrulation (Figure 7). A key event during gastrulation is the delamination of committed mesododerm/DE cells from the epiblast epithelium. This process, called epithelial-mesenchymal transition (EMT) appears to be driven by FGF signalling. *FGFR1* is expressed in the PS at ES stage. The activation of FGFR1 by secreted FGF8 expressed by the epiblast cells in the PS and nascent mesoderm cells leads to the upregulation of *Snai1*, a *bona fide* EMT marker. *Snai1* is responsible for the downregulation of *E-cadherin*, which is necessary for the detachment of cells during EMT (Nieto 2002). In embryos lacking *FGF8* expression,

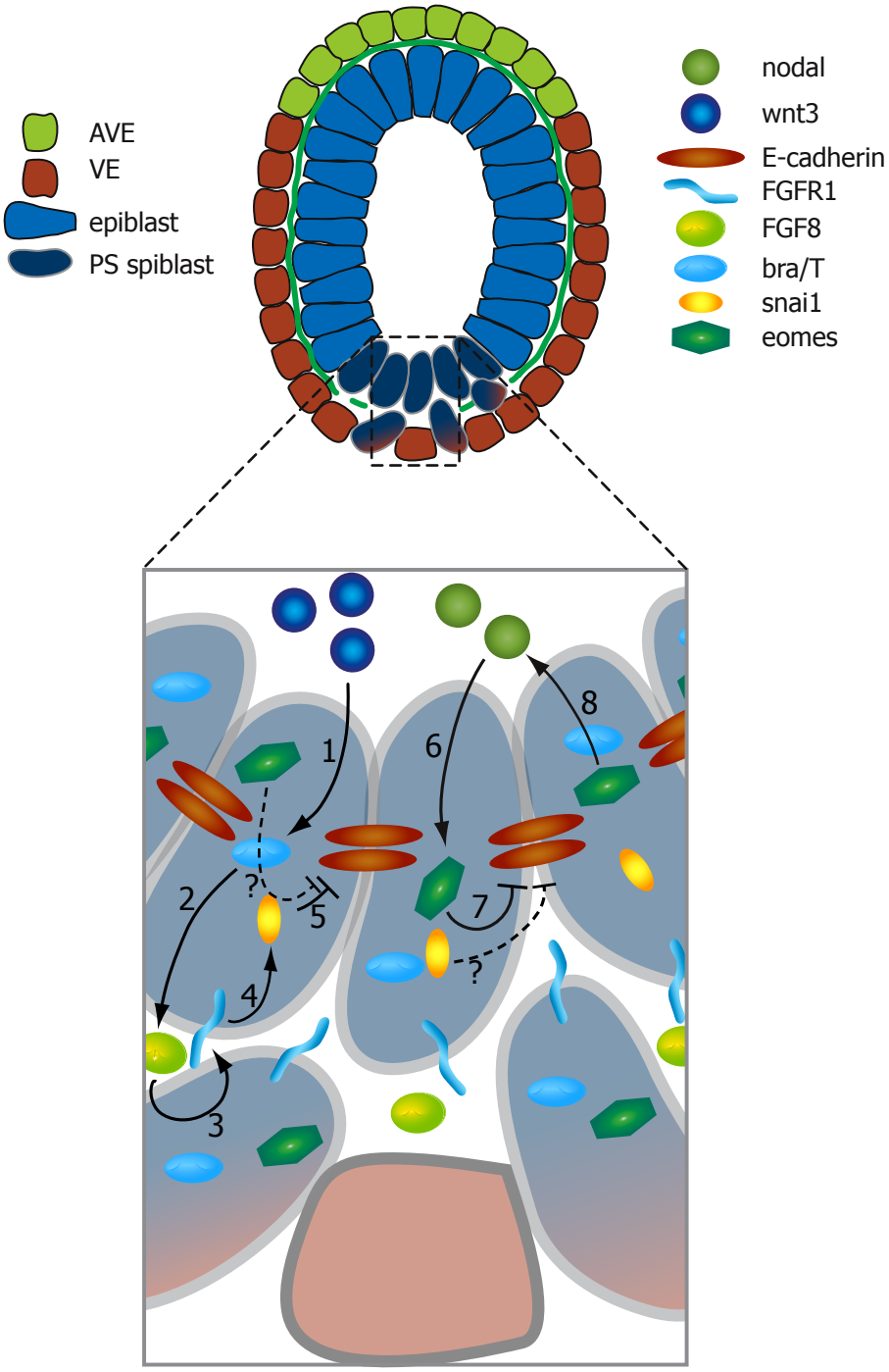

Figure 7 Molecular pathways underlying gastrulation
Three major signalling pathways have been shown to be important for gastrulation. (1) Secreted Wnt3 leads to an upregulation of *Bra/T* in epiblast cells close to and at the PS. (2) The expression of *FGF8* is enhanced by Bra/T. (2) FGF8 is secreted and activates FGFR1 (3), present on posterior epiblast cells. (4) FGFR1 signalling induces the expression of the transcriptional repressor Snai1, which is necessary to downregulate E-cadherin (5). The loss of E-cadherin is important for the delamination of cells that are committed to become mesoderm or endoderm and to leave the PS. (6) Nodal signalling in the PS is important for the specification of lineages but also for the induction of Eomes. (7) Eomes has been shown to be an important regulator of EMT, possibly in conjunction with or upstream of Snai1. (8) However, Eomes is also capable of inducing Nodal expression in posterior epiblast cells via a feedback loop.

nascent mesoderm cells are able to migrate through the primitive streak but then fail to detach and accumulate in the PS. These embryos largely fail to generate mesoderm or DE and their derivatives (Sun, et al. 1999). Similarly, *Snai1* mutant embryos are unable to produce mesoderm because the nascent mesoderm cells cannot detach and migrate (Carver, et al. 2001). Interestingly, Arnold and co-workers have recently shown that Nodal signalling is important for EMT during gastrulation. In *Eomes* deficient embryos, derived from conditional ablation of *Eomes* in the epiblast, cells were unable to leave the primitive streak and were trapped, similar to the case in *FGF8* and *Snai1* deficient embryos. *E-cadherin* expression persisted, although *FGF8* and *Snai1* were expressed at expected levels (Arnold, et al. 2008). This enforces the idea that a well-regulated interplay of different signals is necessary for the establishment of the mammalian body plan.

1.7. Epithelial-mesenchymal transition

The process of epithelial-mesenchymal transition is seen in many places and is a basic requirement for gastrulation to proceed. Epithelial cells are polarized, tightly packed and exhibit strong cell-cell and cell-matrix contacts. In contrast, mesenchymal cells are motile, dispersed and display little cell-cell contact. To change the behaviour and fate of epithelial cells towards mesenchymal cells, several rearrangements are necessary. In general, cells need to detach from the epithelia. This requires a reduction in the adhesion to neighbouring cells, which is mainly achieved by the downregulation and redistribution of E-cadherin. This calcium dependent cell adhesion molecule is widely expressed in epithelial cells and is important in the formation of adherence junctions (Shook and Keller 2003). Adherence junctions normally pave the way for the establishment of other types of cell-cell adhesion complexes such as tight- or gap junctions. A second requirement is the detachment from and the disruption of the basement membrane (BM), a specialized extracellular matrix (ECM) that underlies the epithelium. Cells secrete several matrix metallo proteases (MMP) in order to modulate their surrounding ECM. In the case of gastrulation, very little is known about how the BM is degraded in order to allow migration of the nascent mesoderm cells through the PS. Several processes during embryonic development involve EMT. For instance, the generation of neural crest cells involves EMT in order to allow cells to delaminate from the neuroectoderm and migrate to their designated target areas (reviewed in Trainor 2005). EMT also has important implications in health and disease. The recruitment of blood vessels to solid tumours and the delamination of tumour metastases require EMT. Besides FGF signalling, TGF-beta signalling also plays central roles in the regulation of EMT (Shook and Keller 2003).

1.8. Basement Membrane

The BM is a specialized form of the extracellular matrix. Its function is to provide stability to a tissue. Furthermore, a functional BM is needed for cells to form a polarized epithelial layer. This is important in the formation of PrE during peri-implantation development. Studies have shown by using mouse embryonic stem cell derived embryoid bodies, that a non-functional BM inhibits the formation of the epithelial structures and thus the proper formation of EBs (Aumailley, et al. 2000; Fujiwara, et al. 2007). This process is known to mimic the formation of VE and epiblast in the mouse embryo (Coucouvanis and Martin 1999).

The BM consists of a basic network mainly established by laminin proteins. Laminins are heterotrimers comprised of an alpha, beta and gamma chain (Colognato and Yurchenco 2000). In total five alpha, four beta and three gamma chains are known, which can be combined to, in total, 16 so far known laminin isoforms in mice (Miner and Yurchenco 2004); (Aumailley, et al. 2005). The names of the respective laminin isoforms are derived from the numbers of the alpha, beta and gamma chains used (Aumailley, et al. 2005). The main laminin isoforms found during early embryonic development in mouse are laminin111 (ln alpha1, beta1, gamma1) and laminin511 (Miner 2004). Although laminin is believed to be a critical component of the BM, other proteins are also important for a functional BM. Type IV collagen is widely present in BMs as well as the glycoproteins nidogen1 and 2. In addition, the proteoglycan perlecan is found in many BMs (Handler, et al. 1997). These different components of the BM are thought to serve different functions. Laminins are believed to form a structural scaffold, whereas type IV collagen functions in linking laminin scaffolds to a network. Other components are implicated in protein binding to the BM that also facilitate the adhesion of cells to the BM (Yurchenco 2004).

The assembly of BMs, however, is still not fully understood. It is known that secreted laminin trimers are essential for BM formation. Laminin network assembly is Ca^{2+} dependent and was believed to proceed by self-assembly upon reaching a critical concentration of laminin trimers. This view has changed in recent years. Instead, a so-called surface activated assembly is hypothesized. Thus, a nascent LN network would require interactions with cell surface proteins through its G-domain for assembly. This network would further be stabilized and cross-connected by type IV collagen, nidogen and perlecan (reviewed in Yurchenco 2004). Studies have indicated that LN is critical for the assembly of BM (Yurchenco and Wadsworth 2004; Miner 2004), whereas

components such as nidogen or type IV collagen, are not important for initial assembly but rather for stability (Murshed, et al. 2000; Schymeinsky, et al. 2002; Pöschl, et al. 2004)). Interestingly, the main cell surface receptors for LN, integrin and dystroglycan also seem to play a minor role in BM assembly. In studies using knock out embryoid bodies for integrin beta1 or Dab1, a proper BM could form (Li, et al. 2002). However, integrins and dystroglycans are important for tissue organization and formation during early development (Fässler, et al. 1995; Williamson, et al. 1997). This marks one of the main functions of BMs, aside from its structural requirement. Intact BMs are needed for cells to epithelialize and differentiate, for instance in the formation of the epiblast in the embryo. In addition to this function, BM components are also known to bind and immobilize growth factors (Mongiat, et al. 2001) and thereby affect signalling in a tissue.

1.9. Some questions remain

Despite the increasing understanding of the regulatory processes during early postimplantation development, some questions still remain. The regulation of gastrulation for instance, have been well studied, and are understood to a good extent. Nevertheless, gaps in some of the regulatory pathways still need to be filled, but a variety of effector molecules are known, which are important for morphogenetic movents during mesoderm and endoderm formation. During axis formation, however, very little is known about how the cells actually migrate, and which molecules are involved in cell adhesion or tissue cohesion. It is clear, that AVE cells form filopodial protrusions when they migrate, but it is not fully understood, by which mechanisms this migratory process is executed. So far, mainly transcriptional regulators such as Hex, Lim1 or Otx2 have been found to function in the regulation of AVE cell migration (Srinivas, et al. 2004; Shawlot and Behringer 1995; Ang, et al. 1996). The first data leading towards direct effectors of cell migration was the identification of the involvement of NAP1, which has actin cytoskeleton modulating functions (Rakeman and Anderson 2006). Nevertheless, none of these molecules can directly interact with its environment outside the cell. Therefore the discovery of new molecules that function in the AVE will not only increase the understanding of the way AVE cells are positioned but could also give new insights in the biological role of the AVE during embryonic development.

1.10. Fibronectin leucine rich transmembrane proteins

The FLRT family of proteins is a rather young family. Not only because it was discovered in 1999 in an in silico screen for human muscle ECM interacting proteins (Lacy, et al. 1999), but also because orthologous genes have been found only in vertebrates, such as in Xenopus, zebrafish and mouse. The FLRT family is comprised of three members, FLRT1, FLRT2 and FLRT3 (Lacy, et al. 1999). The three members show a rather high degree of structural homology. These putative type 1 transmembrane proteins with a size of about 650 to 675 amino acids, have an extracellular domain, a transmembrane region and a rather short (about 100 aa long) intracellular C-terminal tail. The extracellular domain consists of 10 leucine rich repeats (LRR), flanked by a characteristic N- and C-terminal LRR, respectively, and a fibronectin type 3 (FN3) domain (Figure 8). This characteristic domain structure gave the name to the entire protein family, FLRT (Fibronectin Leucine Rich Transmembrane protein). However, the intracellular stretch shows no known protein interaction motive. Nevertheless, several putative phosphorylation sites have been predicted and two highly conserved lysine residues were implicated in Rnd1 (a Rho GTPase) interaction (Ogata, et al. 2007).

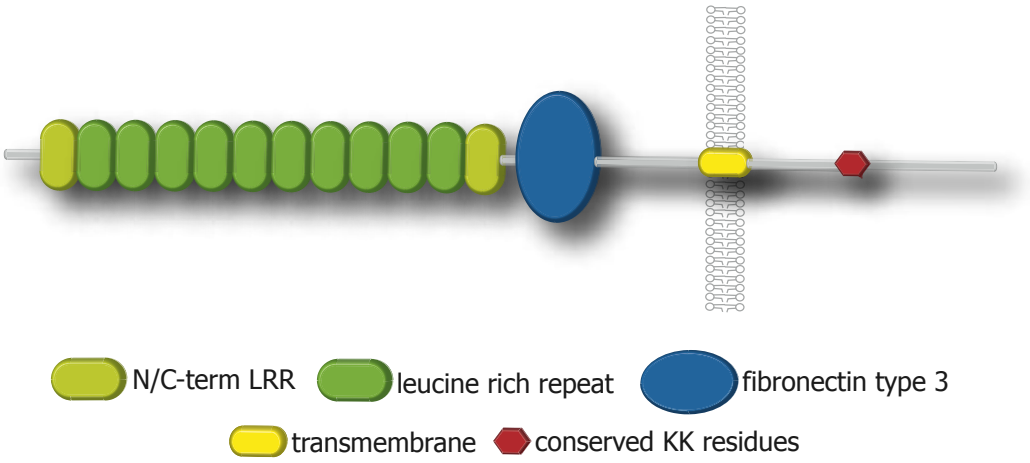

Figure 8 The domain architecture of FLRT3
The name FLRT is derived from the protein's domain structure. FLRT proteins are putative type 1 transmembrane proteins carrying 10 leucine rich repeats (LRR) flanked by a N- and a C-terminal LRR and a fibronectin type 3 domain on its extracellular region. After the transmembrane domain, a short C-terminal domain extends into the cytoplasm without any known protein homology domain but with two highly conserved lysine residues.

Although a great effort has been put into the understanding of the biological roles of FLRT proteins, only a limited but steadily increasing number of studies have been published so far. Yet, research has mainly focused thus far on the biological functions of FLRT3, and almost no published data is available on the functions of FLRT1 or FLRT2. FLRT3, in turn, has been found to be upregulated in PNS neurons after injury (Tanabe, et al. 2003); Robinson et al. 2004), and to promote neurite outgrowth of cerebellar granule cells when grown on a FLRT3 expressing surface layer (Tsuji, et al. 2004). In *Xenopus* embryos, xFLRT3 (the *Xenopus* homologue) was shown to function in the FGFR pathway (Figure 9 A). Injection of *xFLRT3* RNA into *Xenopus* embryos led to ectopic expression of Xbra and Fgf8. This is mediated through the interaction of the FN3 domain of FLRT3, with the extracellular domain of the FGFR1 in presence of the intracellular C-terminal region of FLRT3, followed by downstream activation of the MAP-kinase pathway (Böttcher, et al. 2004). Furthermore, a second study performed in the laboratory of Christof Niehrs showed that FLRT proteins can interact homotypically and are able to promote cell sorting in transfected cells via their LRRs (Karaulanov, et al. 2006) (Figure 9 C). An additional function of FLRT3 was found in conjunction with the Nodal-like TGF-beta signal Activin (Figure 9 B). In *Xenopus*, FLRT3 is involved in a pathway controlling the subcellular localization of C-cadherin in animal cap cells. Upon activation through Activin, FLRT3 and the Rho-type GTPase Rnd1 directly bind and mediate the internalization of C-cadherin via endocytosis. In overexpression experiments, massive detachment of cells was evident after injection of with *xFLRT3* or *Rnd1* RNA (Ogata 2007). The possible biological roles of FLRT3 have so far mainly been addressed in cell culture or amphibian embryo experiments. Initially, very little data on the function of FLRT3 in mouse was available. Haines and co-workers provided some insights into the expression pattern of FLRT3 during postimplantation development. In addition, they have confirmed the possible cell-adhesion function of FLRT3, as well as an interaction with FGFRs (Haines, et al. 2006). The available data on the functions of FLRT3 shows a rather diverse picture. FLRT3, a potential ECM interacting protein, is expressed on regenerating PNS neurons and can facilitate the outgrowth of neurites. Further in vitro studies have implicated a capability of FLRT3 for homotypic binding and mediation of cell sorting. In combination with FGF or activin signalling, it can also influence the formation of the embryonic body axis either by posteriorizing effects or by disturbing axis elongation, at least in the amphibian embryo. Aside from the expression pattern of FLRT3 in mouse embryos, the function in mammalian development remained largely unknown. Only very recently, a publication has claimed a possible role for FLRT3 in the developing mouse embryo. The loss of FLRT3 during development was suggested to result in DE migration defects that are independent of FGF signalling. But no possible mechanism of how FLRT3 is involved in DE generation or migration could be shown, (Maretto, et al. 2008).
In this dissertation, my work on an independently generated FLRT3 knock out mouse will be presented.

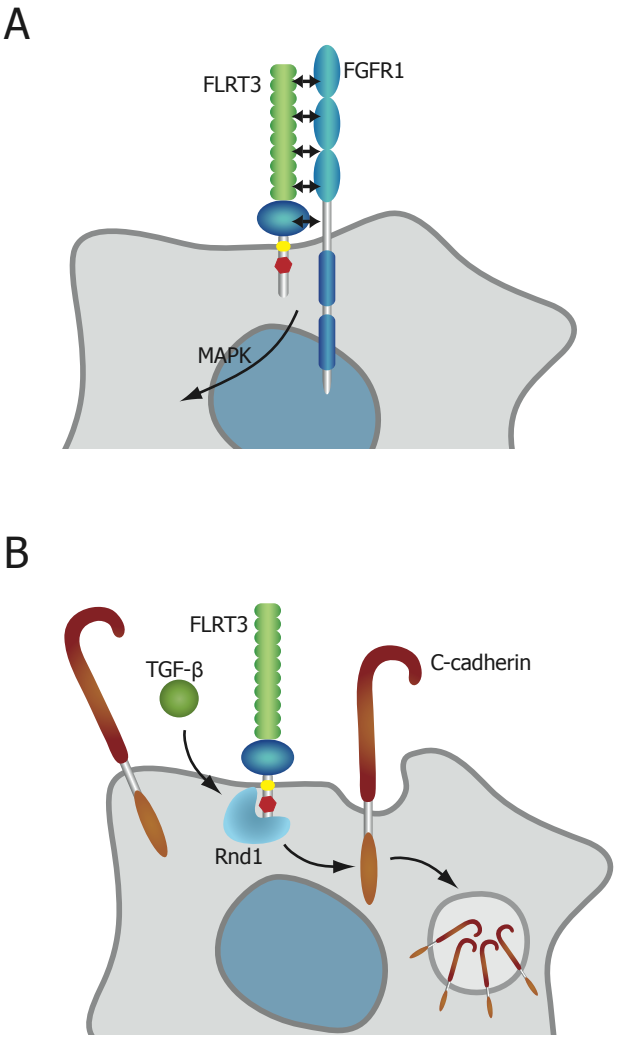

Figure 9 Proposed functions of FLRT3
Although the function of FLRT3 is not yet clear, several roles for FLRT3 have been demonstrated thus far. (A) In Xenopus embryos, FLRT3 interacts with FGFR1 and enhances the signalling function of FGFR1 via the MAPKinase pathway. (B) In addition, during Xenopus gastrulation, FLRT3, in cooperation with Rnd1, is required to regulate C-cadherin levels present in the cell membrane. This pathway is activated through TGF-beta signalling. (C) It has been shown in heterologous cell systems that FLRT3 is able to bind in a homotypic manner and can mediate cell sorting. How this effect is accomplished is so far unclear

2. Results

2.1. Early embryonic expression pattern of FLRT family members

Using whole mount *in situ* hybridization (WISH), a technique to (sequence) specifically visualize mRNA (Wilkinson 1992), the expression pattern of *FLRT1*, *FLRT2* and *FLRT3* during mouse embryonic development was determined. The expression was analyzed during the period of gastrulation, starting from ES stage (~E6.5) until organogenesis stage (E10.5) in the case of *FLRT3*. During the early phases of gastrulation (ES; MS; E6.5 – E7.0), *FLRT1* and *FLRT2* expression was not detected by the riboprobe used in this study (data not shown). *FLRT2* was detected at mid to late streak stages but expression was restricted to the newly generated head fold mesoderm (Figure 10 A-C). At this stage no FLRT1 expression was observed (data not shown). However, *FLRT3* expression was already detected at ES where it was exclusively expressed in the visceral endoderm (VE), the cell layer surrounding the epiblast (Figure 10 D-F), with highest expression anterior in the AVE. Notably, *FLRT3* expression was completely absent from the region of the primitive streak and the epiblast (Figure 10 D-F). FLRT3 was also found to be expressed in the chorion at the proximal extraembryonic region (Figure 10 D) at early streak stage. Also during later stages of gastrulation, *FLRT3* expression remained restricted to the endodermal cell layer. Interestingly, FLRT3 expression persisted in the DE with expression levels comparable to VE (Figure 10 G-I). At early head fold (EHF) stage, FLRT3 expression expanded into the head fold mesoderm, the lateral ectoderm and the posterior neuroectoderm (Figure 10 J-K). Common to all stages, was the absence of *FLRT3* expression in the region of the primitive streak.

During early organogenesis (E8.5) FLRT1 expression was detected exclusively in the midbrain region (Figure 11 A). Also at E9.5, *FLRT1* expression was largely restricted to the midbrain region, although the expression pattern was more refined and showed a clear stripe-like pattern along the mid-hindbrain boundary, the so called isthmus, as well as in a region at the fore- midbrain boundary (Figure 11 B). The expression of *FLRT2* at E8.5 and E9.5 is more widespread compared to *FLRT1* with strong expression in what appears to be the cephalic mesoderm of both E8.5 and E9.5 embryos (Fig results 2 C, D). Furthermore, *FLRT2* expression was visible in the somites and the trunk

mesenchyme caudal to the heart at E8.5 (Figure 11 C). In E9.5 embryos, *FLRT2* was expressed in the somites, the mandibular component of the first branchial arch and in mesoderm tissue surrounding the neural tube (Figure 11 D).

Expression of *FLRT3* in E8.5 to E10.5 embryos continued to be widespread. Expression was detected in the prospective fore- and midbrain regions at E8.5, as well as in the newly formed somites. Also the proepicardial organ showed high *FLRT3* expression. *FLRT3* expression was detected in the prospective forebrain and extended throughout

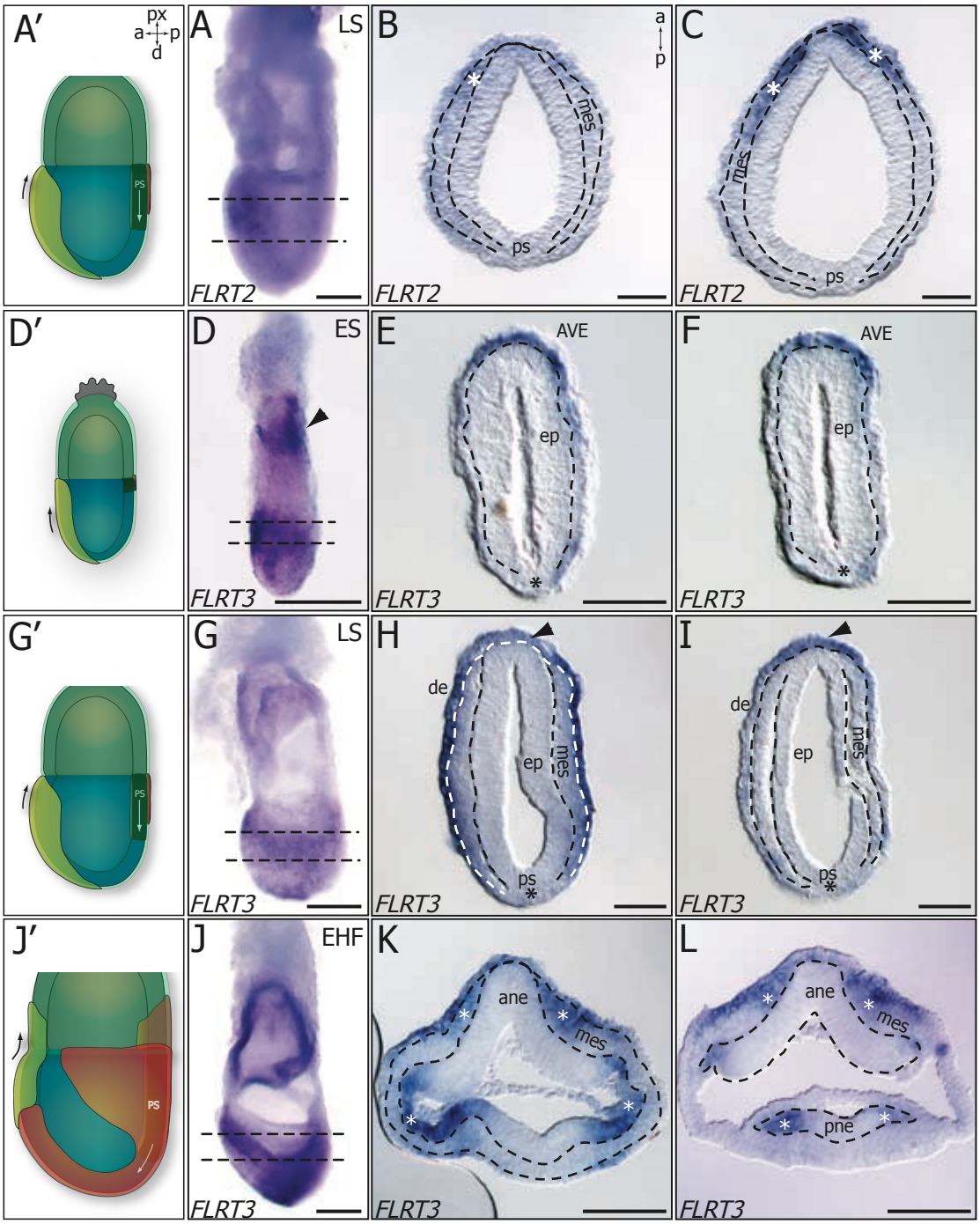

the midbrain. In E9.5 embryos, strong expression of *FLRT3* was detected at the isthmic boundary. However, *FLRT3* expression was restricted to the midbrain side and virtually absent in the hindbrain. In addition, the optic and otic eminences, as well as the mandibular part of the first branchial arches, showed *FLRT3* expression. The somites displayed a very particular expression pattern with strong staining in the dorsal region. Also, the apical ectodermal ridge (AER) and the limb buds were positive for *FLRT3* expression (Figure 11 F). At E10.5 FLRT3 was still expressed at the isthmic boundary, the for- and midbrain, as well as the branchial arches. The somitic expression of FLRT3 remained prominent in a patterned fashion, together with the strong expression at the AER in both, fore- and hind limb buds. *FLRT3* expression in general was restricted to the more anterior structures and was never expressed posterior to the caudal-most somites.

In summary, FLRT1, FLRT2 and FLRT3 displayed interesting and dynamic expression patterns during early post implantation development. In particular, FLRT3 showed a highly dynamic and specific expression pattern during this period, ranging from expression exclusively in the VE, and therefore extraembryonic, before and during gastrulation, to expression in all three germ layers, but with a very distinct expression pattern in the forming somites and the developing nervous system.

Figure 10 Expression of FLRT during early post implantation development
(A',D',G',J') Schematic drawings showing various stages of embryonic development and indicating developmental hallmarks, such as AVE migration (indicated by an arrow), PS initiation, and mesoderm migration. All whole mount embryo images are oriented with the anterior towards left and distal towards the bottom of the image. (A) Using WISH, expression of *FLRT2* was detected in the head fold stage (HF) embryo exclusively in the anterior mesoderm. Dashed lines indicate the location of the histological sections shown in B and C. (B, C) Cryosections of the embryo in (A) showing the expression of *FLRT2* exclusively in the anterior mesoderm (asterisks). The dashed lines separate the three germ layers - definitive endoderm (DE), mesoderm and ectoderm. (D) Early streak stage (ES) embryo after WISH for *FLRT3* showing strong expression in the embryonic VE, especially in the anterior region and in the chorion of the extraembryonic region (arrow). The dashed lines indicate the location of the sections shown in E and F.(E, F) Cryosections of ES embryo showing strong *FLRT3* expression in the VE, especially in the AVE. No *FLRT3* expression was detected in the epiblast and the PS region (asterisk). Dashed lines outline the border between the epiblast and VE. No mesoderm is recognizable yet. (G) Late streak stage embryo (LS) after WISH for *FLRT3*, showing *FLRT3* expression in the embryonic region in the DE and VE. Dashed lines indicate the regions of sections shown in (H) and (I). (H,I) Cryosections of the embryo shown in G revealing strong FLRT3 expression in the DE and the remaining VE in the anterior region (arrow). The dashed lines outline the germ layers. Note, that in the PS region *FLRT3* is absent (asterisk). (J) Early head fold stage (EHF) embryo showing strong *FLRT3* expression in the embryonic region. The dashed lines indicate the region of the cryosections shown in (K) and (L). (K,L) Histological sections showing strong expression of *FLRT3* in the anterior endoderm. In addition, the anterior mesoderm and the lateral regions of the ectoderm, especially the posterior neuroectoderm, show *FLRT3* expression (asterisks). Dashed lines outline the germ layers or the ectoderm.
Scale bars in A, D, G, J are 200 µm and in B, C, E, F, H, I, K, L are 50 µm. Sections are oriented in a way that anterior is directed upwards and posterior downwards.
Abbreviations: ane, anterior neuroectoderm; AVE, anterior visceral endoderm; DE, definitive endoderm; EHF, early head fold stage; ep, epiblast; ES, early streak; LS, late streak stage; mes, mesoderm; pne, posterior neuroectoderm; ps, primitive streak

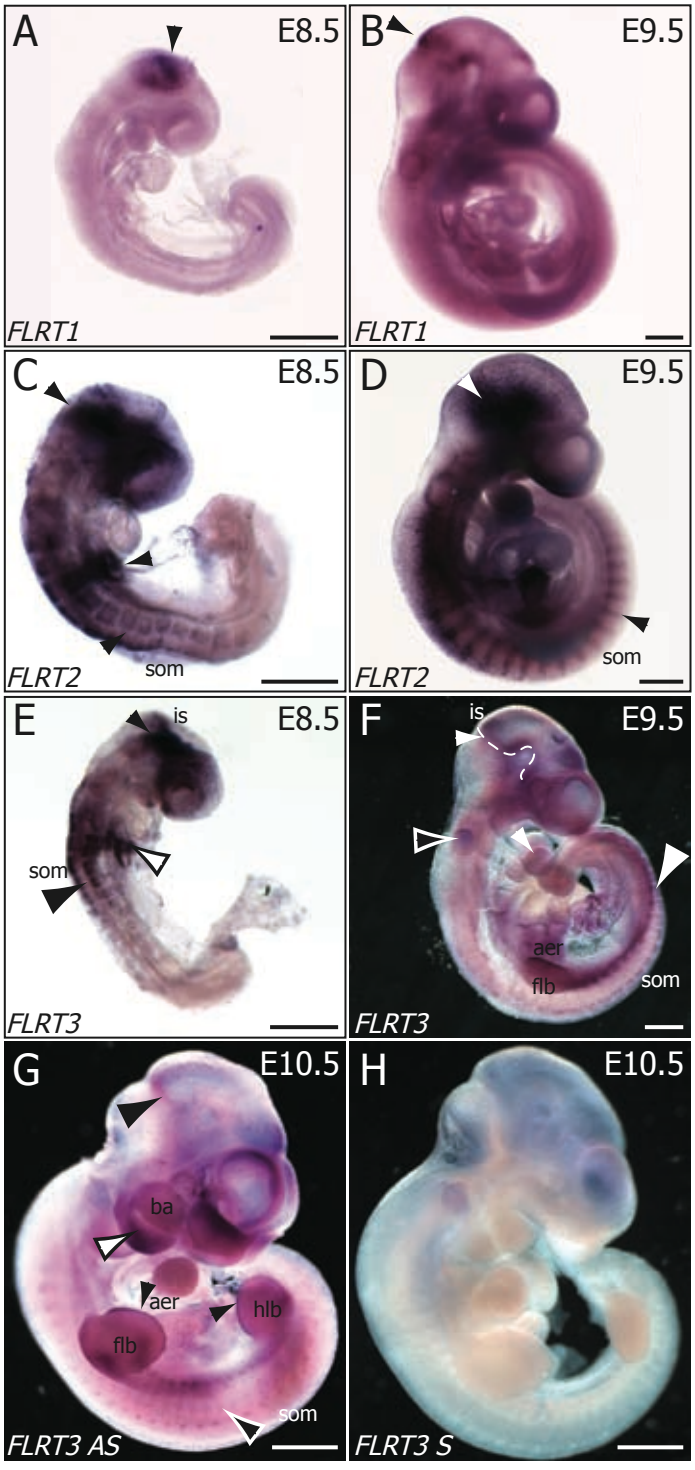

Figure 11 FLRT expression during early organogenesis and embryonic turning

(A) Expression of *FLRT1*, visualized using WISH at E8.5, was restricted to the prospective midbrain region (arrow). (B) At E9.5, expression of *FLRT1* was still exclusively found in the prospective midbrain but more restricted to the isthmic boundary (arrow). (C) *FLRT2* expression at E8.5 was rather widespread and included the prospective midbrain, the developing somites and the foregut diverticulum (arrows). (D) At E9.5, the expression of *FLRT2* appeared widespread in the, most probably, cephalic mesoderm tissue (white arrow) and was refined in the somites (black arrow). (E) The midbrain of E8.5 embryos, analyzed for *FLRT3* expression showed strong expression of *FLRT3* (small arrow), as well as the newly forming somites (arrowhead) and the foregut diverticulum (white arrow). No *FLRT3* expression was detected caudal to the last somite. (F) At E9.5, *FLRT3* expression was still detectable in the prospective midbrain, especially at the isthmic boundary (dashed line and arrow), in the first branchial arch (arrow), the otic vesicle (open arrowhead) and the somites (arrowhead). The newly formed forelimb buds, especially at the aer, showed strong *FLRT3* expression. This is a region of high FGF signalling activity. (G) *FLRT3* expression at E10.5 was largely similar to expression at E9.5 including the isthmic boundary (black arrowhead), the somites (white outline arrow) and branchial arches (black outline arrow). Interestingly, in addition to the expression in the forelimb bud, the expression of *FLRT3* was also detected in the newly formed hind limb bud and the aer (arrow). (H) WISH using the *FLRT3* sense riboprobe and an E10.5 embryo. No staining was detectable in this embryo, suggesting high specificity of the antisense riboprobe used for the study.

The scale bars in A-F are 500 µm and in G and H 1000 µm.

Abbreviations: aer, apical ectodermal ridge; ba, branchial arch; flb, forelimb bud; hlb hind limb bud; is, isthmic boundary; som, somites

2.2. Genetic ablation of FLRT3

2.2.1. The genetic ablation of FLRT3 causes embryonic lethality

The genetic ablation of a gene of interest in the mouse genome has been widely used to discover the function of a molecule in a living animal. In order to understand the function of FLRT3 in the mouse embryo, a knockout allele was generated previously in our laboratory. Briefly, a full knockout allele (*FLRT3*$^{-}$) was generated by replacing the entire coding sequence of FLRT3, which is located in a single exon (exon III), with a neomycin resistance cassette. With homologous recombination in mouse embryonic stem cells, the allele was transmitted through the mouse germ line.

Heterozygous intercrosses with the *FLRT3*$^{-}$ allele yielded a very low number of viable offspring (<3% at weaning age), suggesting that the mutation leads to embryonic lethality. A careful analysis of critical embryonic stages was carried out. Litters of heterozygous intercrosses were dissected and embryos were genotyped using a PCR based strategy. It became apparent that until E9.5, *FLRT3*$^{-/-}$ embryos could be recovered with the expected Mendelian ratio. After E10.5, almost no *FLRT3*$^{-/-}$ embryos could be recovered. This showed that the majority of embryos died between 9 and 10 days of embryonic development (data not shown).

Characterizing the phenotype of the *FLRT3*$^{-/-}$ embryos was an important step on the way to understanding the function of FLRT3 in the mouse embryo. Using embryos at E8.0 to E10.5, a careful analysis of the occurring phenotypes was performed. Embryos at the respective stages were dissected, genotyped and subjected to scanning electron microscopy (SEM) analysis in collaboration with Martin Heß at the Biocenter of the Ludwig-Maximilians-Universität. This method delivered a three dimensional impression of the embryos and also allowed the retrieval of high resolution and high magnification images of *FLRT3*$^{-/-}$ embryos. The observed phenotypes showed varying degrees of severity. Already in embryos around E8.0 to E8.5 an asymmetry of the head folds could be observed. One head fold appeared normal in development, whereas the second head fold seemed smaller and was significantly retarded in growth (Figure 12 B, C). Also, in older embryos, asymmetric head folds could were normally be observed in concert with head fold fusion defects (Figure 13 E, F). Independently of the observed asymmetries, head fold or anterior neural tube fusion defects were observed in embryos at E8.5 (just before or during embryonic turning) and E9.5 (Figure 12 D and Figure 13 G, H). Furthermore, the head fold fusion defect became more pronounced in embryos at

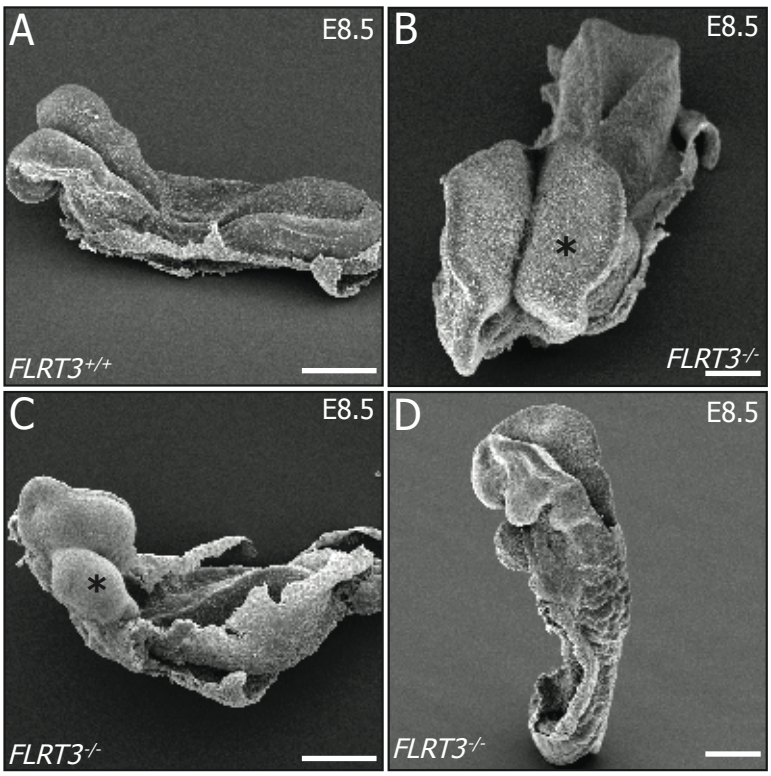

Figure 12 FLRT3$^{-/-}$ embryos exhibit asymmetric head folds at E8.5
(A) Scanning electron microscope image of a wt embryo at E8.5. (B, C) *FLRT3*$^{-/-}$ E8.5 embryos exhibited asymmetric head folds, with one head fold appearing less developed (asterisk) compared to the second. In a slightly older embryo (D), the head folds were not fused, whereas the remaining neural tube had fused.
Scale bars are 200 µm.

E10.5, when few embryos displaying exencephaly could be recovered. These embryos showed asymmetric head folds together with exposed neural tissue (Figure 14 B, C).

Moreover, more severe malformations, such as defects in embryonic turning were frequently observed in embryos recovered at E9.5 (Figure 13 C). Turning defects often resulted in more severe malformations, which affected mainly the anterior region of the embryos. Such Embryos were often not fully enclosed in the visceral yolk sac, showed open head folds and a curved neural tube (Figure 13 G, H and Figure 14 D). A very interesting observation was the discovery of *cardia bifida*, the presence of two primitive hearts, in histological preparations at E9.5. Each of these heart primordia showed signs of septation and patterning (Figure 15 A-I). This finding was further verified using whole mount antibody stainings against GATA4, a marker for early heart development (Molkentin, et al. 1997). In addition, blood filled cavities in the head region were often observed (Figure 15 D, E, G, H). In more severe cases, parts of the embryo or even the entire embryo developed outside of the visceral yolk sac. Remarkably, even in those embryos, the somites were visible (Figure 15 L).

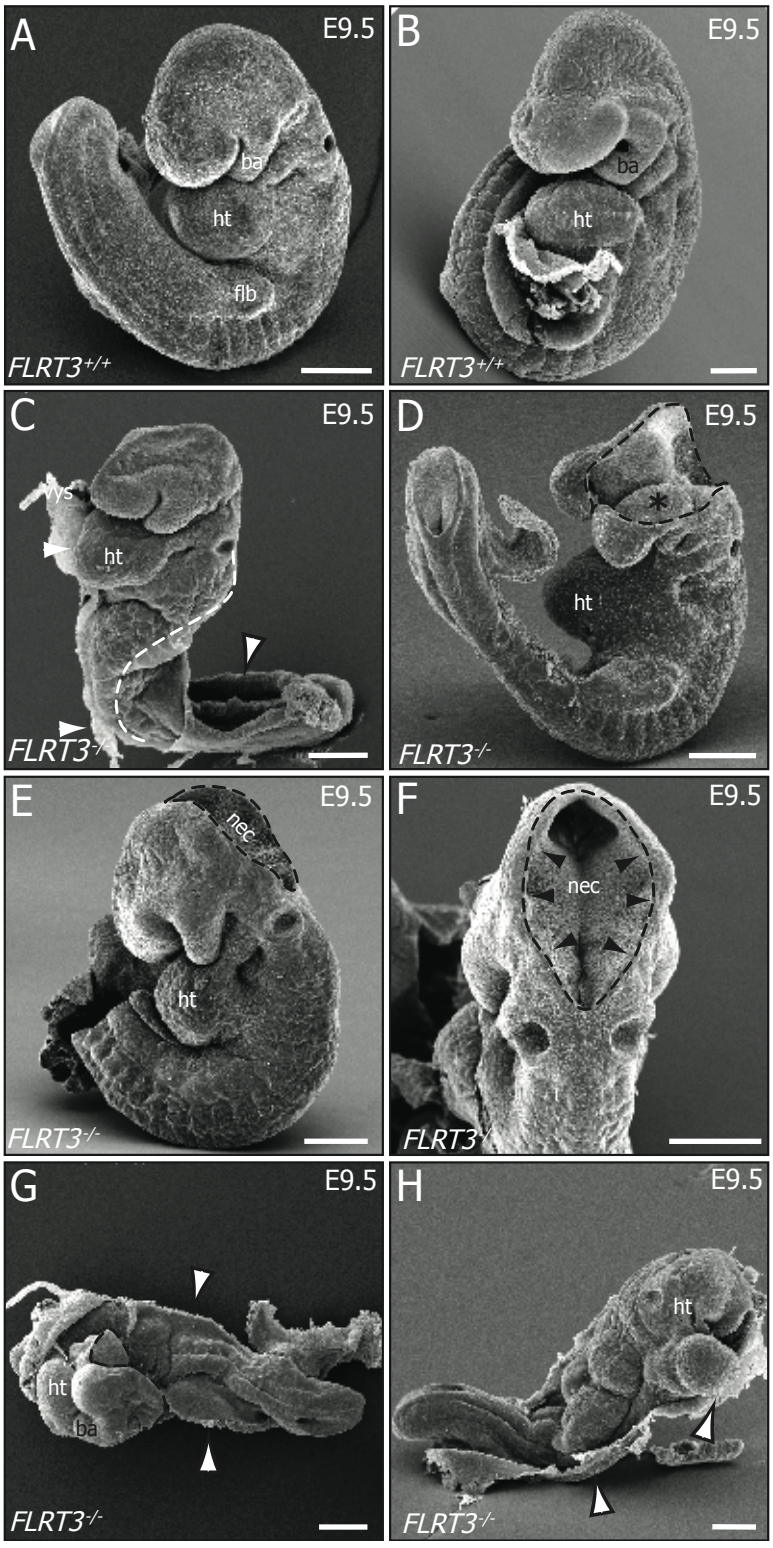

Figure 13 Turning defects and neural tube closure defects at E9.5 in FLRT3$^{-/-}$ embryos

(A, B) Scanning electron microscope images of wt embryos at E9.5. (C) shows a *FLRT3*$^{-/-}$ embryo that has not undergone embryonic turning and was still attached at its ventral side to the VYS (arrows). The dashed line indicates the twisted neural tube exposing the ventral body side at its caudal end (black outline arrow). (C) SEM image showing an E9.5 *FLRT3*$^{-/-}$ embryo with unfused and asymmetric head folds (asterisk) and a laterally mislocalized pericardium (heart). Remarkably, the caudal part of the embryo developed normally. (E, F) At E9.5, this *FLRT3*$^{-/-}$ embryo displayed unfused head folds and the neuroectoderm was still visible (arrows). Nevertheless, the development in general seemed unaffected, as the embryo still underwent the turning process. (G, H) Two E9.5 *FLRT3*$^{-/-}$ embryos that have developed integrated into the VYS and did not undergo embryonic turning. The remaining VYS is clearly detectable (arrow heads) and appeared to be attached to the ventral body wall. Whereas the embryo in (G) showed asymmetric but clearly visible head folds, the embryo shown in (H) seemed more severely affected.

Scale bars are 200 µm.

Abbreviations: ba, branchial arch; flb, forelimb bud; ht, primitive heart; nec, neuroectoderm; VYS, visceral yolk sac.

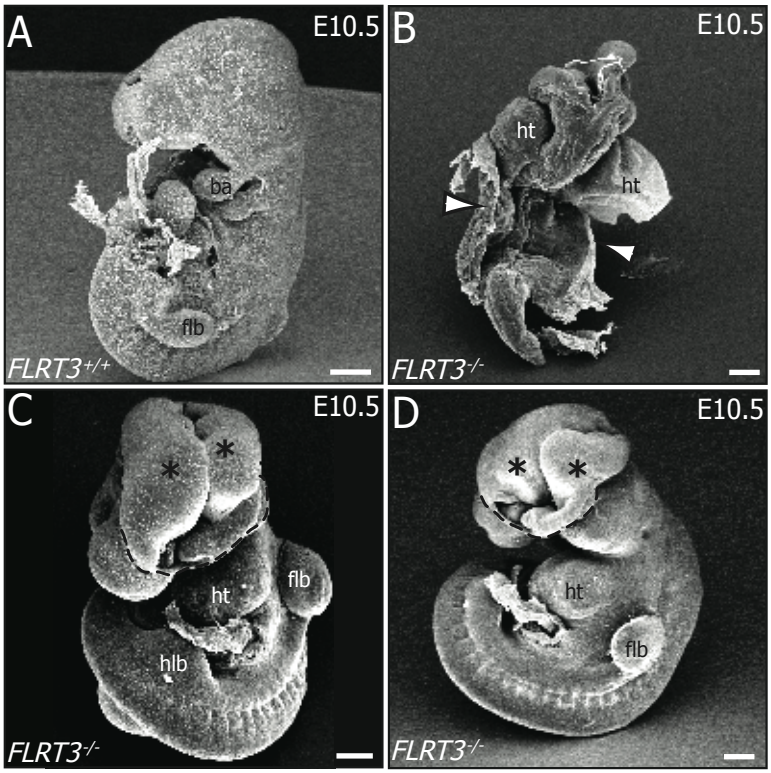

Figure 14 Exencephaly and turning defects in FLRT3$^{-/-}$ embryos at E10.5

(A) Scanning electron microscope image of a wt embryo at E10.5. The caudal part of the embryo was removed. (B) Even at E10.5, *FLRT3*$^{-/-}$ embryos could be recovered that were integrated in the VYS (arrowheads). This image shows an embryo with two individual hearts and therefore, probably, no ventral fusion had occured. The head folds were asymmetric and not fused. This embryo had not undergone embryonic turning. (C, D) SEM images of an E10.5 embryo showing severe exencephaly with the neuroectoderm present at the surface (asterisks), leading to brain development outside of the surface ectoderm. Notably, the more caudal regions of the embryo are unaffected. Scale bars are 200 µm.

Abbreviations: ba, branchial arch; flb, forelimb bud; hlb, hind limb bud; ht, primitive heart; nec, neuroectoderm; VYS, visceral yolk sac.

Taking these observed phenotypes together, *FLRT3*$^{-/-}$ mutant embryos were categorized in three different groups according to the severity of the phenotype. The group "no phenotype" included all embryos at stages E8.5 to E10.5 that were genotyped as mutant but didn't show any obvious defects (Figure 16 i, vi). Embryos displaying asymmetric head folds and/or open anterior neural tubes were grouped as "mild phenotype" (Figure 16 ii, vii); whereas embryos showing strong malformations, including *cardia bifida* and the development outside of the visceral yolk sac were grouped as "severe phenotype" (Figure 16 ii, iv, v, viii ,ix ,x). The distribution of the phenotypes clearly showed, that about half of all recovered and analyzed *FLRT3*$^{-/-}$ embryos, showed severe phenotypes. This was true for both genetic backgrounds used, namely C57BL/6 and CD1.

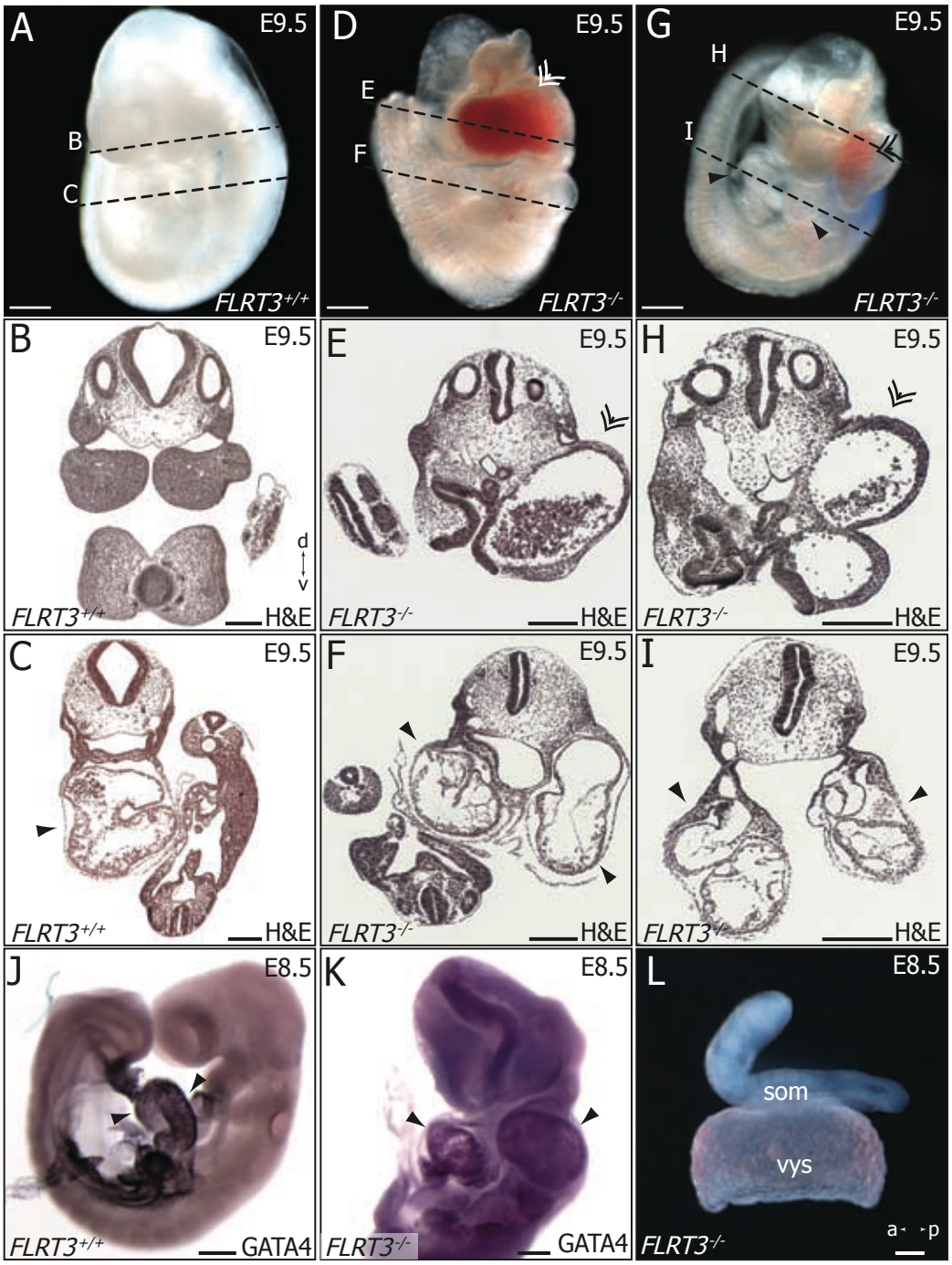

Figure 15 *Cardia bifida* was observed in FLRT3$^{-/-}$ embryos

(A-C) A wt E9.5 embryo served as control for anatomical comparisons. In (A), a whole mount embryo is depicted with dashed lines indicating the position of haematoxylin and eosin stained paraffin sections shown in (B) and (C). The arrow in (C) indicates the location of the single heart. (D, G) Whole mount *FLRT3*$^{-/-}$ embryos displayed *cardia bifida* (solid arrow heads) and blood filled swellings in the head area (double arrows). The dashed lines indicate the location of the respective histological sections. (E, F, H, I) Haematoxylin and eosin stained paraffin sections of E9.5 *FLRT3*$^{-/-}$ embryos shown in D and G. Embryos exhibited large blood filled cavities in the head region (double arrow) and two individual hearts, a characteristic of *cardia bifida*. Markedly, the head regions are severely malformed. Sections are oriented in a way that dorsal points to the top and ventral to the bottom. (J) GATA4 whole mount antibody staining labelled the forming heart at E8.5. (K) In *FLRT3*$^{-/-}$ embryos, two independent GATA4 positive hearts were apparent. (L) In extreme cases, *FLRT3*$^{-/-}$ embryos developed entirely outside of the VYS. Remarkably, structures like the somites were visible.
Scale bars in A, D and G are 500 µm and in B, C, E, F, H, I, J, K and L are 200 µm
Embryos shown in panels A, D, G and L were a "jump start" from Joaquim Egea.

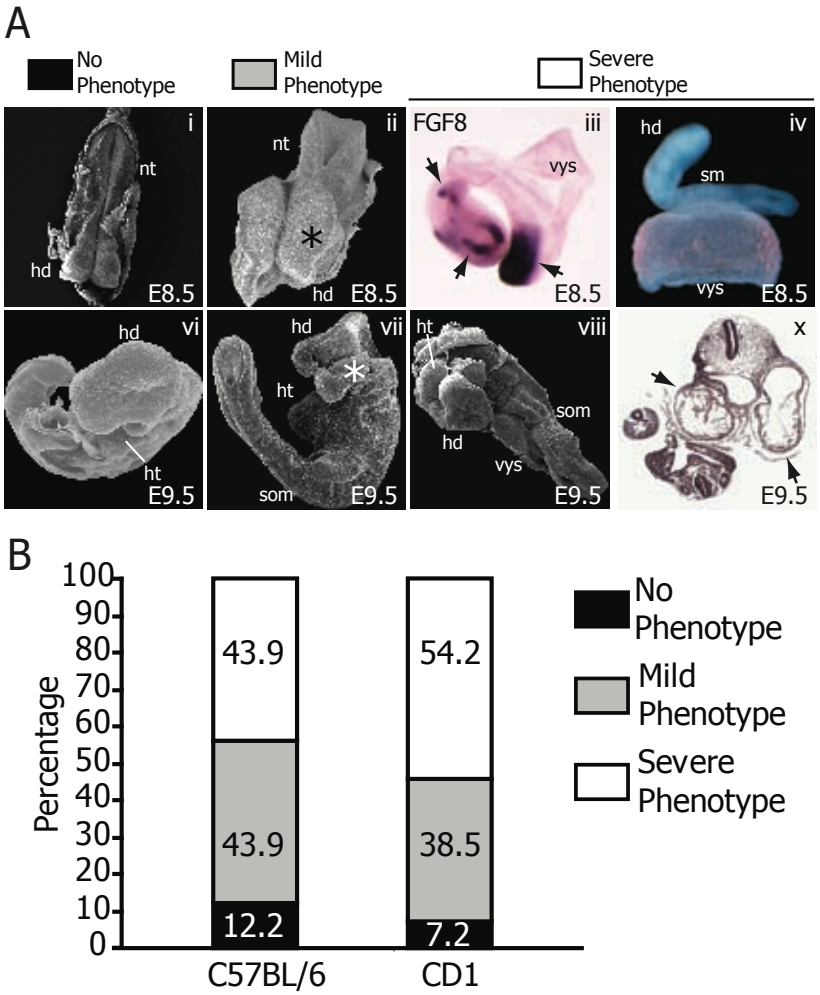

Figure 16 FLRT3$^{-/-}$ phenotype can be categorized by severity
(A) *FLRT3*$^{-/-}$ embryos were grouped according to their phenotype into three categories. In the category "no phenotype" were all embryos that were mutant by genotype but did not show any obvious physical defects (panels i, vi). Belonging to the category "mild phenotype" were mutant embryos that showed only asymmetric head folds and no further defects. (ii, vii). Embryos exhibiting *cardia bifida*, that did not undergo embryonic turning and/or developed partially or entirely outside the VYS, or any combination, were grouped into "severe phenotype" (iii, iv, viii, x). (B) A quantification of the phenotypes showed that about half of the recovered embryos at E8.5 and E9.5 displayed severe malformations in both genetic backgrounds used. Only a very small fraction of embryos was without observable phenotype.
Abbreviations : hd, head; ht, heart; som, somites; vys, visceral yolk sac

2.2.2. FLRT3$^{-/-}$ embryos show no patterning defects

Previous studies have shown hat impairments in the early patterning of mouse embryos can result in severe anterior malformations (Shawlot and Behringer 1995; Ang, et al. 1996). To further investigate, if the induction of anterior structures was impaired in *FLRT3*$^{-/-}$ embryos, an extensive marker gene analysis was carried out using WISH. This included markers for the fore- and midbrain, but also hindbrain structures. In addition markers for axial and paraxial mesoderm derivatives were used to test the proper generation of mesoderm. Otx2 is a transcription factor important for fore- and midbrain development (Acampora, et al. 1995). Testing *Otx2* expression in *FLRT3*$^{-/-}$ embryos at E8.5 and E9.5 showed that *Otx2* was induced and present at both stages (Figures 17 A-D). Due to the severity of the observed phenotypes, the expression domain was somewhat distorted. However, together with *FGF8*, used as a marker for very anterior structures (Crossley and Martin 1995), namely the anterior neural ridge; it became clear that in both wild type and mutant embryos, fore- and midbrain structures were induced. Due to the strong malformations, the expression domain appeared smaller and was sometimes difficult to interpret (Figure 17 D, H). Notably *FGF8* expression at the isthmic boundary was detectable in mutant embryos as well. In addition, *Krox20* and *Hoxb1* were used to investigate possible patterning impairments in the hindbrain region. The hindbrain is subdivided into seven stripe-like domains called rhombomeres. *Krox20* expression is known to be restricted at E8.5 and E9.0 to the rhombomeres 3 and 5 (Nieto, et al. 1991), whereas *Hoxb1* is expressed in rhombomere 4 and the tail bud (Pöpperl, et al. 1995) (Figure 17 I, K, M, O). Also *FLRT3*$^{-/-}$ embryos showed expression of *Krox20* and *Hoxb1* in rhombomeres 3, 5 and 4, respectively. However the expression was again sometimes slightly disturbed by the severe malformations (Figure 17 J, L, N, P). Interestingly, even severely affected mutant embryos displayed the expected pattern of expression (Figure 17 N, P).

The investigation of midline and mesoderm marker genes suggested the proper formation of these structures. *Foxa2* is expressed in the anterior mesoderm, the notochord (a derivative of the axial mesoderm), and the floor plate (Klingensmith, et al. 1999). The expression pattern of *Foxa2* was largely unchanged in *FLRT3*$^{-/-}$ embryos, especially in the notochord (Figure 18 A-D). Similarly, the expression pattern of a second notochord marker gene in *FLRT3*$^{-/-}$ embryos, sonic hedgehog (Shh), was indistinguishable from that in the wild type (data not shown). Furthermore, the expression of *Meox1*, a

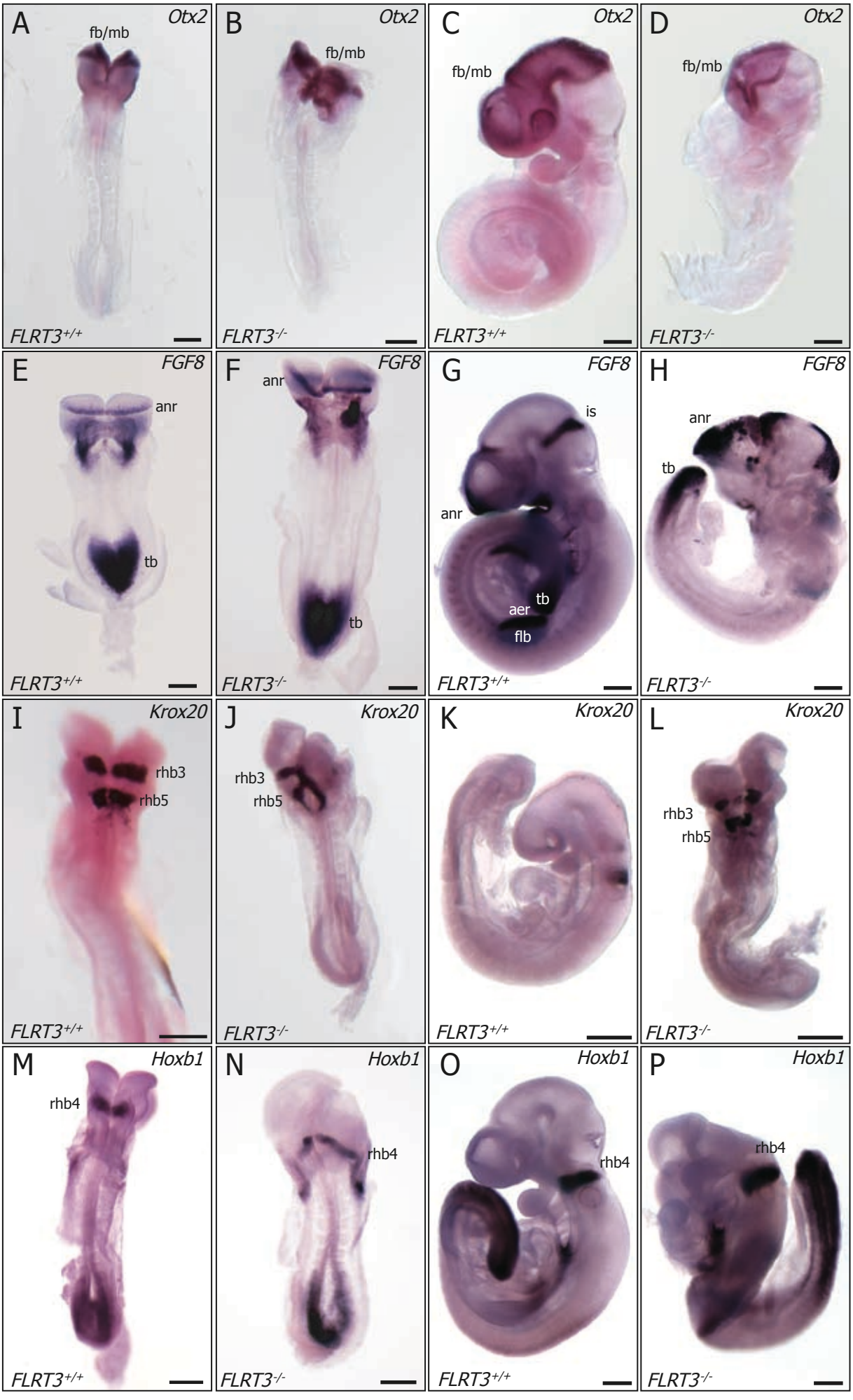
A
Otx2
fb/mb
FLRT3+/+
B
Otx2
fb/mb
FLRT3-/-
C
Otx2
fb/mb
FLRT3+/+
D
Otx2
fb/mb
FLRT3-/-
E
FGF8
anr
tb
FLRT3+/+
F
FGF8
anr
tb
FLRT3-/-
G
FGF8
is
anr
tb
aer
flb
FLRT3+/+
H
FGF8
anr
tb
FLRT3-/-
I
Krox20
rhb3
rhb5
FLRT3+/+
J
Krox20
rhb3
rhb5
FLRT3-/-
K
Krox20
FLRT3+/+
L
Krox20
rhb3
rhb5
FLRT3-/-
M
Hoxb1
rhb4
FLRT3+/+
N
Hoxb1
rhb4
FLRT3-/-
O
Hoxb1
rhb4
FLRT3+/+
P
Hoxb1
rhb4
FLRT3-/-

marker for the (paraxial) mesoderm-derived somites (Candia, et al. 1992) in *FLRT3*$^{-/-}$ embryos was analyzed. Wild type and mutant embryos exhibited a clearly defined pattern of expression indicating a proper formation of somites (Figure 18 E-H). Also, the number of somites in stage-matched embryos did not differ between wild type and mutant embryos. In summary, this suggests that the production of mesoderm in *FLRT3*$^{-/-}$ embryos was not impaired.

To investigate neural crest cell (NCC) behaviour, *Sox10* a marker for NCC induction and migration was used. Neural crest cells contribute to many structures in the mouse including the branchial arches. At E8.5 the pattern of Sox10 expression in *FLRT3*$^{-/-}$ embryos was largely similar to that seen in wild type embryos. Interestingly, at E9.5 the number of Sox10 positive cells seemed to be strongly reduced, although the overall location of the cells appeared to be preserved (Figure 18 I-L). Overall, it became clear that *FLRT3*$^{-/-}$ embryos did not exhibit a general patterning impairment that could account for the observed phenotypes at embryonic days 8.5 to 10.5. Moreover, *FLRT3*$^{-/-}$ embryos do not suffer from axis truncations or dorsalization as previously reported in *Xenopus* embryos and other mouse mutations.

Figure 17 Anterior patterning is not impaired in FLRT3$^{-/-}$ embryos
(A, C) *Otx2* was expressed in the prospective fore- and midbrain of wt E8.5 and E9.5 embryos, as shown by WISH. (B, D) In *FLRT3*$^{-/-}$ embryos, expression of *Otx2* was detected by WISH. The mutant embryo shown in (D) however, displayed massive malformations in the head region with unfused head folds. Therefore the expression area of *Otx2* were reduced. (E, G) The expression of *FGF8* was detected in wt embryos using WISH. (E) At E8.0, *FGF8* was expressed in the tail bud, the foregut endoderm and the anr, the anterior most region of the forebrain. (G) At E9.5, anterior expression persisted and expression at the isthmic boundary, as well as at the aer, was detected. (F, H) *FLRT3*$^{-/-}$ embryos showed a largely similar pattern of *FGF8* expression, especially in less affected E8.0 embryos, where clear anr expression was detected (F). At E9.5 (H), severe malformations made the interpretation more complex. Nevertheless, very anterior expression, as well as more caudal expression in the distorted anterior region, was detected. (I, K) In wt E8.5 and E9.5 embryos, *Krox20* expression was detected in rhombomeres 3 and 5, subdividing the hindbrain region. (J, L) *Krox20* expression was evident in rhombomeres 3 and 5 in *FLRT3*$^{-/-}$ embryos. Due to the anterior malformations, the expression appeared to be shifted and sometimes a little distorted, especially in older, more severely affected mutants (L). (M, O) *Hoxb1* served as another marker for hindbrain development. Expression was detected in E8.5 and E9.5 embryos in rhombomere 4 of the developing hindbrain. (N, P) Also in *FLRT3*$^{-/-}$ embryos, *Hoxb1* expression was detected in rhombomere 4, even in severely affected embryos.
Scale bars in A, B, E, F, I, J, M, N are 200 µm and in C, D, G, H, K, L, O, P are 500 µm.
Abbreviations: aer, anterior ectodermal ridge; anr, anterior neural ridge; fb, forebrain, flb, forelimb bud; is, isthmic boundary; mb midbrain; rhb, rhombomere; tb tail bud

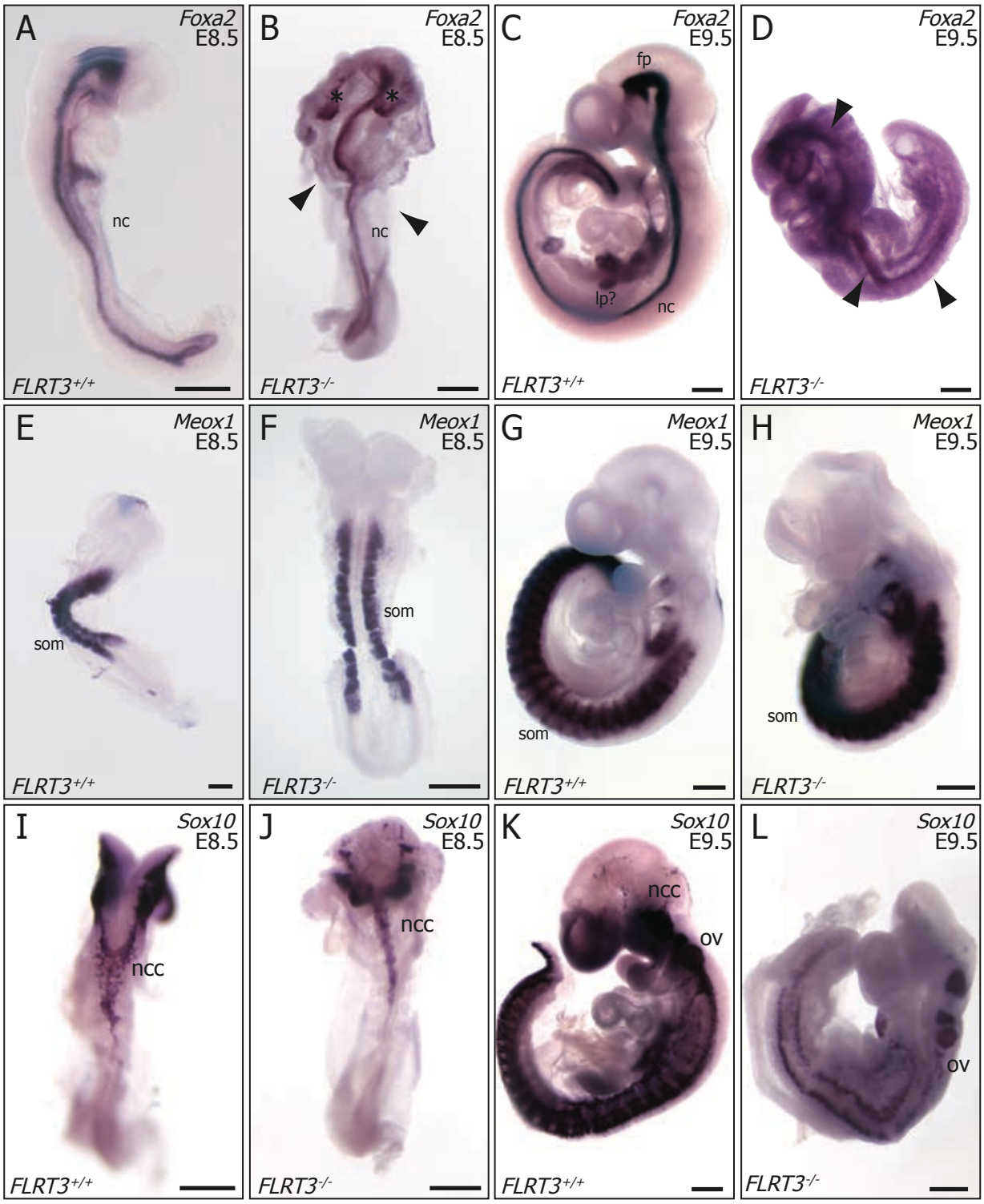

Figure 18 Analysis of mesoderm derivatives and neural crest cells in FLRT3$^{-/-}$ embryos

(A, C) *Foxa2* expression was detected in wt embryos in derivatives of mesoderm/DE such as the notochord or the prechordal plate. Moreover, the floor plate of the midbrain showed *Foxa2* expression at E8.5 and E9.5. (B, D) In *FLRT3*$^{-/-}$ embryos, the expression of *Foxa2* was detected by WISH at E8.5 and E9.5. (B) Even in a severely affected embryo, showing defects in ventral closure (arrows), *Foxa2* expression in the notochord was detected. Ectopically localized *Foxa2* expression (asterisks) may represent the floor plate that was misplaced due to the unfused head folds. (E, G) In the somites of wt embryos at E8.5 and E9.5, the expression of *Meox1* was detected using WISH. (F, H) Similarly, in *FLRT3*$^{-/-}$ embryos, essentially undisturbed expression of *Meox1* was evident at E8.5 and E9.5. (I, K) The expression of *Sox10*, which labels neural crest cells, was detected in wt embryos at E8.5 and E9.5 using WISH. While at E8.5 only a limited number of neural crest cells were seen, the number of *Sox10* positive cells increased dramatically at E9.5. Especially in somites, strong *Sox10* expression was seen.

2.2.3. Discontinuous endoderm in head fold stage FLRT3$^{-/-}$ embryos

To further describe the *FLRT3*$^{-/-}$ phenotype, it was necessary to investigate earlier stages of embryonic development. High resolution scanning electron microscopy had already proven to be a valuable tool in characterizing the mutant phenotype. Therefore, head fold stage (E7.5) embryos were analyzed using SEM. In a frontal view of a wild type, head fold stage embryo, two cell types could be easily distinguished (Figure 19 A). Small round cells with clear outlines and the surface covered by microvilli (Ishikawa 1986) represented extraembryonic visceral endoderm cells (Figure 19 A, F). These cells formed a columnar epithelium, which, at this stage, covered mainly the extraembryonic region. The second type of cell displayed less clear outlines with a smoother surface (Figure 19 A, E). These larger cells were embryonic definitive endoderm cells, which formed a squamous epithelium (Hashimoto and Nakatsuji 1989). Extraembryonic and embryonic regions were clearly separated by the circumferential groove (outlined in Figure 19 A). In the mutant case, both cell types, visceral and definitive endoderm, were present. However in *FLRT3*$^{-/-}$ embryos the endodermal cell layer appeared discontinuous with one, or rarely two holes formed in the endoderm at the border between the extraembryonic and embryonic regions (Figure 19 B-D). The holes were either deep or sometimes resembled more shallow pits. Interestingly, those holes or pits uncovered a third, as yet unseen cell type. These cells were small and displayed a regular shape, with a smooth surface (Figure 19 G, H). Depending on the size of the hole, these new cells mostly originated from the hole and seemed restricted to the area close to the hole (Figure 19 B, C, G). In more severe cases however, these cells were seen in higher numbers and at a greater distance from the hole (Figure 19 D, H). The shape and the origin of this third cell type seen in the SEM images suggests that these cells belonged to the epiblast, a pseudo stratified epithelium.

(J, K) Already at E8.5, the number of *Sox10* positive cells in *FLRT3*$^{-/-}$ seemed reduced. However, at E9.5 a strong reduction in the number of *Sox10* positive cells in *FLRT3*$^{-/-}$ compared to wt embryos was evident.
Scale bars in panels A, B, E, F, I, J are 200 µm and in panels C, D, G, H, K, L are 500 µm.
Abbreviations: fp, floor plate; nc, notochord; ncc, neural crest cells; ov, otic vesicle; som, somites.

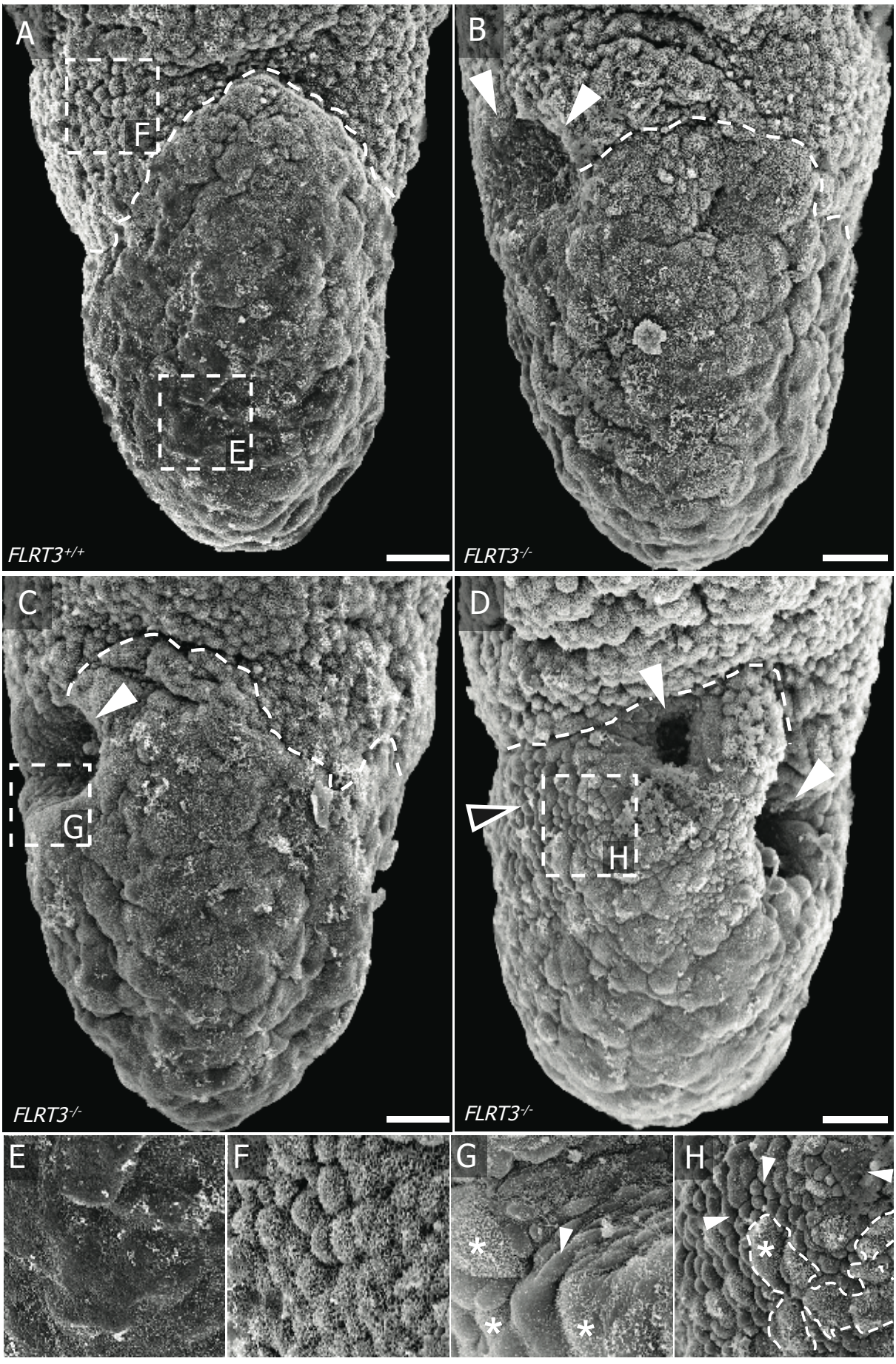
A
F
E
FLRT3+/+
B
FLRT3-/-
C
G
FLRT3-/-
D
H
FLRT3-/-
E
F
G
H

Figure 19 SEM analysis revealed holes in the endoderm of FLRT3$^{-/-}$ embryos
(A-H) SEM images of head fold stage mouse embryos. (A) A frontal view of a wt embryo clearly showed the different cell types on the surface of the embryonic (distal) and the extraembryonic region (proximal). The dashed line indicates the circumferential groove, the border between embryonic and extraembryonic region. (B-D) In a frontal view of FLRT3$^{-/-}$ embryos, holes in the endoderm layer were discovered (white arrowheads). The appearance of these holes varied from a shallow pit (B) to a much deep hole, reaching into the amniotic cavity of the embryo (D). In addition to the holes, embryos exhibited an ectopic cell type on their surface (white outlined arrow). (E) In a high magnification image of the region indicated in (A), DE cells with a smooth surface were visualized. (F) Cells of the VE in the region indicated in A, viewed in higher magnification, displayed a rough surface, covered with microvilli and a clear round outline. (G) A magnified view of a region at the rim of the hole in embryo shown in panel C revealed an as yet unseen type of cells, which is present on the surface of the hole. These cells were apparently growing from the inside of the embryo outwards (arrowheads) and have a smooth surface with clear outlines. Endoderm cells are present at the rim of the hole (asterisks). (H) Similar cells as shown in (G) were found in the proximity of the hole in embryo (D, arrowheads). These cells were found at greater distance from the hole and intermingled in patches with DE cells (dashed line and asterisk).
Scale bars are 200 µm.

2.2.4. Histological analysis reveals the breakage and discontinuity of the anterior visceral/definitive endoderm in FLRT3$^{-/-}$ embryos.

Since the SEM analysis has shown an ectopically occurring cell type on the surface of *FLRT3*$^{-/-}$ embryos, which originated from holes in the endoderm, the identity of those cells needed to be clarified. In order to determine the fate of the endoderm, WISH using the Wnt-signalling inhibitor *Dkk1* as a marker for anterior visceral and definitive endoderm was performed. In the wild type case, anterior endoderm cells were *Dkk1* positive (Figure 20 A). Although the expression of *Dkk1* is somewhat variable, *Dkk1* positive cells populated a comparably large area in the anterior endoderm. Histological sections of embryos after *Dkk1* whole mount *in situ* hybridization showed, that the endoderm formed a continuous epithelium at the anterior of the embryo (Figure 20 B). In *FLRT3*$^{-/-}$ embryos however, a clear discontinuity in *Dkk1* expression was visible (Figure 20 C). Taking a closer look at the whole mount preparations, it became clear that the *Dkk1* free region represented a hole in the endoderm. This resembled what was seen in the scanning electron microscopy images (Figure 20 C, dashed white line). Histological sections revealed that the endoderm, marked by *Dkk1* expression, was discontinuous. Cells, most likely originating from the epiblast, disrupted the endoderm epithelium. These endoderm substituting cells were clearly *Dkk1* negative and appeared to have epithelial properties (Figure 20 D). In early head fold stage embryos the discontinuity of the endoderm seemed was more pronounced. The ectopically positioned epiblast cells protruded outwards and substituted endodermal cells over a large surface. Interestingly, the ectopic epiblast cells seemed to retain the shape and structure of a pseudo-stratified epithelium (Figure 20 F).

Figure 20 Epiblast replaces the endoderm of FLRT3$^{-/-}$ embryos
(A) Frontal and lateral views of a wt LS stage embryo after WISH for *Dkk1* showed the expression of *Dkk1* in the entire anterior endoderm region. (B) Cryosection at the level indicated in (A) confirmed that the endoderm formed a continuous layer that is *Dkk1* positive in the anterior of the embryo. The dashed lines in black and white outline the ectoderm and the endoderm, respectively. The mesoderm occupied the space between endoderm and epiblast and already reaches the anterior of the embryo. (C) At LS stage, *FLRT3*$^{-/-}$ embryos displayed a discontinuity in the *Dkk1* expression in the lateral anterior endoderm, visualized by WISH, which was reminiscent of the SEM images (white dashed line in frontal and lateral view). (D) Cryosection of the embryo shown in (C) at the indicated level. The discontinuous *Dkk1 in situ* staining was a result of a discontinuous endoderm (VE and DE) layer in the anterior of the embryo. The anterior epiblast has protruded out of its usual territory and replaced the endoderm. (E) A similar situation was seen in early head fold stage embryos after WISH for *Dkk1*. Although *Dkk1*

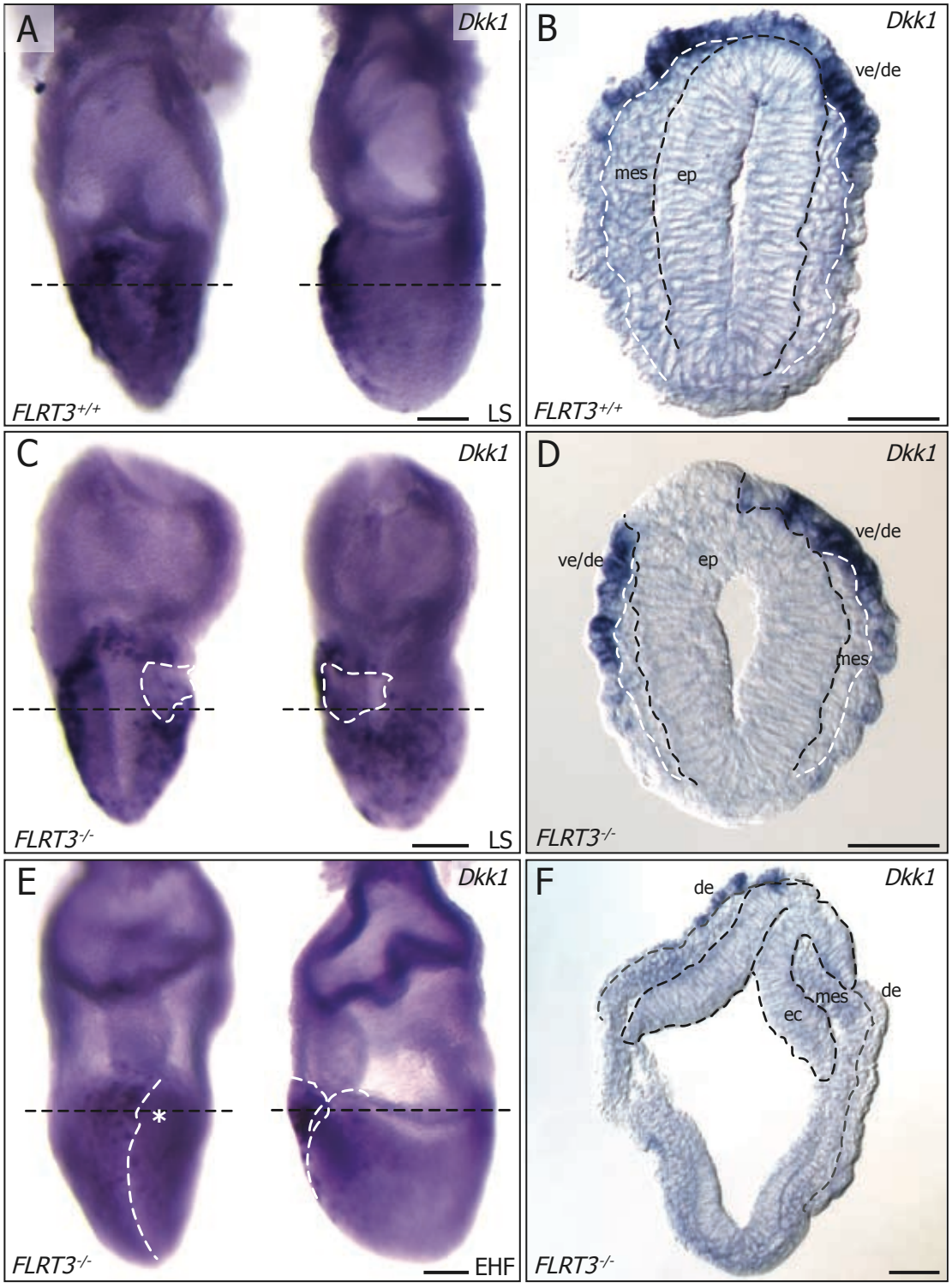

expression was not as strong anymore, no staining for *Dkk1* could be detected on the left side of the embryo close to its proximal end (asterisk). In addition, the midline of the extruding head folds was bent, as indicated by the white dashed line. (F) A cryosection of the embryo shown in (E) at the level indicated by the black dashed line uncovered a clear protrusion of the ectoderm in the anterior of the embryo, replacing the DE at this region.
Scale bars in A, C, E are 100 µm and in panels B, D, F 50 µm.
Abbreviations: de, definitive endoderm; ec, ectoderm; ep, epiblast; mes, mesoderm; ve, visceral endoderm

2.2.5. FLRT3$^{-/-}$ embryos show no difference in proliferation or apoptosis

Previous publications have suggested a role for FLRT3 in FGFR signalling (Böttcher, et al. 2004). It was shown that FLRT3 is able to interact with FGFR1 in *in vitro* systems and in *Xenopus* embryos. In mouse embryos at streak stage, both *FGFR1* and *FGFR2* expression were detected by *in situ* hybridization. *FGFR1* was found mainly in the epiblast in early streak stages and was restricted to the posterior region in late streak to early head fold stage embryos. *FGFR2* however, was mostly expressed in the chorion and anterior endoderm of early streak to late stages. FLRT3 could, possibly through an interaction with FGFR signalling, affect cell proliferation or survival. Therefore, the rate of proliferation in ES to MS stage and EHF to LHF stage embryos was determined using phosphorylated histone H3 (PHH3) as a marker for mitotic cells. The mitotic index was determined by counting the number of PHH3 positive cells in histological sections and comparing this number to the total number of cells, assessed by counting stained nuclei (Figure 22 A-F). Determination of the mitotic index was achieved individually for

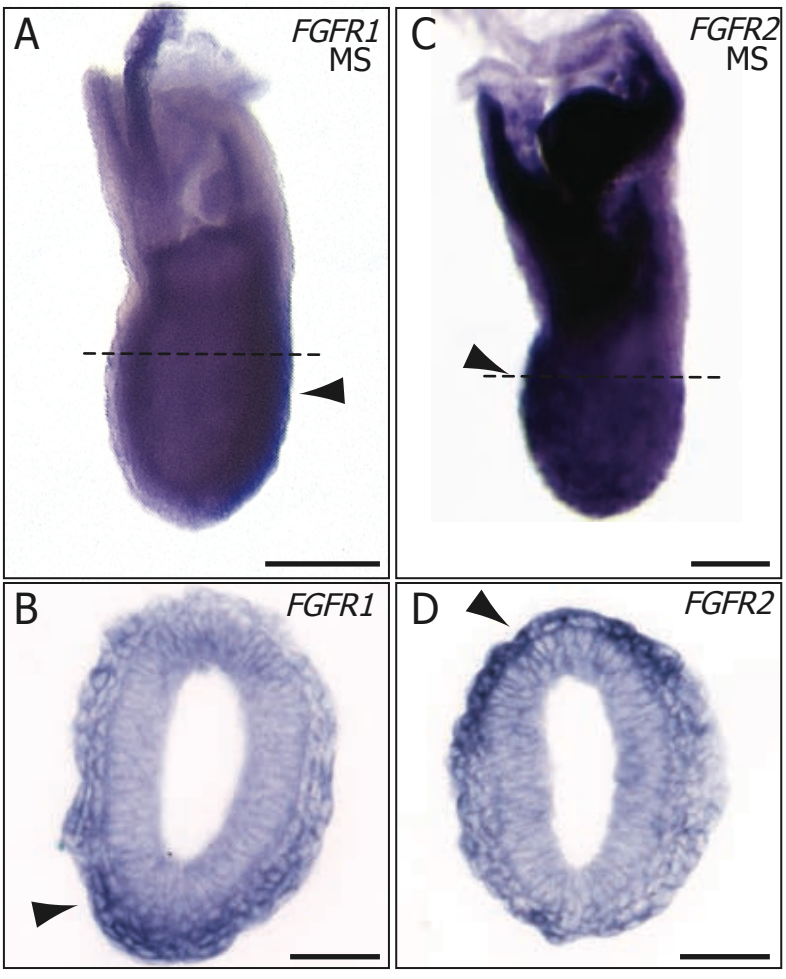

Figure 21 FGFR1 is expressed in the posterior and FGFR2 in the anterior region of MS mouse embryos
(A) *FGFR1* expression at the MS stage visualized by WISH. Expression of *FGFR1* was detected in the posterior region of the embryo, at the region of the PS (arrowhead).
(B) Cryosection at the level indicated by the dashed line in (A) showed expression of *FGFR1*, mainly in the cells leaving the PS (arrowhead).
(C) *In situ* hybridization for *FGFR2* revealed strong expression in the anterior endoderm (arrowhead) and in the extraembryonic chorion region. (D) In a cryosection of the indicated region in (C), strong expression of *FGFR2* in the anterior endoderm was evident (arrowhead).
Scale bars are 100 µm for panels A and C and 50 µm for panels B and D.

each germ layer, as they were easily distinguishable. The counting procedure was done blind with regard to the genotype of the respective embryos.

In ES to MS stage wild type embryos, the mitotic index determined for mesoderm and endoderm (visceral and definitive) was lower than that in the epiblast. *FLRT3*$^{-/-}$ stage-matched embryos however, displayed similar mitotic indices as in wt embryos. In later stage embryos, the mitotic indices of the three germ layers were determined to be 4-5.5% depending on the germ layer in wild type embryos. The mitotic index of *FLRT3*$^{-/-}$ embryos did not differ significantly from their wt littermates. Taken together, these results show that the lack of FLRT3 had no influence on cell proliferation in ES to LHF stage embryos.

Next, we wanted to know if the loss of FLRT3 could influence the survival of endoderm cells in mutant embryos. To test this possibility, antibody staining was performed using activated caspase 3 (casp-3) as a marker for apoptotic cells. No apoptotic index could be determined since the number of apoptotic cells in wild type early streak to head fold stage embryos was very low. As with the wild type embryos, very few apoptotic cells were detected in mutant embryos. This suggests that survival of endoderm cells in *FLRT3*$^{-/-}$ embryos was not altered (Figure 22 I-K).

In Summary, this suggests that neither a decrease in proliferation nor an increase in programmed cell death has resulted in a reduction in endoderm cell number that could be responsible for the endodermal discontinuities. Also the epiblast cells do not show increased proliferation that could lead to the holes in the endoderm of *FLRT3*$^{-/-}$ embryos. Therefore other mechanisms must operate to generate the endodermal defect that was observed. In deed, careful analysis of the BM in *FLRT3*$^{-/-}$ embryos has revealed, that a breakdown of the anterior BM precedes the appearance of the holes (Egea, et al. 2008). This was reminiscent of processes occurring in the PS of wt embryos.

Figure 22 No alterations of proliferation or apoptosis as a consequence of the loss of FLRT3 were evident

(A-F) Cryosections of MS stage control (A-C) and *FLRT3*$^{-/-}$ (D-F) embryos after phospho-histone H3 (PHH3) immunostaining were used to determine the mitotic index of the respective embryos. To determine the total number of cells, sections were counterstained using DAPI (B, C and E, F). (G, H) To determine the mitotic index, the number of PHH3 positive cells was divided by the total number of cells. The mitotic index was compiled individually for each germ layer in MS (G) and HF stage embryos (H). The graphs shown were the mean of five mutant and three control embryos for MS and four control and four wild type embryos for HF stage embryos. No significant differences were seen ($p>0.15$; Student's *t-test*). Error bars represent the standard deviation. (I-K) Using cryosections immunostained for activated caspase 3 (casp3) and counterstained with DAPI, a quantifiable amount of apoptotic cells was not seen. Therefore no apoptotic index was determined. The dotted line outlines the epiblast. In panels (I-K), representative images of control embryos can be seen. Note the casp3 positive cells in the decidual tissue surrounding the embryo.
Scale bars represent 20 µm.
Abbreviations: ec, ectoderm; en, endoderm; mes, mesoderm; n.s., non significant

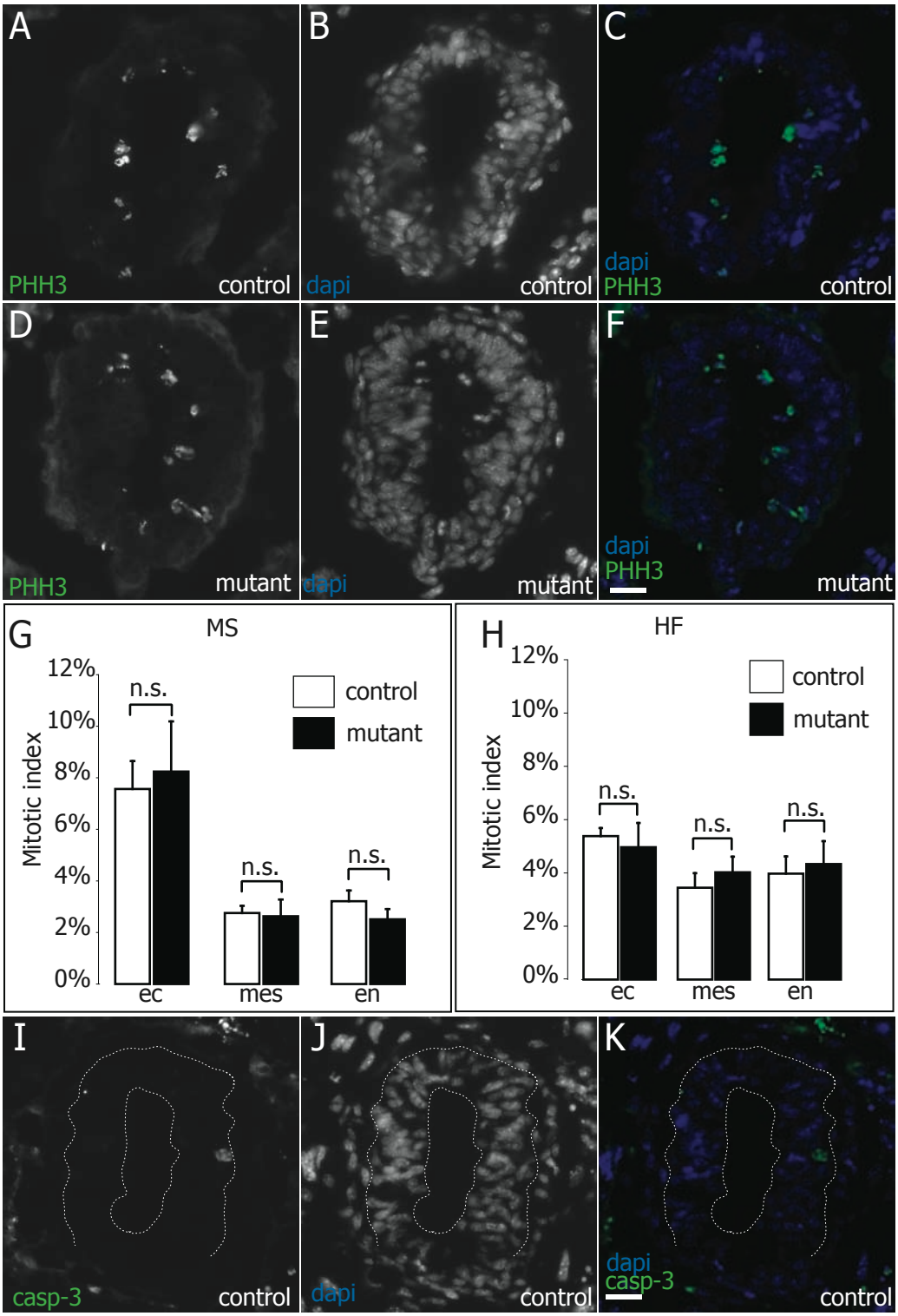
A
PHH3
control
B
dapi
control
C
dapi
PHH3
control
D
PHH3
mutant
E
dapi
mutant
F
dapi
PHH3
mutant
G
MS
Mitotic index
12%
10%
8%
6%
4%
2%
0%
n.s.
n.s.
n.s.
control
mutant
ec
mes
en
H
HF
Mitotic index
12%
10%
8%
6%
4%
2%
0%
n.s.
n.s.
n.s.
control
mutant
ec
mes
en
I
casp-3
control
J
dapi
control
K
dapi
casp-3
control

2.2.6. Ectopic induction of mesoderm markers

The generation of mesoderm is, amongst others, one of the key events during gastrulation. Epiblast cells in the primitive streak begin expressing mesodermal genes, such as *Bra/T*. This T-box transcription factor is at later stages used as a marker for the notochord, a descendent of the axial mesoderm (Figure 23 A). During the analysis of anterior patterning markers, *Bra/T* was used to ensure the integrity of the notochord. Interestingly, ectopic expression of *Bra/T* was detected in several *FLRT3*$^{-/-}$ embryos at E8.5 and E9.5 (Figure 23). Further analysis of the ectopic expression revealed that *Bra/T* expression was seen in areas of ectopically localized epithelia (Figure 23 C, D). These ectopic epithelia were very similar to the ectopically localized epiblast seen in head fold stage embryos (Figure 20 D, F). To verify this observation, whole mount in situ hybridization for *Bra/T* was performed using EHF to LHF stage embryos. In wild type embryos, strong *Bra/T* expression was observed in the epiblast and the newly formed mesoderm around the PS region and anterior at the prechordal plate (Figure 24 A, B). In the *FLRT3*$^{-/-}$ embryos however, ectopic expression of *Bra/T* was very often detected at the distal portion of ectopic ectoderm (Figure 24 E-H). Although not every *FLRT3*$^{-/-}$ embryo showed this ectopic expression (Figure 24 C, D), the occurrence of ectopic *Bra/T* expression was high. Six out of eight *FLRT3*$^{-/-}$ embryos with ectopic ectoderm, from a total of ten *FLRT3*$^{-/-}$ embryos analysed; showed ectopic expression of *Bra/T*. Interestingly, ectopic expression was always localized to the distal regions of the ectopic ectoderm.

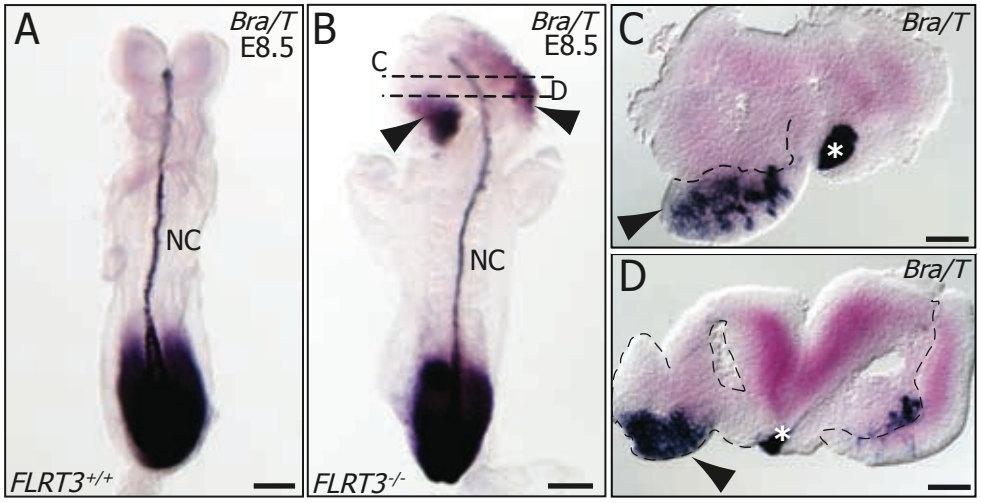

Figure 23 Bra/T is ectopically expressed in FLRT3$^{-/-}$ embryos at E8.5
(A, B) Whole mount *in situ* hybridization for *Bra/T* using E8.5 wt (A) or *FLRT3*$^{-/-}$ (B) embryos. While in the wt embryo *Bra/T* expression is strong only in the tail bud and the notochord, in the *FLRT3*$^{-/-}$ embryo additional ectopic expression of *Bra/T* was evident in the head folds (arrowheads). (C, D) Trisections of the embryo and at the levels indicated in (B), showed strong expression of *Bra/T* in an epithelial structure (arrowhead) continuous with the neuroectoderm, outlined with the dashed line. Note the strong expression in the notochord (asterisks).
Scale bars represent 200 µm in panels A and B and 50 µm in panels C and D.

The upregulation of *Bra/T* in epiblast cells and the migration of Bra/T positive mesoderm cells are hallmarks of gastrulation. But of course *Bra/T* is not the only factor necessary for mesoderm induction; other important mesoderm markers include *FGF8* (Sun, et al. 1999), and eomesodermin (*Eomes*). To investigate the idea that ectopic induction of mesoderm could be caused by the loss of FLRT3, whole mount *in situ* hybridizations were performed using *FGF8* and *Eomes*. In wild type LHF stage embryos, *FGF8* expression is restricted to the PS region and to regions in the head fold mesoderm, as seen in histological sections (Figure 25 A). In four out of eight *FLRT3*$^{-/-}$ embryos however, *FGF8* expression was also detected in ectopic ectoderm (epiblast) (Figure 25 B, C). Similarly to ectopic *Bra/T* expression, *FGF8* expressing cells were localized to more distal regions of the ectopic ectoderm (Figure 25 C). This ectopic expression of *Bra/T* and *FGF8* suggested that cells in the anterior epiblast acquire mesodermal features, similar to what takes place in the primitive streak. The t-box transcription factor *Eomes* is a very early gene in mesoderm specification. It is only active in the primitive streak region and in migrating mesoderm cells for a short period of time. At mid-to late head fold stage, *Eomes* expression was already restricted to the extraembryonic chorion and was no longer active in the embryonic region (Ciruna and Rossant 1999). Wild type embryos at head fold stage showed expression of *Eomes* in the chorion region (Figure 25 D). However, in *FLRT3*$^{-/-}$ embryos at head fold stage, *Eomes* expression was detectable in the ectopic ectoderm of all mutant embryos analyzed (Figure 25 E, H, I; n=2 mutant embryos). Also the expression of *Eomes* was localized to the distal region of the ectopic ectoderm.

Generation of mesoderm also involves the delamination of newly specified mesodermal cells at the primitive streak. Hence, the cells need to undergo an epithelial-mesenchymal transition. It has recently been shown that eomes is an important regulator of gastrulation EMT (Arnold, et al. 2008). To verify whether an EMT process is initiated in ectopic epiblast cells of *FLRT3*$^{-/-}$ embryos, the expression of a second general EMT marker,

Figure 24 Loss of FLRT3 leads to expression of Bra/T in the ectopic ectoderm
Panels (A, C, E, G) show frontal and lateral views of wt (A) and mutant (C, E, G) embryos at LS to LFH stages after WISH using a riboprobe for *Bra/T*. In the wt embryo, *Bra/T* was strongly expressed in the PS as well as in the prechordal plate mesoderm in the anterior embryo. Analysis of cryosections as shown in (B) at the indicated level confirmed this observation. (C) In LS stages, a hole in the endoderm was already present that could be seen in the whole mount preparation (white dashed line). (D) In a cryosection at the indicated level (dashed line in C), the protrusion of the ectoderm was evident. However, no expression of *Bra/T* was detected on the ectopic tissue (asterisk). Notably, the protrusion of the ectoderm was rather mild, representing an early stage of this phenotype. (E, G) In the embryos at HF stage, ectopic expression of *Bra/T* was evident in the whole mount preparation (arrowheads). Histological sections revealed that the expression of *Bra/T* was localized to the patches of ectopic ectoderm tissue, replacing the endoderm (arrowheads). Please note that *Bra/T* expression was localized at the frontal tips of the ectopic ectoderm.
Scale bars in panels A, C, D, E represent 200 µm and in panels B,D,F,H represent 50 µm.
Abbreviations: ec, ectoderm; en, endoderm; mes, mesoderm; ps, primitive streak

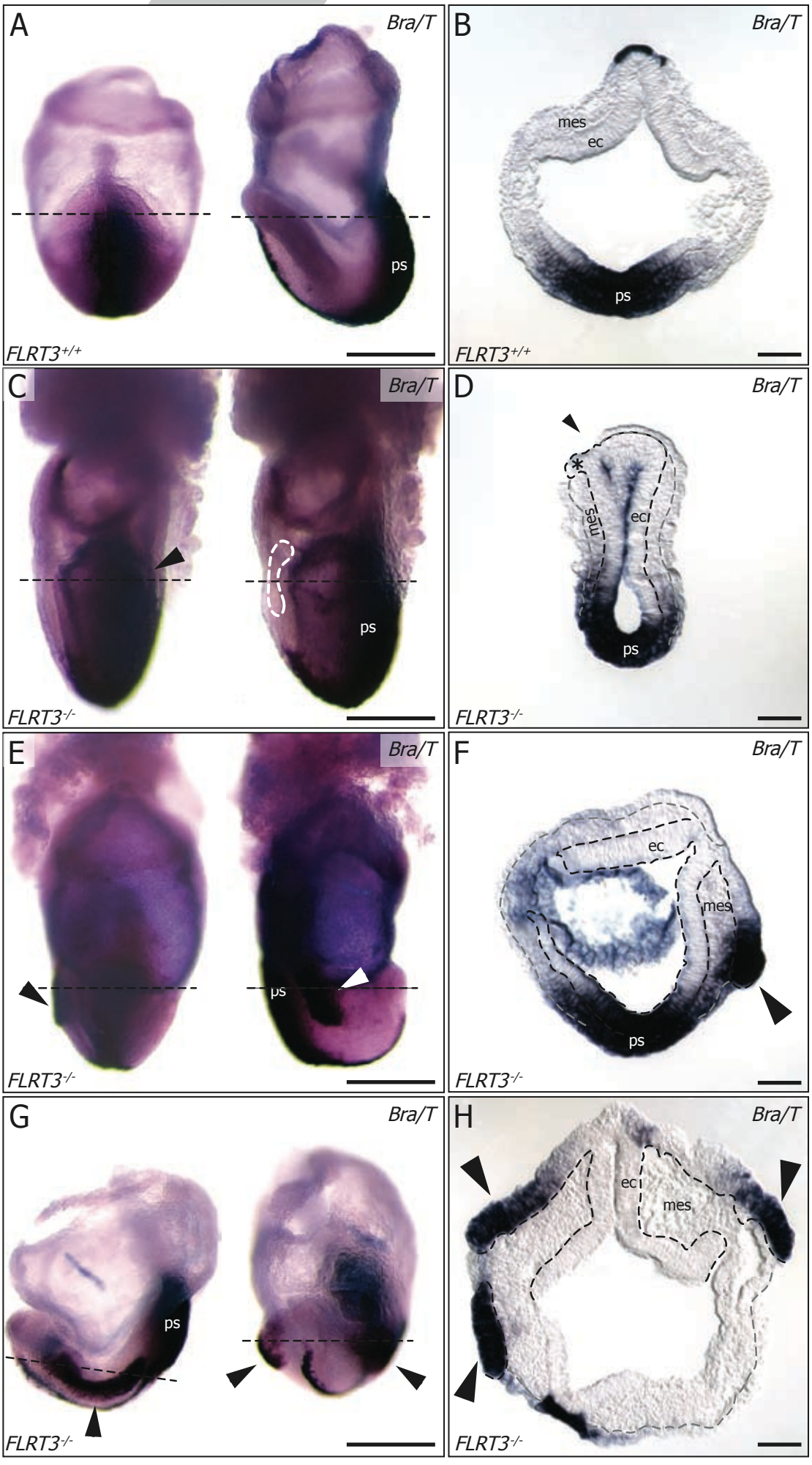
A
Bra/T
ps
FLRT3+/+
B
Bra/T
mes
ec
ps
FLRT3+/+
C
Bra/T
ps
FLRT3-/-
D
Bra/T
mes
ec
ps
FLRT3-/-
E
Bra/T
ps
FLRT3-/-
F
Bra/T
ec
mes
ps
FLRT3-/-
G
Bra/T
ps
FLRT3-/-
H
Bra/T
ec
mes
FLRT3-/-

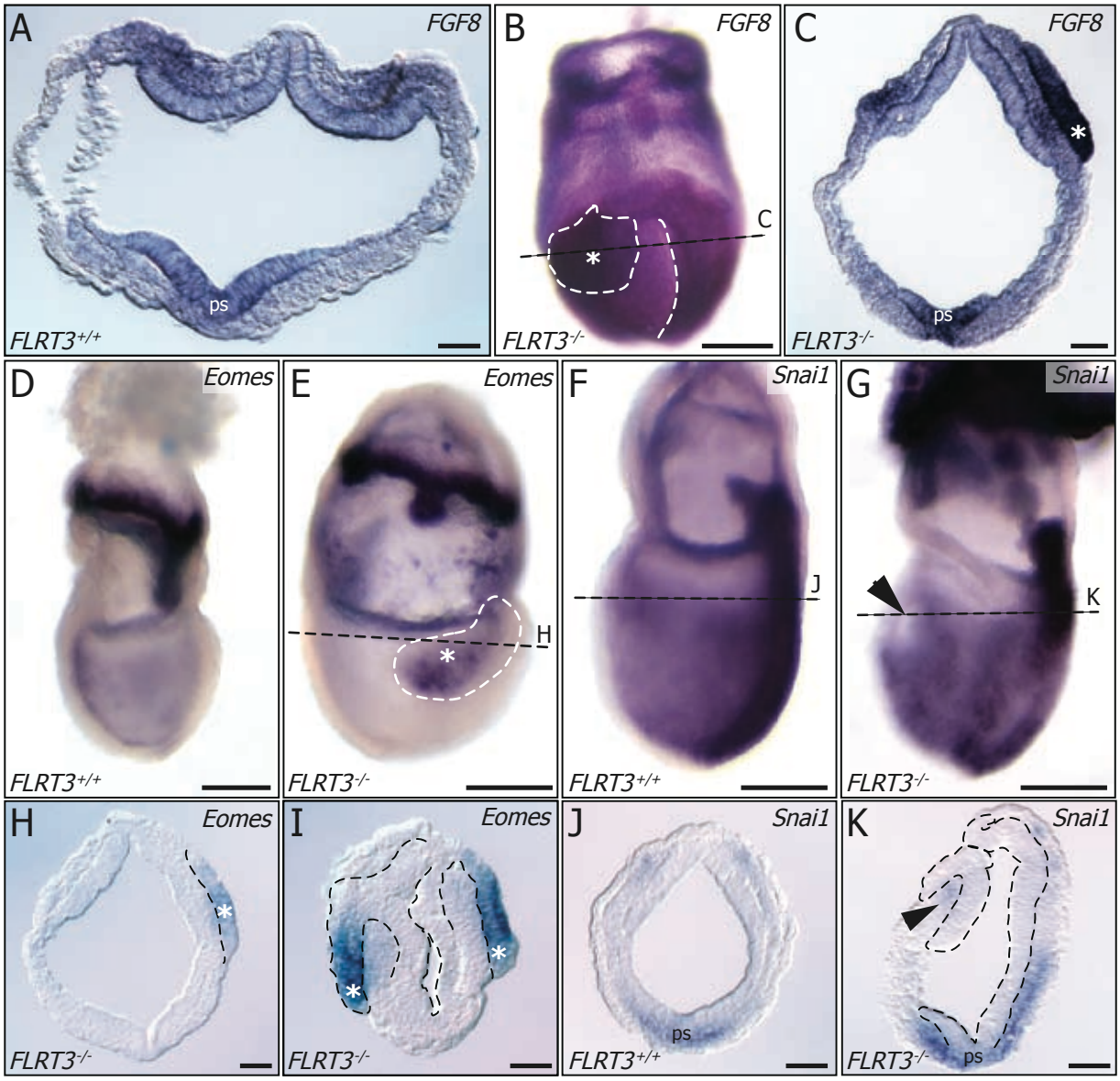

Figure 25 Ectopic induction of mesoderm markers occurs in FLRT3$^{-/-}$ embryos

(A) Cryosectioning of a wt LHF stage embryo after WISH for *FGF8*, showed *FGF8* expression in the region of the primitive streak and in the anterior head fold mesoderm. (B) After *FGF8* WISH, ectopic expression of *FGF8* in *FLRT3*$^{-/-}$ whole mount embryos was evident (asterisk). The ectopic expression was localized to a region of ectopic ectoderm on the surface of the embryo (dashed white line). (C) Cryosectioning at the level indicated by the dashed line in (B) confirmed that *FGF8* expression, in addition to the PS and the head fold mesoderm was evident in the ectopic ectoderm, present on the surface of the embryo (asterisk). Remarkably, *FGF8* was, similar to *Bra/T*, mainly expressed at the frontal tip of the ectopic ectoderm. (D, E) *Eomes* expression was visualized by WISH using LS to EHF stage embryos. In the wt embryo, *Eomes* expression was already restricted to the chorion (D), whereas in the mutant embryo, ectopic expression of *Eomes* was localized to a stretch of ectopic ectoderm (white dashed line in E). Embryos were oriented with the anterior to the right. (F, G) The expression of the EMT gene *Snai1* in HF stage embryos was mainly restricted to the PS region, both in wt (F) and mutant embryos (G). Despite the visible hole in the endoderm (arrowhead), no ectopic expression of *Snai1* was detected. Embryos were oriented with the anterior to the left. (H, I) Cryosections of mutant embryos after WISH for *Eomes*, showed expression of *Eomes* (asterisks) in the ectopically localized ectoderm (outlined by the dashed line). In panel (H), a section at the indicated region in (E) is shown, whereas the section in (I) is an example from a different embryo. (J) Cryosectioning of a LS wt embryo, showed *Snai1* expression in the PS region and in the migrating mesoderm cells. (K) Similarly, in the mutant embryo, cryosections showed *Snai1* expression was restricted to the PS and migrating mesoderm cells. No expression of *Snai1* was detected in the ectopic ectoderm (outlined by the dashed line) but rather in the mesoderm. All histological sections are oriented with anterior to the top and posterior to the bottom.
Scale bars in panels A, C, H, I, J, K represent 50 µm and in panels B, D, E, F, G 200 µm.

Snai1 (Nieto 2002) was assessed. *Snai1* expression was detected in epiblast cells in the PS region of EHF stage embryos and nascent mesoderm cells migrating towards anterior (Figure 25 F, J; n=4 wild type embryos). In *FLRT3*$^{-/-}$ embryos, expression of *Snai1* in the PS was comparable to wild type embryos. Surprisingly, no ectopic expression of *Snai1* was found in any of the four mutant embryos analyzed (Figure 25 G, K). All together, this data suggests that the loss of FLRT3 in the anterior endoderm causes premature and ectopic induction of mesoderm, but clearly the formation of real mesoderm was not fully completed, as was shown by the missing expression of *Snai1* and the epithelial structure of the ectopic cells.

2.2.7. The signalling functions of the AVE are not affected in FLRT3$^{-/-}$ embryos

Since the AVE is known to have organizer-like properties in gastrulating embryos, a disturbance in the interplay of signalling factors can cause severe defects in axis formation, gastrulation and mesoderm development. To investigate the signalling properties in *FLRT3*$^{-/-}$ embryos, WISH studies were carried out, using genes important in Wnt and TGF-beta signalling as markers. These signalling systems are important for early anterior-posterior patterning and axis formation. The AVE expresses inhibitors such as *Dkk1* for Wnt signalling, and *Cer1* and *Lefty1* for TGF-beta signalling. In early streak stage embryos, the inhibitor for TGF-beta signalling *Cer1* was strongly expressed in a subpopulation of AVE cells (n=9 wt embryos) (Figure 26 A). As expression of *Cer1* is very dynamic at this stage, it expanded more laterally when embryos proceeded from ES to MS or LS stage. Similar expression patterns were observed in *FLRT3*$^{-/-}$ embryos (n=4 mutant embryos), where *Cer1* was strongly expressed in the AVE and expanded its expression domains more laterally at MS to LS stage (Figure 26 and data not shown). *Lefty1*, the second inhibitor of TGF-beta signals was also expressed in the AVE in wild type embryos at ES to MS stage (n=5 embryos). Its expression was less dynamic but the riboprobe used also detected a second homolog, *Lefty2*, which was not expressed at ES stage. At MS to LS stage, *Lefty2* was expressed in a horseshoe like fashion in the primitive streak region. In *FLRT3*$^{-/-}$ embryos, no alteration of the expression pattern of *Lefty1* was detected (n=7 embryos) (Figure 26 B, G). The Wnt inhibitor *Dkk1* was strongly expressed in the AVE of ES to LS stage embryos (n=3 embryos). In *FLRT3*$^{-/-}$ embryos the expression pattern of *Dkk1* was indistinguishable from that in wild type embryos (n=3 embryos) (Figure 26 C, H). This is consistent with the observation that in head fold stage embryos, except for the holes, the expression of *Dkk1* was similar in wild type and mutant embryos (Figure 20 A, C).

Although the inhibitors of Wnt and TGF-beta signalling were expressed normally, the expression of *Wnt3* and the TGF-beta ligand *Nodal* may have been changed in *FLRT3*$^{-/-}$ embryos. To investigate this possibility, the expression patterns of *Nodal* and *Wnt3* were analyzed using *in situ* hybridization. The expression of *Nodal* extended in a wing-like pattern in the posterior region from the extraembryonic- embryonic border along the PS into the sides of the embryo (Figure 26 D; n=4 wild type embryos). *Nodal* expression in *FLRT3*$^{-/-}$ embryos appeared unchanged when compared to wild type embryos (Figure 26 I; n=3 mutant embryos). The expression of *Wnt3* was

somewhat similar to *Nodal*. Also *Wnt3* was expressed in the posterior of the embryo along the primitive streak but extended proximally into the extraembryonic region and was laterally more restricted (Figure 26 E; n=8 embryos). *FLRT3*$^{-/-}$ embryos displayed no changes in the expression of *Wnt3* (Figure 26 J; n=4 mutant embryos). Taken together, the unchanged expression patterns of *Wnt3*, *Nodal* and the Wnt- and Nodal inhibitors, suggests that *FLRT3*$^{-/-}$ embryos have no alterations in the signalling properties of the AVE. It rather seems that the ectopic induction of mesoderm is a consequence of the breakage of the anterior endoderm.

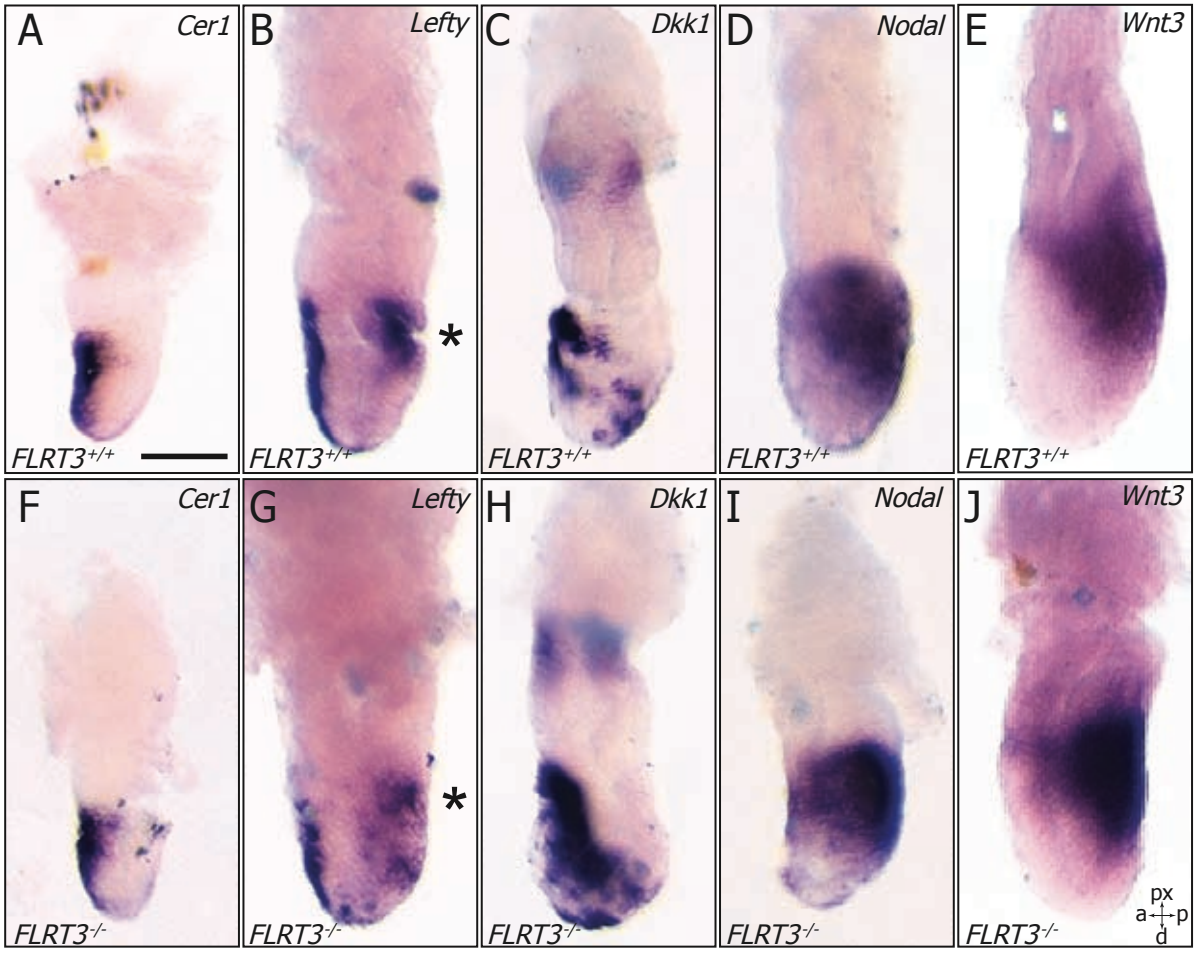

Figure 26 The AVE displays normal signalling properties in FLRT3$^{-/-}$ embryos
(A-J) Whole mount *in situ* hybridization images of ES to MS stage control and mutant embryos assayed for the expression of *Cer1* (A, F), *Lefty* (B, G), *Dkk1* (C, H), *Nodal* (D, I) and *Wnt3* (E, J). Expression of any of the tested Nodal/Wnt signalling inhibitors did not differ from wt to mutant embryos. In the case of Lefty, a riboprobe was used that detected both *Lefty1* and *Lefty2*, the latter in the PS region (asterisks in B and G). (D, I) Similar to the expression of Nodal inhibitors, the expression of *Nodal* was not altered in *FLRT3*$^{-/-}$ embryos. (E, J) Also, the expression of the Wnt ligand *Wnt3* did not differ between wt and mutant embryos.
All embryos were oriented with the anterior to the left.
Scale bar represents 100 µm

2.3. In vitro systems used to study FLRT3 function

2.3.1. HeLa cells as a model system to study FLRT3 function

Addressing the cellular function of FLRT3 is an important step to understand the biology of FLRT3, especially in the context of the loss of function phenotype during early mouse development. Since several previously published mechanisms were ruled out in this study, other mechanisms needed to be discovered. Analysing the effect of FLRT3 on cell-cell adhesion or cell-matrix adhesion would give important information about FLRT3's cellular functions, but addressing these questions seemed rather difficult in the living mouse embryo was rather difficult. Therefore, a system to study FLRT3 function was needed; one that was easy to handle, readily allowed manipulations and in which established assay systems were applicable. HeLa cells were the first choice for in vitro studies to unravel the function of FLRT3 because HeLa cells do not express any endogenous FLRT family proteins (Figure 27 and SY, JE personal communication), and overexpression constructs for mouse and dog FLRT3 could be used in HeLa cell transfections.

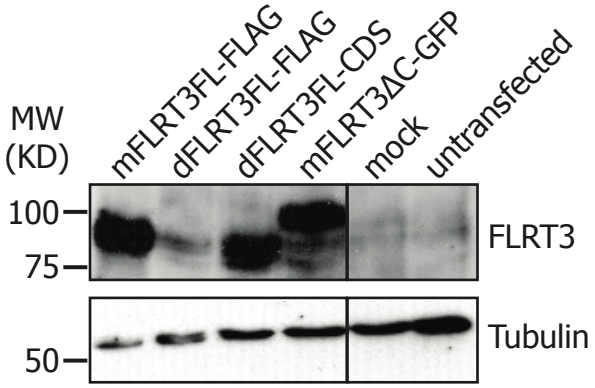

Figure 27 Expression of different FLRT3 constructs in HeLa cells

Total cell lysates of HeLa cells transiently overexpressing full length mouse FLRT3, carrying a FLAG tag (mFLRT3FL-FLAG), full length dog FLRT3 carrying a FLAG tag (dFLRT3FL-FLAG), full length dog FLRT3 without tag and 3' UTR (dFLRT3FL-CDS) or a c-terminally truncated version of mouse FLRT3 carrying a GFP tag (mFLRT3ΔC-GFP) were separated by SDS-PAGE and immunoblotted with a FLRT3 antiserum, detecting the extracellular domain of FLRT3 (#1134). Expression of the constructs was detected, although the expression of dFLRT3FL-FLAG was very weak. Lysates of cells transfected with an empty pcDNA3 vector (MOCK) or of untransfected cells, displayed no FLRT3 expression. Immunoblotting of a Tubulin antibody was used for loading control.

2.3.2. Adhesion assays using transfected HeLa cells did not show an effect of FLRT3 on cell-matrix adhesion

To test whether FLRT3 affected the binding of cells to the extracellular matrix, an adhesion assay protocol was established using transfected HeLa cells. The cells were either transfected with a mFLRT3FL construct or an empty vector as mock transfection. Subsequently, cells were seeded in multiwell plates coated with different substrates. The number of cells bound to the substrate in the given time and at a restrictive concentration of substrate was used as a measure of adhesion to the ECM. The ECM components laminin, collagen type I (collagen I), collagen type IV (collagen IV) and

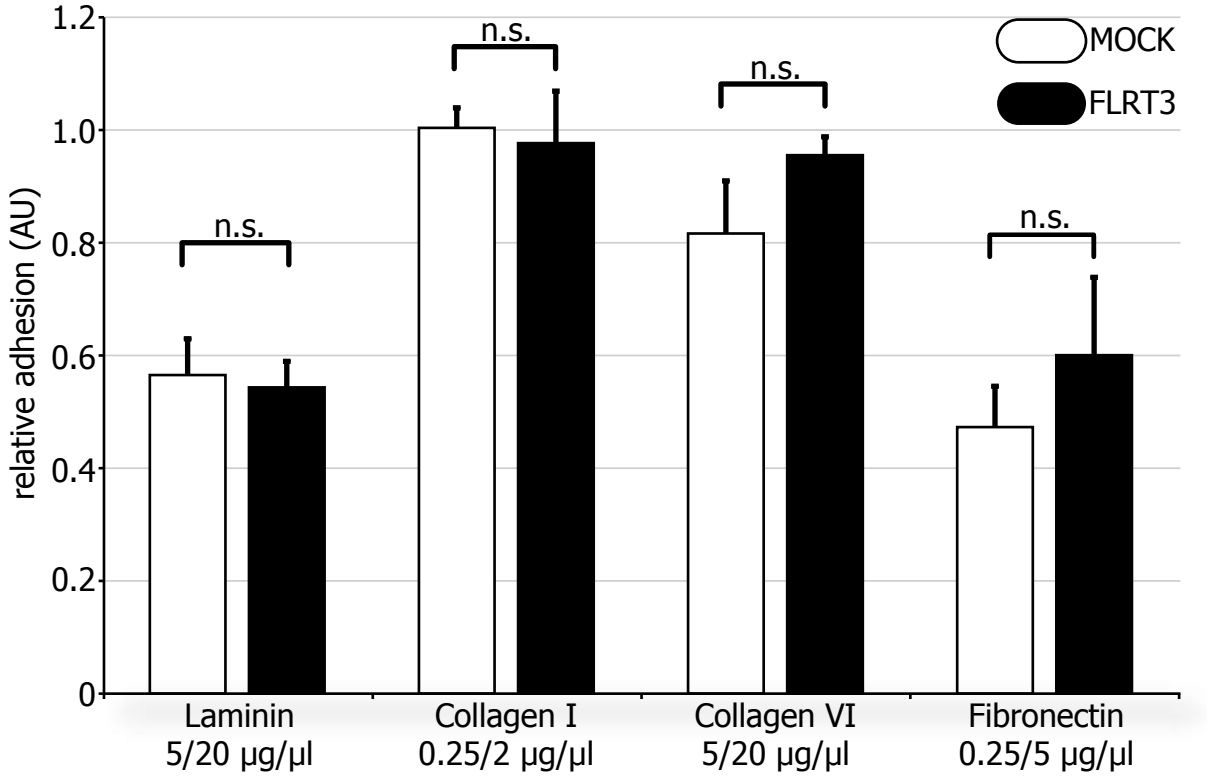

Figure 28 Overexpression of FLRT3 in HeLa cells did not affect cell-matrix adhesion

Cell matrix adhesion assays, carried out using transiently transfected HeLa cells and different extracellular matrix proteins were pooled, with the average of three experiments shown here. After the assay, cells were fixed, washed, stained with Crystal violet and the dye was solubilised in acetic acid. The absorbance was measured in a spectrophotometer. The so derived measure of cell numbers was normalized against samples containing only the protein coat. The absorbance at limiting concentrations was compared to the absorbance at saturated conditions to obtain the relative adhesion. A significant difference in binding in presence or absence of FLRT3 was not detected in any of the tested ECM components ($p>0.1$; Student's *t-test*.). The error bars represent the standard error.

fibronectin served as substrates. The concentrations used for the experiments were determined by acquiring binding curves of cells to different concentrations of the substrates (data not shown). Overexpression of FLRT3 in HeLa cells did not change the adhesion of HeLa cells to the ECM significantly (Figure 28). In particular, binding to laminin or collagen I was not altered. Also in the case of fibronectin and collagen IV no differences in binding could be observed, although a slight trend towards higher binding in the FLTR3 expressing cells seemed apparent. The variations between experiments were considerably high and no consistent data could be obtained. In addition, the expression of FLRT3 was intended to be monitored by coexpression of GFP, but the measurement of GFP fluorescence in these experiments was unreliable. Therefore, no data concerning the expression of FLRT3 was obtained. However, the transfection efficiency and the level of protein production of the cells used were typically rather high.

2.3.3. MDCK cells as an experimental model

Using an epithelial cell line to study the effects of FLRT3 on cell-matrix or cell-cell adhesion appeared to better resemble the cellular events in the mouse endoderm in vivo. Madin Darby Canine Kidney (MDCK) cells represent a well-established epithelial cell line, which can, when grown on plastic dishes or filter supports (two-dimensional cultures), form a fully polarized single layer epithelium. Grown in three-dimensional

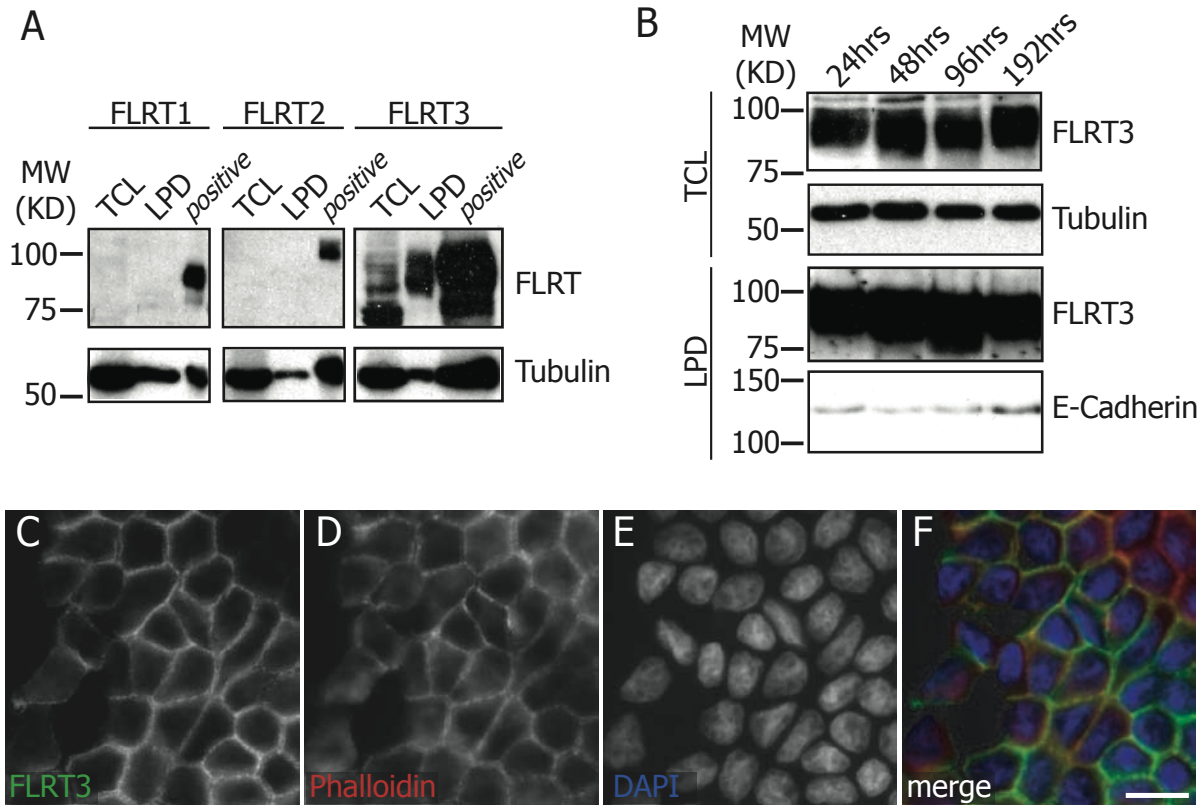

Figure 29 FLRT3 expression in Madin Darby Canine Kidney (MDCK) cells
(A) Total cell lysates (TCL) and lectin pull downs (LPD) of untransfected MDCK cells were separated by SDS-PAGE and immunoblotted with antibodies/antisera against either FLRT1, FLRT2 or FLRT3. Immunoprecipitations of cells transiently transfected with FLRT1 or FLRT2 and a TCL of cells transiently transfected with FLRT3 were used as respective positive controls. Correct loading was tested by immunoblotting using an anti-tubulin antibody. (IPs were a generous gift of SY and the TCL of FLRT3 transfected cells was a generous gift of JE). MDCK cells were found to endogenously express FLRT3, but not FLRT1 or FLRT2. (B) Cell lysates of untransfected MDCK cells were collected after various culture times and separated by SDS-PAGE. Total cell lysates or lectin pull down experiments were loaded and immunoblotted using a FLRT3 antiserum (#1134). Levels of loaded protein were assayed by immunoblotting against tubulin in the case of TCL and E-Cadherin in the case of LPD experiments. FLRT3 protein expression peaked after reaching confluence (around 96 hrs after plating) and was again reduced 192 h after plating. (C- F) Immunofluorescence of confluent MDCK cells grown on filter supports to allow polarization. Cells were stained with an antibody against FLRT3 (R&D) (C), phalloidin (D) to visualize the actin cytoskeleton, and DAPI (E). FLRT3 is localized to the plasma membrane, especially in cell-cell contacts.

cultures, in a collagen gel for instance, MDCK cells can form cysts, which are sphere-like structures.

Prior to the analysis, the endogenous expression of FLRT proteins in MDCK cells was investigated. It was previously shown in our laboratory that MDCK cells expressed endogenous FLRT3 (JE, personal communication). To test the presence of FLRT1 and FLRT2 in MDCK cells, western blot analysis using confluent and untransfected MDCK cells was performed. Lysates of cells transfected with overexpression constructs for FLRT1, FLRT2 or FLRT3 (mFLRT3FL-FLAG) served as positive controls. Expression of FLRT1 or FLRT2 was not detected, whereas expression of FLRT3 was evident in the total cell lysate (TCL) and in the lectin pull down (LPD).

To test whether the expression of FLRT3 was stable over time in MDCK culture, time course experiments were performed, using cells that had been in culture for different times. Beginning with cells growing in isolated islands, expression of FLRT3 was analysed until cells had formed a dense epithelial layer. The expression of FLRT3 seemed to increase as they were growing more dense, and peaked when the cells reached confluency. Interestingly the level of FLRT3 protein was again lower in cells growing in a dense epithelium (Figure 29 B). This could be seen in both the total cell lysate and the lectin pull down. Finally, the subcellular localization of FLRT3 protein was assessed using antibody staining against FLRT3. Especially in polarized cells, FLRT3 protein was mainly localized at the cell membrane, with regions of cell-cell contacts showing high levels of FLRT3 protein expression (Figure 29 C-F).

2.3.4. FLRT3 overexpression in MDCK cells did not alter cell-matrix adhesion

To continue studying the effect of FLRT3 on cell-matrix adhesion, MDCK cells overexpressing mouse FLRT3 were compared to MOCK transfected MDCK. Similar to the experiments performed in HeLa cells, MDCK cells were seeded in multiwell plates coated with either laminin or collagen I. The relative adhesion was determined by comparing the number of cells bound to low concentrations compared to saturated concentrations of the substrates. The binding of MDCK cells to laminin was not altered significantly by overexpression of FLRT3 (Figure 30). However, generally a very low number of cells bound to lower concentrations of laminin. Similarly, the binding of MDCK cells to collagen I seemed to be unaffected by the overexpression of FLRT3. In all of the performed experiments, high intra- and inter-experimental variations were observed. In addition, the level of expression of exogenous FLRT3 was not clear. Since the transfection efficiency of MDCKs was comparably low, a plasmid coding for GFP was cotransfected to monitor the FLRT3 expressing cells. Similar to experiments performed in HeLa cells, the measurement of GFP positive cells adhering to the substrate was unreliable (data not shown). Therefore no data obtained from GFP-fluorescence measurements was used for the evaluation.

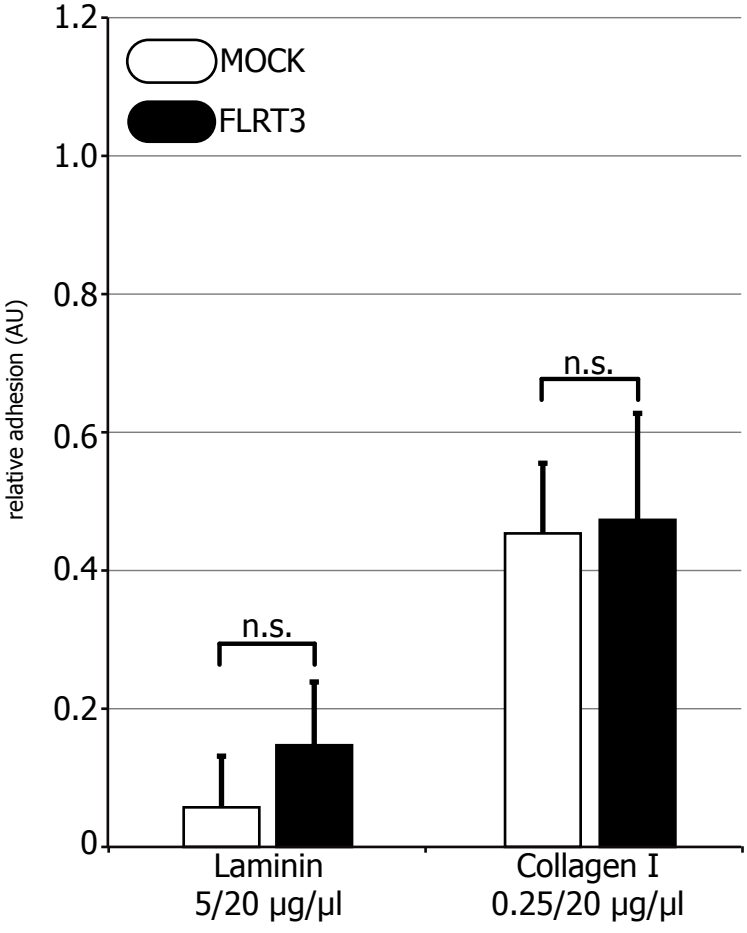

2.3.5. Establishment of FLRT3 shRNA knock down cell lines

Since the potential gain-of-function experiments using overexpression of FLRT3 were not sufficient to address the influence of FLRT3 on cell-matrix adhesion, a short hairpin RNA mediated RNA knock down for FLRT3 in MDCK cells was established. For these loss-of-function experiments potential target regions in the sequence of dog (*canis familiaris*) FLRT3 transcript were identified using a web-based search algorithm (www.Dharmacon.com – see MM for details). Several possible target regions were chosen and the respective oligonucleotides were cloned into the pSUPER.retro. puro shRNA vector (Oligoengine – see MM for details) for sustained expression in mammalian cells. The efficiency of the cloned shRNAs in downregulating FLRT3 was tested by cotransfecting dog FLRT3 with the respective shRNA vectors (Figure 31 A) in HeLa cells. Two shRNA constructs, RNAi11 and RNAi14, consistently showed an efficient reduction of FLRT3 in several HeLa transfection experiments (Figure 31 A). Transient transfections of MDCK cells with the shRNA vectors showed only slight reductions in the level of FLRT3 protein (data not shown). This was most probably due to the relatively low transfection efficiency achieved with MDCK cells. In order to do functional experiments, a low number of cells expressing the shRNA construct was not desirable. Therefore cell lines stably expressing the shRNA RNAi11 or RNAi14 were generated by clonal selection. Stable cell lines carrying the empty pSUPER vector (MOCK) were generated to serve as control cells. The clonal cell lines obtained were analyzed by western blot analysis for the expression of FLRT3 protein (Figure 31 B). For the following experiments, a total of four cell lines carrying the shRNA (three carrying RNAi14 and one carrying RNAi11), and three control cell lines were used. The cell lines were referred to as RNAi14-1, RNAi14-2, RNAi14-3, RNAi11-1 and MOCK1-3, respectively.

Figure 30 FLRT3 overexpressing MDCK cells did not show differences in cell-matrix adhesion

Cell matrix adhesion assays were carried out using MDCK cells, transiently overexpressing mFLRT3 and GFP (FLRT3), and control cells transfected with an empty vector and GFP (MOCK). Cells were allowed to adhere to laminin or collagen I for 30 min before washing and fixation. Cells were stained using crystal violet, which was subsequently solubilised using acetic acid and the absorbance measured was used as a quantification of the number of cells bound to the substrate. Relative adhesion was determined by comparing the number of cells bound to a limiting concentration of substrate with the number of cells bound to saturated substrate concentrations. Each condition was repeated in triplicates. Values presented are the mean of four individual experiments. Error bars represent the standard error. No significant differences could be detected between the (potentially) FLRT3 overexpressing cells and the control cells (n.s.; $p>0.2$; Student's *t-test*).

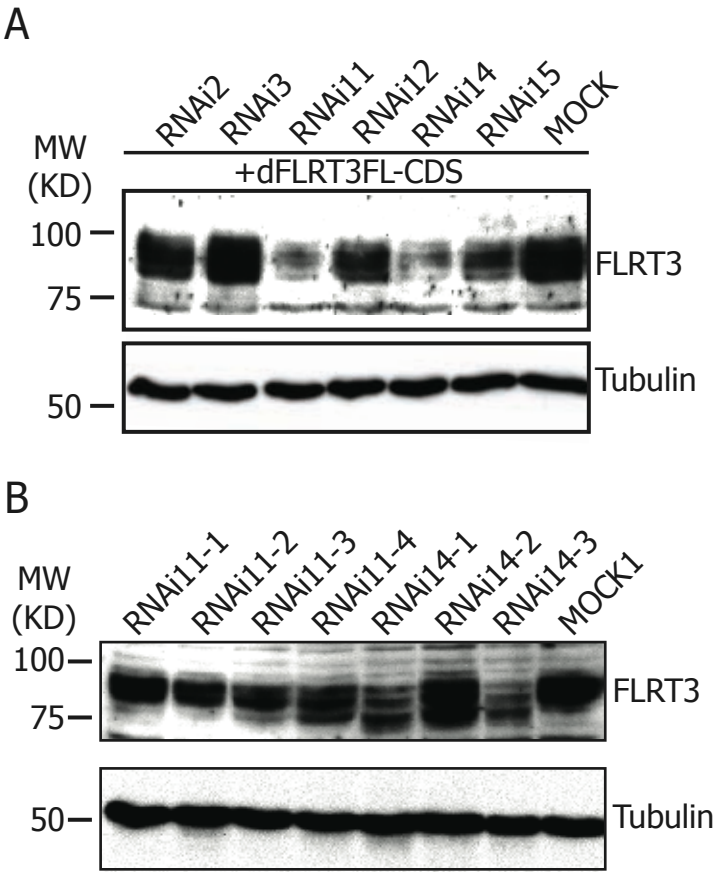

Figure 31 Generation of MDCK cells stably expressing shRNA constructs to knockdown endogenous FLRT3

(A) To test the efficiency of the chosen shRNA constructs in knocking down dog FLRT3, HeLa cells were cotransfected with dFLRT3FL-CDS and the respective shRNA vector or the empty pSUPER.retro.puro vector. Total cell lysates were separated by SDS-PAGE and immunoblotted using FLRT3 antisera (#1134). Tubulin antibody was used to control the level of loaded protein. The shRNA constructs RNAi11 and RNAi14 showed a reliable reduction of dFLRT3 protein. (B) Example image of western blot analysis testing the knock down efficiency in clonal MDCK cell lines stably expressing shRNA constructs targeting FLRT3 mRNA. TCLs of respective cell lines were separated by SDS-PAGE and immunoblotted with a FLRT3 antiserum (#1134) and protein loading was assessed by using an anti tubulin antibody. The most efficient reduction of FLRT3 protein level was seen in the cell lines RNAi14-1 and RNAi14-3, both expressing the shRNA construct RNAi14.

Figure 32 FLRT3 knock down cell lines did not show an alteration in cell-matrix adhesion

Cell matrix adhesion assays were carried out using stable FLRT3 knock down MDCK cell lines RNAi14-1, RNAi14-3 and the control cell line MOCK1. Relative adhesion was determined by comparison of the number of cells bound to limiting substrate concentrations with the number of cells bound to saturated concentrations of substrate, both determined by colorimetric measurements. Each condition was repeated in triplicate and a total of at least three experiments were pooled to obtain the presented data. Although a tendency towards increased binding in the knock down lines was apparent, no statistically significant difference was obtained ($p>0.2$; Student's *t-test*). Error bars represent the standard error.

2.3.6. Binding of FLRT3 knockdown cell-lines to extracellular matrix components

To perform matrix adhesion assays, cell lines carrying the RNAi14 construct were employed. For the initial experiments, only lines RNAi14-1 and RNAi14-2 were used. Cells were seeded to laminin and collagen I substrates. Although there was an observable tendency towards increased binding of the knockdown cell lines to laminin, no significant differences could be accounted. Similar observations were made, using collagen as a substrate (Figure 32). Also in this case, a tendency towards increased binding of knockdown cells to collagen I seemed apparent. Nevertheless, no significant differences were observed for both substrates after averaging the experiments, due to the high intra- and inter-experimental variations. The expression level of FLRT3 protein was monitored by western blot analysis subsequent to the experiment. Although a clear reduction of FLRT3 protein was detected, the remaining relative protein levels were still considerably high (Figure 33). Notably, the tendency in relative binding behaviour of the cell lines seemed to correlate with the measured relative protein expression.

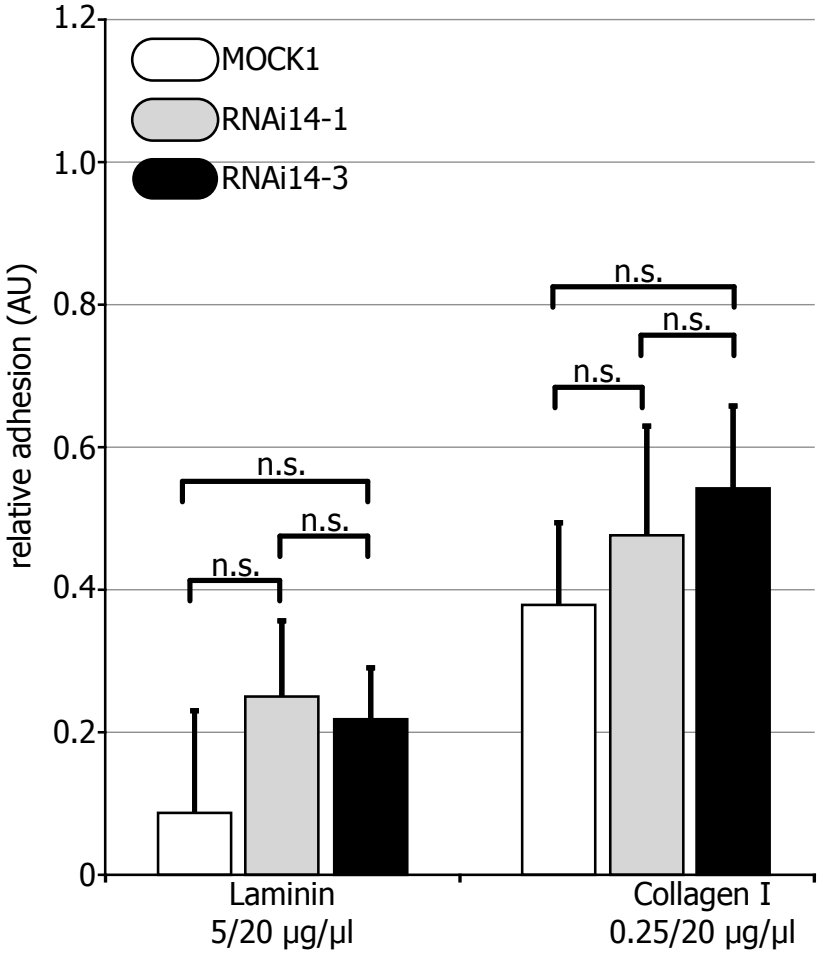

2.3.7. Scatter Assay using MDCK cells

MDCK cells grow in an epithelial monolayer in two dimensional culture systems, as well as cysts in three-dimensional culture systems. When MDCK cysts are treated with recombinant Hepatocyte Growth Factor (HGF), the cysts undergo branching morphogenesis and start forming tubes. In two-dimensional culture systems where MDCK cells are grown under subconfluent conditions, HGF treatment induces scattering of the cells. Upon HGF stimulation, MDCK cells, growing as epithelial islands; loose cell-cell contacts, become migratory and change their cell shape from the normal epithelial shape to a more fibroblast like shape with thinner processes (Weidner, et al. 1990). This assay can be used to study the motility of cells, but also the adhesion properties of cells.

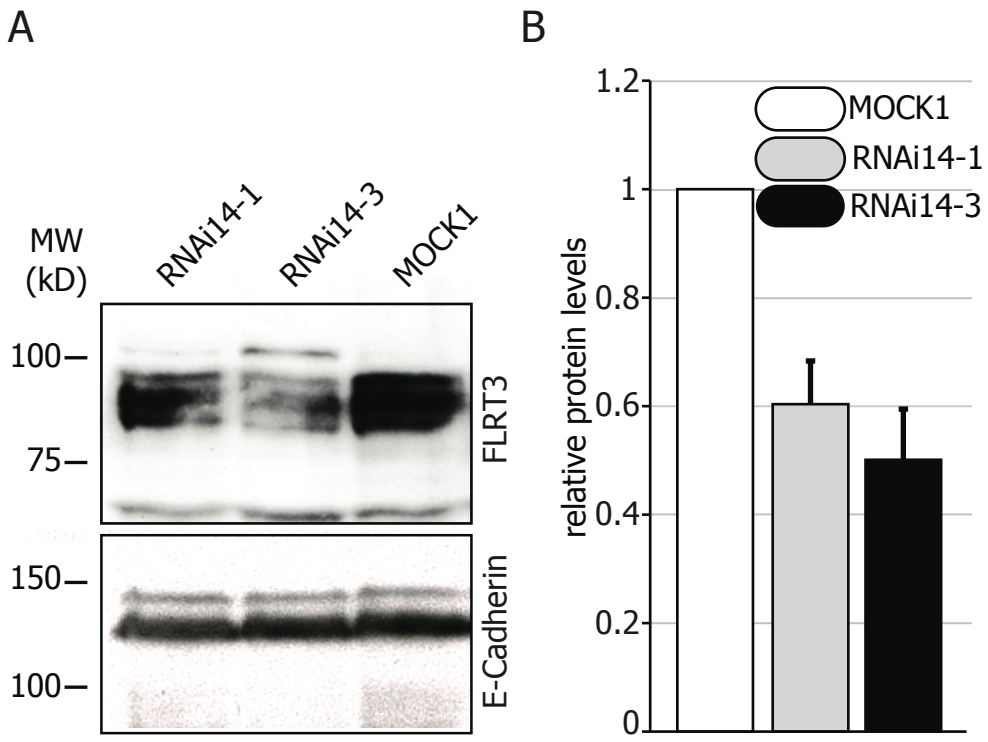

Figure 33 Relative FLRT3 protein levels in knock down cell lines
(A) Cell lysates used for assays shown in Figure 32 and Figure 34 were collected and analyzed for FLRT3 expression by western blotting. Proteins were immunoblotted using FLRT3 antisera (#1134) and protein loading was assayed using an anti E-cadherin antibody. (B) Quantification of the relative protein levels using densitometry with scanned images of developed X-ray films. The levels of the control cell line (MOCK) were set to 100% and compared to the levels of the shRNA-expressing knock down cell lines. The quantification represents a mean of four individual experiments.

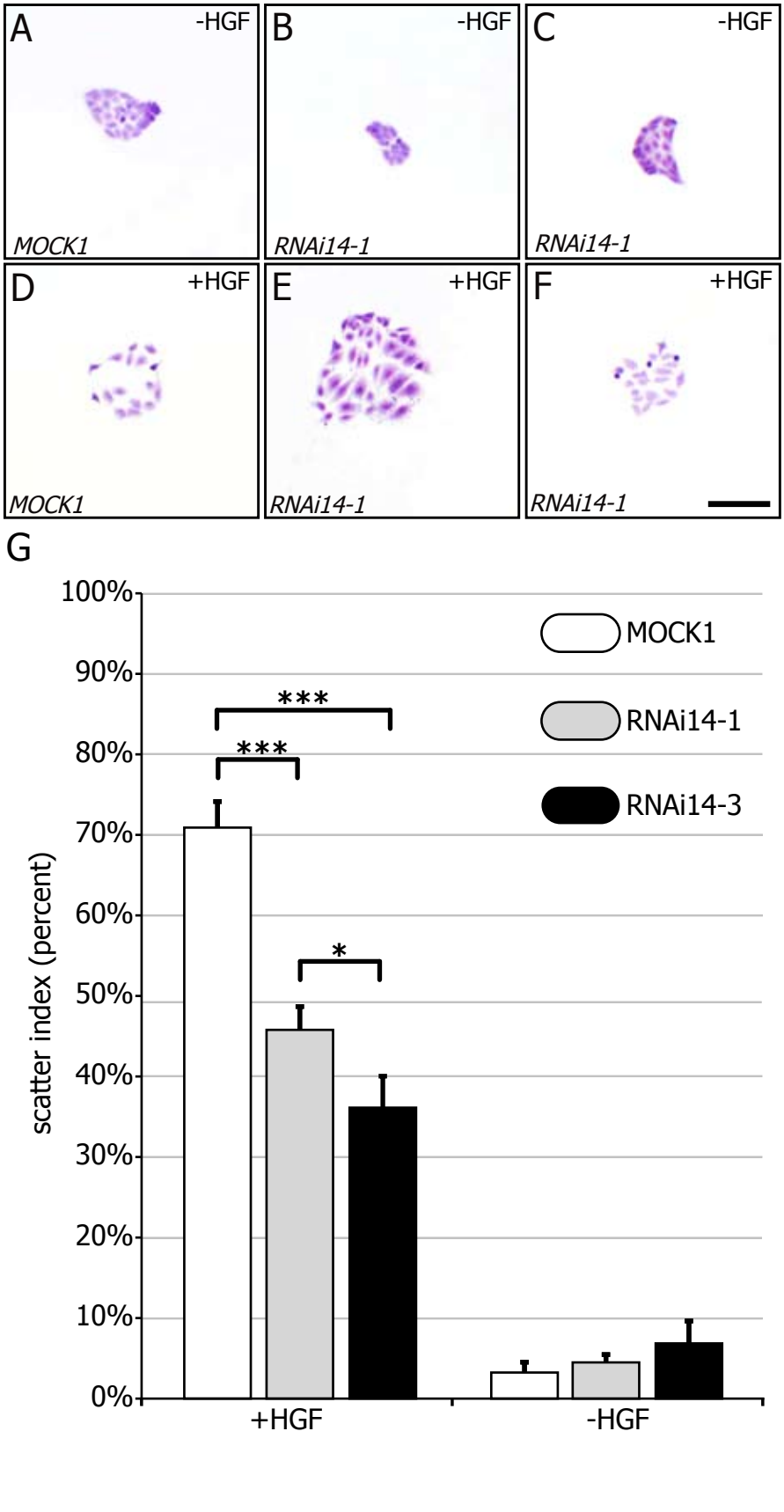

Figure 34 Knock down of endogenous FLRT3 affected scatter behaviour of MDCK cells

(A-F) Representative images of scatter assays performed with control cells (A, D) or knock down cell lines RNAi14-1 (B, E) and RNAi14-3 (C, F). MDCK cells incubated for 24hrs in reduced serum conditions without HGF showed epithelial morphology and grew in islands attached to each other (A-C). Cells treated with HGF in reduced serum medium for 24 hrs showed the typical scatter behaviour, including a change of morphology and the loss of cell adhesion (D-F). (G) Although the knock down cell lines showed scattering, the percentage of scattered colonies was reduced in the knock down cell lines. A scatter index was determined by comparison of the number of scattered colonies with the number of total colonies. All experimental conditions were repeated in triplicate. The graph represents a mean of five individual experiments. Error bars represent the standard deviation. Reductions observed are statistically significant (***=$p<0.001$, *$p<0.05$; Student's *t-test*).

Using the FLRT3 knock down cell lines RNAi14-1 and RNAi14-2, scatter assays were performed and quantified. Briefly, cells were seeded as single cells at very low density and allowed to grow to small islands of 3-6 cells over a period of two days. Cells were stimulated for 24h with 20 ng/ml HGF in reduced serum media, then fixed and stained for further analysis. The scatter index was determined by quantifying the number of scattered colonies versus total number of colonies (for more details see MM). A colony was considered as scattered if 50% or more of the cells had lost cell-cell contacts, started migrating and acquired a fibroblast like morphology (see Figure 34 for examples). Clearly, the scattering activity of the knock down cell lines was reduced compared to the control cell line. The spontaneous scattering however was not altered as shown for the non-stimulated conditions. Here, the knockdown cells lines showed the same level of scattering as compared to the control cells. For these experiments, the same cells were used as for the adhesion assays shown in Figure 32. The level of FLRT3 expression seemed to correlate with the observed reduction in scattering. This could indicate an increase in cell-cell adhesion, a reduction in cell motility or simply a defect in the activation of the HGF pathway. To rule out the possibility that the HGF pathway was perturbed in the FLRT3 knock down cell lines, an HGF stimulation time course experiment was performed. The respective

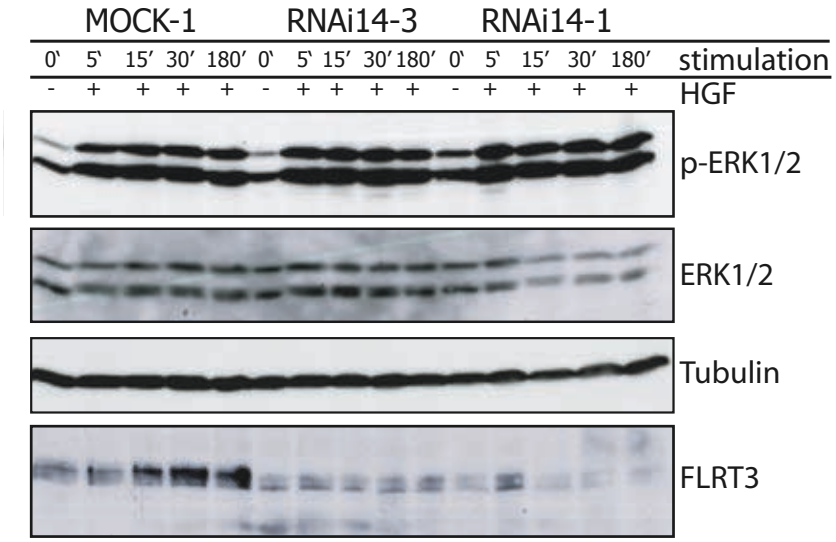

Figure 35 Persistent activation of the ERK-MAPK pathway is not altered in MDCK knock down cell lines RNAi14-1 and RNAi14-3
Control and knock down cell lines were stimulated for various time periods with HGF. Afterwards, the cell lysates were analyzed by western blotting for the phosphorylation of the MAPKinases ERK1 and 2 using a phospho-ERK1/2 specific antibody. As a control for the total levels of ERK1/2, an anti ERK1/2 antibody, and for loading control purposes, an anti tubulin antibody, were used. To monitor the reduction of FLRT3 in the cells used, an anti FLRT3 polyclonal antibody (R&D) was used. Even after 180 min of stimulation with HGF, the level of phosphorylated ERK1/2 remained high, whereas the total level of ERK1/2 did not change over time.

cells were stimulated for 5 min, 15 min, 30 min or three hours with 20 ng/ml HGF and afterwards, the activation of the MAP Kinase pathway was tested by western blot analysis. The stimulation with HGF activated the MAP Kinase pathway persistently during the time of stimulation as shown by phosphorylation of ERK1/2 in the control cells (MOCK-1) (Figure 35). Similarly, the knock down cell lines showed a robust and persistent activation of the MAP Kinase pathway over the time of stimulation. The level of total ERK protein remained unchanged. FLRT3 levels were noticeably reduced in the knock down cell lines when compared to the control line. This indicates that the activation of the HGF pathway was not disturbed in the knock down cell lines.

By using two control cell lines, MOCK-2 and MOCK-3, one additional cell line for RNAi14, RNAi14-4 and one cell line for RNAi11, RNAi11-1, possible effects of the clonal selection or off-target effects should be ruled out. Scatter experiments with these cell lines showed no consistent change in the scattering behaviour of these cells. Furthermore, the control cell lines already showed reduced scattering compared to MOCK-1 (Figure

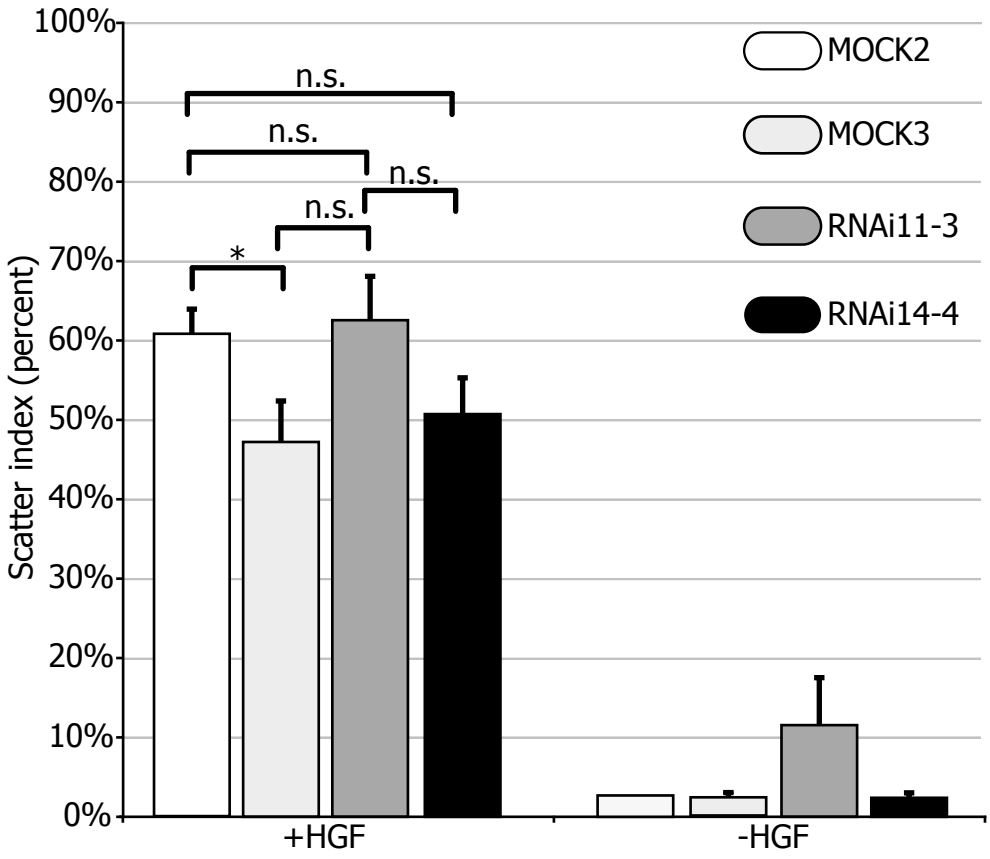

Figure 36 Additional knock down and control MDCK cell lines did not show consistent changes is scattering behaviour

Analyzing additional FLRT3 knock down and control MDCK cell lines for their scattering reaction upon HGF stimulation did not result in persistent and significant alterations. Only the control cell lines differed significantly in their scattering behaviour. The data represents the mean of three individual experiments. In each experiment all conditions were performed in triplicate. The error bars represent the standard deviation. (n.s. $p>0.05$, * $p<0.05$; Student's *t-test*).

36). Together with the relative expression of FLRT3 that was again determined by western blot analysis, no clear correlation between the reduction of FLRT3 protein level and the scattering activity could be made. Even the strongly reduced level of FLRT3 expression in RNAi14-4 compared to MOCK-3 resulted in a similar scattering index.

Summarizing these data, it became clear that with the experimental conditions and setups used so far, no clear results could be obtained. Therefore no further experiments with additional control shRNAs were performed. Unfortunately, the question of the function of FLRT3 on the cellular level has not yet been answered.

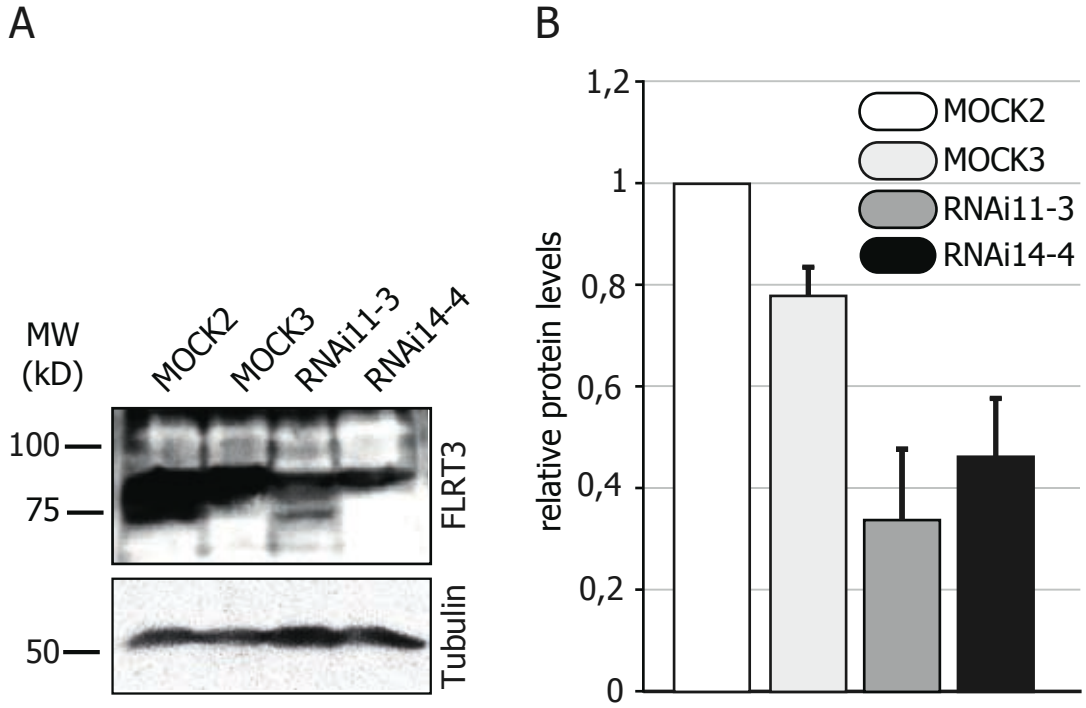

Figure 37 Quantification of relative FLRT3 protein levels in cells used for scatter assay

(A) Cell lysates of cells used for the scatter assay shown in Figure 36 were collected and analyzed for FLRT3 expression by western blotting. Proteins were immunoblotted using FLRT3 antisera (#1134) and protein loading was assessed using an anti tubulin antibody.(B) Quantification of the relative protein levels using densitometry and scanned images of developed X-ray films. FLRT3 protein levels in the control cell line MOCK1 were set to 100% and compared to the levels in the second control cell line MOCK2 and the shRNA expressing knock down cell lines. The quantification represents a mean of three individual experiments.

3. Discussion

3.1. FLRT3 expression during early postimplantation development

Leucine rich repeat (LRR) proteins have been shown to have important functions during embryonic development. A relatively novel family of LRR proteins is the family of FLRT proteins. The expression of these proteins can first be detected during the early post implantation development stages of the mouse. In this study, *FLRT1* expression was seen from E8.0 onwards, earlier than previously reported in (Haines, et al. 2006); and *FLRT2* expression in the anterior mesoderm was already evident at head fold stages (see Figures 10 and 11). However, using ß-Gal reporter lines, *FLRT3* expression was detected as early as E5.5 (PrS) (Egea, et al. 2008; Maretto, et al. 2008) or at the ES stage using in situ hybridization (see Figure 10). The pattern of *FLRT3* expression at the PrS and ES stages was very specific. Prior to PS formation, *FLRT3* expression in the embryonic region was found to be localized over the entire endoderm and became restricted to the AVE as the PS was induced and progressed distally (Egea, et al. 2008).

The AVE has been shown to have important functions in axis formation and anterior patterning (Rossant and Tam, 2004). It has been shown to execute the shift of the embryonic axis from PD to AP, and the spatial regulation of Wnt and Nodal signalling. A set of genes expressed in the AVE has been implicated in its proper function. Amongst those are the *bona fide* AVE marker *Hex*, the TGF-beta inhibitors *Lefty1* and *Cer1* and the transcription factor *Otx2* (Thomas, et al. 1998; Belo, et al. 1997; Biben, et al. 1998; Perea-Gomez, et al. 2001). Interestingly, most gene products shown to influence AVE function, either by influencing cell migration or by modulating signalling activites, are intracellular transcription factors (Lim1, Otx2) or secreted molecules (Lefty1, Cer1). As yet, no transmembrane protein has been implicated in the function of the AVE. Therefore, FLRT3 is not only the first leucine rich repeat protein, but the first transmembrane protein, known to have a (morphogenetic) role in the AVE. *FLRT3* expression, similar to that of other genes expressed in the AVE, persists in the newly generated DE. Interestingly, FLRT3 expression was not detected in the PS region, even at later stages of development. This is in contrast to observations made in

Xenopus embryos, where FLRT3 is involved in the regulation of cell-adhesion molecule levels present in the plasma membrane of cells in the PS equivalent (Ogata, et al. 2007). At later stages of development, the expression of *FLRT3* expanded to encompass the mesoderm and ectoderm. From E8.5 on, *FLRT3* expression became more widespread anterior to the tail bud but still showed a distinct and non-ubiquitous expression pattern. In addition to its expression in the developing somites, which gave rise to some speculation about possible roles of FLRT3 in somite formation (Haines, et al. 2006), *FLRT3* was found to have a distinct expression pattern in the developing nervous system (Haines, et al 2006, Maretto et al. 2008, this study). Similarly, also *FLRT1* and *FLRT2* are expressed in interesting areas of the developing nervous system.

LRR containing proteins have often been implicated in several processes in nervous system development and function. It has been shown that in flies and mammals for instance, LRR proteins are involved in fasciculation (Kuja-Panula, et al. 2003), synapse formation (Kim, et al. 2006) and neurite outgrowth (Lin, et al. 2003). LRR proteins have also been implicated in causing neurological disorders such as epilepsy and Tourette's syndrome (reviewed in Matsushima, et al. 2005). In addition, FLRT3 has previously been implicated in an enhancing function on neurite outgrowth in vitro (Tsuji, et al. 2004). Expression of *FLRT3* in the developing fore- and midbrain regions and the optic eminences and the otic pit from days 8 to 10 of embryonic development, may point to a possible function for FLRT3 in nervous system development. Given that in *Xenopus* embryos FLRT3 have been shown to modulate FGFR signalling (Böttcher, et al. 2004), the coexpression of *FLRT3* with components of the FGF signalling pathway, for example at the isthmic boundary (Jukkola, et al. 2006), suggests a possible functional role for FLRT3 in the nervous system. Also, *FLRT1* and *FLRT2*, which are expressed in the developing nervous system with *FLRT1* being exclusively expressed in the future midbrain regions at E8.5 and E9.5 and *FLRT2* seemingly expressed in the cranial mesoderm; may function in nervous system development. Although there is very little data currently available concerning FLRT1 and FLRT2, an involvement in nervous system development seems likely, since it has already been shown for other LRR repeats (Kuja-Panula, et al. 2003; Kidd, et al. 1999).

Differences in the assay systems and respective protocols and riboprobes used, could account for minor differences in the expression patterns for FLRT3 shown so far (Haines, et al. 2006; Maretto, et al. 2008; Egea, et al. 2008; this study). Nevertheless, the overall expression pattern seen in all studies showed extensive overlap. It is clear that the role of FLRT family proteins, not only during embryonic development but also in somite formation and nervous system development, needs to be further investigated.

3.2. The FLRT3$^{-/-}$ Phenotype

In recent years, dramatic effects from the loss of a single gene product on embryonic development have been shown in many studies (Shawlot and Behringer 1995; Shawlot, et al. 1999; Acampora, et al. 1995; Ang, et al. 1996; Klingensmith, et al. 1999; Ding, et al. 1998). Recently, Maretto and co-workers published the generation of a deletion allele of FLRT3 (Maretto, et al. 2008), embryos from which were reported to have defects in neural tube closure, heart fusion (*cardia bifida*), DE migration and displayed embryonic lethality. In this study, using an independently generated genetic ablation of FLRT3, largely similar phenotypes were observed, such as embryonic lethality after 10 days of development, *cardia bifida* and neural tube closure defects, often in combination with asymmetric head fold development. As neural tube closure defects are seen with a high incidence in newborn human babies, possible causes of these disorders have received considerable attention (reviewed in Harris and Juriloff 2007). In addition to the known influence of folate metabolism on neural tube closure, a long list of mutations has been collected which cause neural tube closure defects in mice (Harris and Juriloff 2007). Potential target genes are involved in different molecular pathways, such as programmed cell death or the planar cell polarity pathway, to name just a few (Harris and Juriloff 2007; Kibar, et al. 2007). But only around 15% of the reported cases in humans are syndromic cases, where in addition to the defective neural tube closure other abnormalities can also be observed (Harris and Juriloff 2007; Hall, et al. 1988; Hunter 1984). Also, in the majority of human disease cases studied (85% of the cases), no embryonic lethality was observed. Gene mutations that cause neural tube closure defects in concert with other abnormalities and embryonic lethality, are believed not to be involved in disease relevant, so called canonical, neural tube disorders. Thus, it seems unlikely that FLRT3 could be added to the list factors causing canonical neural tube disorders. Interestingly, failures of neural tube closure have been previously reported to occur in concert with *cardia bifida* (Lickert, et al. 2002), a condition which is characterized by the development of two individual hearts. In GATA4 deficient embryos, *cardia bifida* has been reported to be a consequence of failures in ventral fusion (Molkentin, et al. 1997). The promyocardiae are located between the foregut endoderm and the yolk sac endoderm. Starting at a thickening of the splanchnic mesoderm and the underlying endoderm - the so-called anterior intestinal portal (AIP); the ventral body side closes in a zipper like fashion, due to the folding of the mesoderm and endoderm. In GATA4 mutant embryos, the AIP was not formed (Molkentin, et al. 1997). GATA4 was found

to be responsible for the expression of N-cadherin, which is important for heart field fusion (Zhang 2003). However, in Beta-catenin conditional mutants (Lickert, et al. 2002), it became evident that *cardia bifida* and neural tube closure defects were the consequence of endodermal deficiencies. Similarly, the loss of definitive endoderm production in Furin mutant embryos, a proprotein convertase involved in the activation of Nodal, was shown to be the cause for, amongst other conditions, *cardia bifida* and neural tube closure defects (Constam and Robertson 2000b). Nodal signalling, transduced by SMAD2/3, is required for the production of definitive endoderm during mouse gastrulation (Dunn, et al. 2004). Together with the phenotype of *FLRT3*$^{-/-}$ embryos, this could suggest that FLRT3 is involved in the production, specification or maintenance of definitive endoderm. Interestingly, no axis truncation, as in the case of Beta-catenin deficient embryos, was observed in *FLRT3*$^{-/-}$ embryos.

Also, the expression of *Foxa2*, a marker for anterior primitive streak derivatives (Ang, et al. 1993; Sasaki and Hogan 1993), shows no appreciable difference between mutant and control embryos, although in some severely malformed embryos the interpretation could be difficult. Moreover, in time-lapse microscopy experiments using the HEX-GFP transgenic mouse line (Rodriguez, et al. 2005) in the *FLRT3*$^{-/-}$ background, HEX-GFP positive cells were able to migrate away from the anterior primitive streak towards the anterior of the embryo (Egea, et al. 2008). Finally, a role for FLRT3 in the definitive endoderm as a cause of the observed phenotypes has been proven to be highly unlikely. The initial phenotype could be first seen before the DE began to populate the anterior of the embryo (see below). Furthermore, a strong line of evidence came from tetraploid aggregation experiments. In these experiments, almost the entire embryo was derived from mutant ES-cells, whereas the extraembryonic tissue was entirely wild type (Tam and Rossant 2003; Kwon, et al. 2008). It became apparent that the role of FLRT3 was restricted to the extraembryonic visceral endoderm (Egea, et al. 2008). All embryos derived from *FLRT3*$^{-/-}$ embryonic stem cells injected in electrofused tetraploid wt mouse blastocysts were phenotypically normal and showed no apparent defects (Egea, et al. 2008). Notably, none of the embryos generated by tetraploid aggregation showed ectopic *Bra/T* expression, as analyzed by in situ hybridization (data not shown, and see below). In conclusion, it seems very unlikely that FLRT3 is involved in the generation, maintenance or, as suggested by Maretto and co-authors, migration of definitive endoderm derived from the anterior primitive streak.

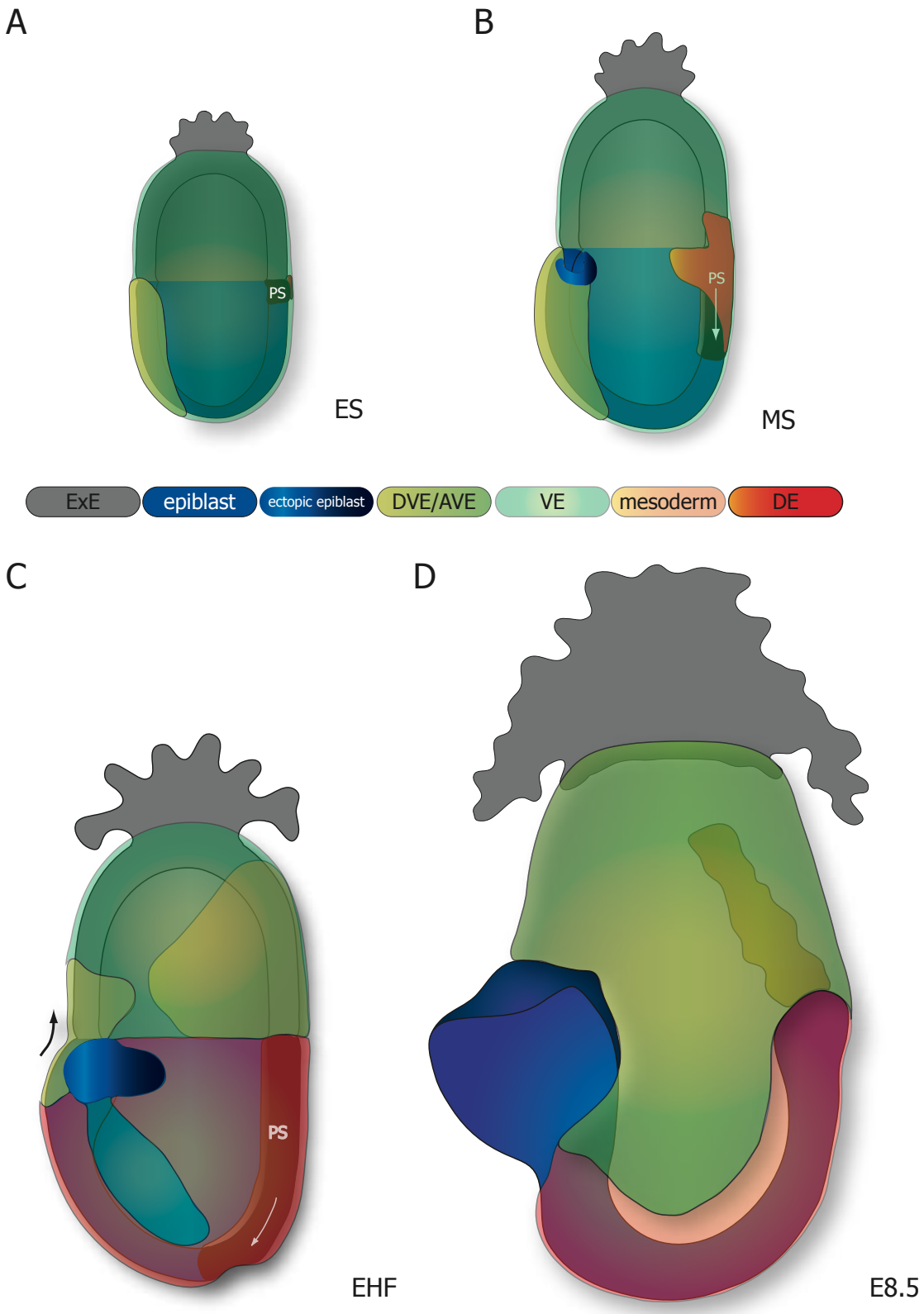

Figure 38 Summary of the FLRT3$^{-/-}$ phenotype.
(A) ES *FLRT3*$^{-/-}$ embryos did not show an obvious phenotype. (B) At MS stage, a discontinuity in the anterior endoderm could be seen, together with ectopic localization, and expression of mesodermal marker genes, such as *Bra/T.* (C) At EHF stage, a prominent hole in the endoderm could be seen, from which ectopic ectoderm cells were protruding outwards. The expression of mesodermal marker genes was evident at the frontal tips of the ectopic ectoderm. (D) At E8.5, at least the head of the embryo was very often localized outside of the VYS. In more severe cases, the entire embryo could be found outside of the VYS. Due to the improper enclosure of the embryo into the VYS, resulting from the hole in VE, ventral body closure could not be completed in the anterior region and caused *cardia bifida*.

3.3. The loss of FLRT3 does not disrupt early embryonic patterning

The AVE is known to be an important signalling centre for anterior posterior development and gastrulation (Kimura, et al. 2000). In a classical experiment, the mechanical ablation of the AVE resulted in anterior patterning abnormalities (Thomas and Beddington 1996). Also in genetic studies, the ablation of genes expressed in the AVE such as Otx2 and Lim1, led to anterior truncations. In embryos lacking *Lim1*, no fore- and midbrain structures, characterized by the expression of *Otx2*; and a reduced size of the developing hindbrain, determined by the expression of *Krox20*; could be observed (Shawlot and Behringer, 1995). Similarly, in double heterozygote *Otx2*$^{+/-}$:*Foxa2*$^{+/-}$ embryos, a shortening of the fore- and midbrain region, demonstrated by a dramatic reduction of the expression domain of *Otx2*, has been reported (Jin, et al. 2001). The expression of *Krox20*, and therefore the size of the hindbrain, was not altered in *Otx2* deficient mice (Ang, et al. 1996). Furthermore, in embryos deficient for *Lim1* or *Otx2*, the formation of the somites, seen as the disturbed expression of meox1, was found (Ang, et al. 1996; Shawlot and Behringer, 1995). In *FLRT3*$^{-/-}$ mutant embryos however, no anterior truncations were observed as judged by the presence of the fore-, mid- and hindbrain markers, *FGF8*, *Otx2*, *Krox20* and *HoxB1*. In some cases, somewhat distorted expression of *Otx2* and *Krox20* was detected in few *FLRT3*$^{-/-}$ embryos. This was mainly a consequence of the malformations in these severely affected mutant embryos. Altogether, this shows that *FLRT3*$^{-/-}$ embryos did not display anterior truncations due to defects in anterior patterning. This is in contrast to the interpretation by Maretto and co-authors that *FLRT3*$^{-/-}$ embryos suffer from anterior truncations (Maretto, et al. 2008). However, also Maretto et al. detected *FGF8* expression at the anterior most regions of the embryo. Data obtained from in situ hybridization experiments performed using *FGF8* and *Bra/T* riboprobes, together with the expression pattern of *Meox1*, indicates that the formation and induction of mesoderm during gastrulation is not disturbed. Together with the expression of *Foxa2* in the prechordal plate of *FLRT3*$^{-/-}$ embryos, it is clear that loss of FLRT3 does not cause patterning abnormalities.

3.4. Endodermal discontinuities are apparent at E7.5

Similar to results published by Maretto et al, discontinuous expression of *Dkk1* and *Cer1* was observed in *FLRT3*$^{-/-}$ embryos (see Figure 20 and data not shown). Both are expressed in the AVE/ADE, which forms the outside surface of the embryo during gastrulation (Glinka, et al. 1998; Biben, et al. 1998). Histological and SEM analysis revealed discontinuities or holes in the anterior endoderm layer. *Dkk1* and *Cer1* negative cells in histological sections and the ectopic cells lining the holes in the SEM images appeared similar to epiblast cells populating these holes. The detection of Sox2 positive cells in the ectopic tissue finally provided evidence that the ectopically localized cells belong to the epiblast (Egea, et al. 2008), as Sox2 serves as a marker for epiblast cells at this stage (Wood and Episkopou 1999). Moreover, time-lapse video microscopy experiments, carried out at the Helmholtz Center in Munich, showed that *FLRT3*$^{-/-}$ embryos could break through the visceral yolk sac that encloses the embryo and then continue developing either partially or entirely outside of the visceral yolk sac (Egea, et al. 2008). Similarly, GATA4 deficient embryos exhibit a comparable development outside of the visceral yolk sack (Molkentin, et al. 1997). As previously mentioned, these embryos display amongst other phenotypes *cardia bifida*. It is likely that the *FLRT3*$^{-/-}$ phenotypes observed at later stages, in particular the severely affected embryos, are a result of the ruptured and discontinuous endoderm. The subsequent partial or entire development of the embryo outside the visceral yolk sac may, in turn, lead to the severe malformations observed.

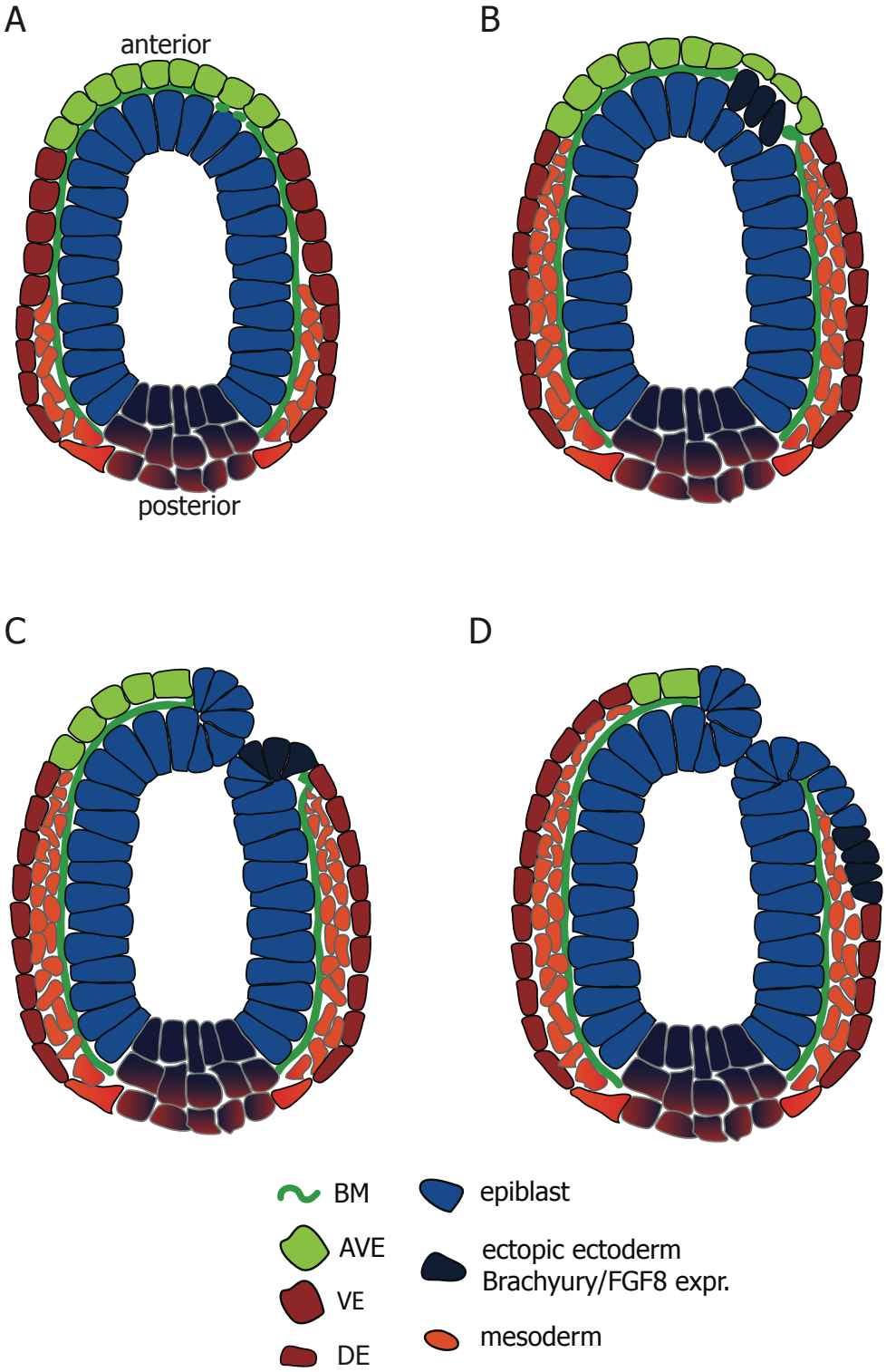

Figure 39 Cellular events underlying the FLRT3$^{-/-}$ phenotype
Already at MS stage, the loss of FLRT3 shows consequences. (A) The BM of *FLRT3*$^{-/-}$, separating the epiblast and the VE ruptures in the lateral anterior region. This leads to a change of behaviour in epiblast cells at the site of BM break down (B). These cells begin to upregulate mesodermal markers, such as Brachyury, and appear to undergo a kind of EMT and invade the newly formed space between epiblast and VE. (C) The VE ruptures and the epiblast cells facing the site of the rupture fill the gap. Epiblast cells now populate the surface of the embryo and have displaced the VE. (D) Most probably due to the morphogenetic forces acting in the fast growing embryo, the ectopic epiblast cells expand into more lateral regions. Still, the frontal tips of the ectopic cells express mesodermal marker genes.

3.5. The loss of FLRT3 in the gastrulating embryo does not affect proliferation or survival

During the process of gastrulation, the embryo gains significantly in size. During a 24 hr period of development (between E6.5 and E7.5, for instance), the embryo almost triples in size (Downs und Davies 1993). Cells in the mouse embryo exhibit a high rate of proliferation during this stage (Bellomo, et al. 1996). It has been shown previously that alterations in cell proliferation during early embryonic development can cause severe developmental defects including growth retardation, shortening of the embryonic axis, neural tube closure defects and may lead to embryonic lethality (Sirard, et al. 1998; Yamaguchi, et al. 1999; Hakem, et al. 1996). In light of the published functional interaction of FLRT3 with the FGFR signalling pathway (Böttcher, et al. 2004), a possible effect of FLRT3 on proliferation or survival was worth investigating. It is known that FGF signalling is involved in many important processes during embryonic development (Böttcher 2005), and in regulating cell proliferation and survival (Eswarakumar, et al. 2005). The overlapping expression of *FLRT3* with FGFR signalling components could indicate that the cooperation shown in Xenopus occurs during gastrulation in mice as well. Two simple scenarios are possible that could link cell proliferation with the observed phenotypes. One possibility would be reduced proliferation of endoderm cells in the AVE, resulting in a shortage of cells covering the underlying epiblast. The epiblast cells would simply make use of the newly formed space and therefore, be ectopically located. Or, secondly, epiblast cells could, in a non-cell autonomous fashion, display increased proliferation and, together with the mechanical forces in the growing embryo, break the endoderm layer and populate this space actively. The data obtained from proliferation assessments establishing the mitotic index, indicates no alteration in cell proliferation, neither in the endoderm, nor in the epiblast of mutant embryos when compared to wt embryos. Also, the quantification of proliferation in the anterior embryo at HF stage did not result in different levels of proliferation when comparing wild type and mutant embryos (data not shown).

However, it is not only the rate of proliferation, but also the survival of cells that influences the total number of cells. There are examples of elevated programmed cell death in early postimplantation embryos that result in early embryonic lethality or severe malformations (Gladdy, et al. 2006). A possible increase in apoptosis of AVE cells of mutant embryos could lead to a shortage of cells and thus to the generation of holes in the anterior embryo. Interestingly, no elevation of the generally low level of

apoptosis could be seen in *FLRT3*$^{-/-}$ embryos. It was only at later stages (E8.5 and E9.5), that elevated levels of apoptosis were detected, mainly in the region of the unfused head folds (data not shown). This is very likely a secondary consequence of the severe phenotype. Altogether, the loss of FLRT3 neither changes cell proliferation in the early embryo, nor directly influences the survival of endoderm cells. This argues against a function for FLRT3 in the mitogenic pathway of FGF signalling in the anterior embryo, which is in agreement with data obtained from a study determining phospho-MAP Kinase (MAPK) levels using an FGFR inhibitor in gastrulation stage mouse embryos. FGFR dependent activation of MAPK was shown in the ExE, but not in embryonic structures or the VE (Corson, et al. 2003). Furthermore, Maretto et al recently provided evidence against the idea that FGF signalling is involved in the *FLRT3*$^{-/-}$ phenotype (Maretto, et al. 2008). A marker gene analysis of typical FGF target genes in the early mouse embryo showed no altered expression in *FLRT3*$^{-/-}$ embryos. Furthermore, FLRT3 expression in wt embryos treated with a FGF specific inhibitor showed no difference. Also, embryos treated with an FGF signalling inhibitor did not show signs of the *FLRT3*$^{-/-}$ phenotype (Maretto, et al. 2008). Altogether, no evidence for FGFR dependent or independent alterations of cell numbers could be found in this study.

3.6. Ectopic induction of mesoderm markers in FLRT3$^{-/-}$ embryos

The induction of mesoderm is an important process during early embryonic development and usually occurs in the posterior region of the embryo at the newly formed PS (Liu, et al. 1999; Ben-Haim, et al. 2006). A hallmark of mesoderm induction is the expression of a well-characterized set of genes connected to mesodermal fate, such as *Bra/T*, *Eomes* or *FGF8*. Bra/T was the first T-box transcription factor described (Wilkinson, et al. 1990), and its role as a transcriptional activator has been well established (Kispert and Herrmann 1993). Amongst brachyury's transcriptional targets in *Xenopus* embryos is eFGF, which is equivalent to FGF4 in mice, where it is expressed in the PS (Isaacs, et al 1994; Isaacs, et al. 1995; Niswander and Martin 1992). Nonetheless, Bra/T has been shown to be a direct target of the Wnt/Beta-catenin pathway in mice (Arnold, et al. 2000). Indeed, regulation of Bra/T expression by FGF8 and FGF4, mediated by FGFR1 has been reported. However, this regulation occurs in an indirect fashion - E-cadherin sequesters Beta-catenin at the membrane and thereby suppresses its transcriptional activating functions, and is downregulted after FGFR1 activation through FGF4 or 8. Subsequently, beta-catenin is available to transduce wnt signalling (Yamaguchi, et al. 1999; Ciruna and Rossant 2001). Eomes, another T-box transcription factor, has been shown to precede *Bra/T* expression and is induced by TGF-beta like Nodal signalling (Ciruna, et al. 1999). Eomes in turn, has been shown to activate Nodal indirectly, possibly through Furin or SPC4, and thereby sustain a high level of Nodal signal, at least in the ExE. Nodal and Eomes act cooperatively to specify definitive endoderm in the anterior primitive streak (Arnold, et al. 2008). FGF8 has been shown to be important in mesoderm migration at the primitive streak through the FGFR1 dependent activation of snail (Sun, et al. 1999). Interestingly in FLRT3 mutant embryos, *Bra/T*, *FGF8* and *Eomes* have been found in the ectopically localized epiblast cells that protrude through the holes formed in the visceral and definitive endoderm. Although not all of the analyzed embryos showed the expression of mesoderm markers, the majority of embryos that displayed ectopic ectoderm also showed *Bra/T* expression (6 out of 8, see Figure 24). In addition, about half of the embryos analyzed showed ectopic *FGF8* expression. Together with the expression of *Eomes*, this suggests that loss of FLRT3 in the AVE potentially leads to ectopic induction of mesoderm in the anterior embryo.

Nodal/TGF-beta, Wnt and FGF signalling pathways are mainly responsible for the regulation of mesoderm induction and production (Arnold and Robertson 2009). Whereas FGF signalling functions in the delamination of mesoderm, Nodal and Wnt

signals are important inducers for mesoderm in the primitive streak. To restrict these inductive signals to the posterior of the embryo, the AVE secretes several Wnt and TGF-beta inhibitors such as Cer1, Lefty1 or Dkk1. The analysis of Wnt and TGF-beta inhibitors in *FLRT3*$^{-/-}$ embryos has shown that the expression of these inhibitors is not altered at ES to MS stage and also the expression of *Nodal* and *Wnt3* is not altered. Hence, it seems very unlikely that loss of FLRT3 causes deregulation of the Nodal or Wnt signalling pathway in the anterior embryo. Ectopic expression of *Bra/T* has been shown for *Cer1*$^{-/-}$:*Lefty1*$^{-/-}$ double mutant embryos (Perea-Gomez, et al. 2002), but only a subset of the embryos (one out of four) displayed ectopic *Bra/T* expression, unlike *FLRT3*$^{-/-}$ embryos, where a majority of embryos showed ectopic expression of mesodermal genes.

Although only the mRNA expression was analyzed and no differences were found, this does not ultimately exclude a lack of nodal inhibitor activity at local sites of the anterior embryo due to protein mis-localization. In light of the BM break down in the anterior of *FLRT3*$^{-/-}$ embryos (see below), it is important to note that growth factors can interact with extracellular matrix components to modulate their functions (reviewed in Macri, et al. 2007). Also, for Nodal it is known that Cripto, an EGF-CFC domain protein is needed as a coreceptor (Whitman 2001; Sakuma, et al. 2002). Although it is clear that Lefty competes with Nodal for the binding to Cripto and Cryptic (Chen and Shen 2004), there is still the possibility that interactions with the extracellular matrix may enhance or interfere with binding of Lefty or Nodal. On the other hand, Lefty1, Cer1 and Dkk1 are secreted as long-range inhibitors (Sakuma, et al. 2002; Glinka, et al. 1998; Belo, et al. 1997) and are able to suppress Nodal and Wnt signals in distances of more than 100 mm.

In *FLRT3*$^{-/-}$ embryos however, ectopic expression of *Bra/T* was detected already at early stages of the BM breakdown phenotype, involving an area of only a few cell diameters (see below; Egea, et al. 2008). Hence, it seems unlikely that a very local rupture of the BM will have such strong effects on Nodal or Wnt activity in the anterior embryo. Although it was recently shown that FLRT3 is a direct target of Nodal/Activin signalling in *Xenopus* and is involved in the Rnd1-mediated relocalization of C-cadherin from the cell membrane of animal cap cells (Ogata, et al. 2007), it seems unlikely that FLRT3 could act along the same pathway during mouse gastrulation. In mice, *FLRT3* and *Nodal* expression patterns in the embryonic region do not overlap (Egea, et al. 2008; Maretto, et al. 2008; this study). *FLRT3* expression was not detected in the PS region during gastrulation. Furthermore AVE cells, also in FLRT3 mutant embryos, displayed high levels of E-Cadherin in the cell membrane (Egea, et al. 2008).

3.7. The ectopic mesoderm marker expression is a consequence of ectopic basement membrane breakdown

Recently it became evident that a local breakdown of the anterior BM can cause ectopic mesoderm induction. In culture experiments using embryoid bodies, it was shown that loss of BM due to the lack of the Laminin gamma1 chain leads to premature differentiation of ectodermal cells into mesoderm, as visualized by enriched Bra/T and Snai2 expression (Fujiwara, et al. 2007). Solid evidence has been provided, that FLRT3 mutant embryos fail to maintain an intact BM at MS stage. In addition, it was shown that Brachyury protein was already evident in epiblast cells that have just encountered the BM breakdown (Egea, et al. 2008). This is in agreement with the finding that the ectopic expression of mesoderm markers in *FLRT3*$^{-/-}$ embryos is always localized to the "tips" of the ectopic ectoderm (see Figures 24 and 25). Interestingly, a recent publication has provided new insights into the timing of EMT events during gastrulation in chicken embryos. It is known that one of the several important steps for EMT is the local breakdown of the BM. Nakaya and co-workers have elegantly shown that the first event in avian gastrulation EMT is the breakdown of the BM, mediated by RhoA driven destabilization of microtubules (Nakaya, et al. 2008). A similar situation could be envisaged in the anterior of *FLRT3*$^{-/-}$ embryos. After the BM breaks down, a default mesodermal program is initiated, including the upregulation of mesodermal genes, foremost the expression of *Eomes* and *Bra/T*. Eomes has just recently been shown to be an important factor in EMT during mouse gastrulation. A conditional deletion of Eomes specifically in the embryonic region blocked the delamination of nascent mesoderm cells from the PS and the cells therefore accumulated in this region (Arnold, et al. 2008). Interestingly, the expression of mesoderm markers such as *FGF8* and *Snai1* was largely unchanged. Both factors are known to be important for the downregulation of E-cadherin. In the case of FLRT3 however, *Eomes* expression was seen in ectopically localized epiblast epithelium, but *Snai1* expression could not be detected. Possibly, Eomes and Snai1 need to cooperate in order to downregulate E-cadherin, allowing mesoderm cells to migrate (Arnold, et al. 2008).

In summary, the epithelial organization of these ectopically localized cells, the expression of *bona fide* mesoderm markers and the lack of *Snai1*, a typical EMT marker, suggest that loss of FLRT3 in the AVE induces ectopic mesoderm induction but the cells fail to detach. Unlike in the PS, EMT in the anterior of *FLRT3*$^{-/-}$ embryos cannot be completed. The cells remain in tight epithelial contact and fail to express *Snai1*, a key regulator for

EMT in general (Nieto 2002) and in the mouse PS (Carver, et al. 2001). It is obvious that the cells encounter different environments. In the PS, strong Nodal signalling is active, whereas in the anterior of *FLRT3*$^{-/-}$ embryos, according to the expression of Nodal and Wnt inhibitors, Nodal activity cannot be expected. Moreover, other signalling factors are also not present in cells of the anterior embryo, such as FGFR1, which is important for the maintenance of *Snai1* expression (Nieto 2002). Although *FGF8* expression is present, it does not seem to function as in gastrulation EMT.

Together, this suggests that the AVE, in addition to its well-established function in signalling, has an additional role in the developing mouse embryo. By an as yet unknown mechanism, FLRT3 is required in AVE cells to maintain the integrity of the BM and thereby inhibit ectopic EMT and mesoderm induction. As FLRT3 is absent in AVE cells, the underlying epiblast cells are able to protrude through the discontinuous BM and push aside the visceral endoderm cells and thereby populate the outside of the embryo. This may, in turn, lead to partial or entire development of the embryo outside of the visceral yolk sac and eventually will give rise to the aforementioned phenotypes observed at E8.5 to E10.5.

Interestingly, *FLRT3*$^{-/-}$ embryos analyzed for the expression of *Sox10*, a marker for neural crest cells (reviewed in Kiefer 2007), showed a distorted *Sox10* expression, especially at E9.5. This could reflect the overall poor condition of *FLRT3*$^{-/-}$ embryos at these stages. On the other hand, one could speculate about a link of FLRT3 with neural crest cells (NCC). Prior to migration, NCCs must delaminate from the neuroepithelium by EMT. Snai1 can be used as a marker for NCC formation (Mayor, et al. 1995). Perhaps FLRT3 also functions in a more general sense in EMT, not only by inhibiting EMT in the AVE. Either conditional gene targeting strategies, or additional tetraploid aggregation experiments are needed, to bypass the function of FLRT3 during gastrulation.

3.8. The involvement of FLRT3 in cell-matrix adhesion

The binding to an extracellular matrix is essential for epithelialisation and survival of cells. Especially during embryonic development, disturbances in the interaction of cells with a specialized ECM, the basement membrane (BM), lead to embryonic lethality (Yurchenco, et al. 2004; Miner 2004). In vitro experiments using embryoid body cultures have shown that a lack of BM leads to failures of differentiation of epithelial cells, and finally to apoptotic cell death (Li, et al. 2002). In recent years, cell surface receptors, such as integrins and dystroglycans, have been found to bind to the ECM (reviewed in Li, et al. 2003). Interestingly, neither integrins nor dystroglycans appear to be necessary for the assembly of the BM from its secreted components.

Human FLRT1 (and subsequently FLRT2 and FLRT3) was identified using an *in silico* screen for extracellular matrix proteins in human muscle tissue (Lacy, et al. 1999). Several recent studies have provided evidence that FLRT3 is upregulated after nerve injury and promotes neurite outgrowth (Robinson, et al. 2004; Tanabe, et al. 2003; Tsuji, et al. 2004). In addition, it has been suggested that overexpression of FLRT3 reduces cell adhesion by redistributing E-Cadherin (Ogata, et al. 2007). Also, in *Xenopus*, FLRT3 was shown to increase cell adhesion, and mediate cell sorting by homophilic interactions (Böttcher, et al. 2004; Karaulanov, et al. 2006). Nevertheless, an interaction of FLRT3 with the extracellular matrix could be possible. Unfortunately, none of the adhesion assays performed were able to give a clear answer to this question. Using HeLa cells overexpressing mouse FLRT3, a significant alteration of cell-matrix adhesion was not evident. Although the tracing of potentially FLRT3 positive cells by coexpression of GFP did not give reliable results, the possibility that FLRT3 may be involved in matrix binding cannot be ruled out. As Karaulanov and co-authors have shown, FLRT3 mediated cell sorting upon overexpression was cell line specific. HeLa cells did not show any increased cell sorting, whereas HEK 293T cells did (Karaulanov, et al. 2006; Egea, et al. 2008). As the mode of action of FLRT3 is still largely undefined, it cannot be ruled out that as yet unknown cofactors are essential for the function of FLRT3, which may not be present in all cell types. To circumvent this problem, MDCK cells endogenously expressing FLRT3 were used. In addition, an epithelial cell line, such as MDCK, seemed to better represent the *in vivo* events in the embryonic epithelia.

However, the relatively low transfection efficiency of this line, the difficulties in tracing transfected cells, and the large variations in the adhesion experiments argued against the use of transiently transfected MDCK cells. Unfortunately, using clonally selected

stable FLRT3 knockdown cell lines, no conclusive differences in matrix adhesion were evident. As the variations between individual experiments were considerably high and the binding of MDCK cells, especially to laminin, was unexpectedly low, problems in the experimental design and/or conductance seem likely. In addition, it can be doubted that possible effects are due to the specific knockdown of FLRT3 by the shRNA. In experiments using additional knock down cell lines, using the same or a second target sequence did not show consistent effects (data not shown). Similar results could be observed in a different assay system (see below).

3.9. A role for FLRT3 in HGF mediated MDCK cell scattering?

MDCK cells grown at low density in two dimensional culture form epithelial islands. Treatment of MDCK cells with HGF (previously called scatter factor) induces a so-called scatter response. These cells change their epithelial organization into a fibroblast like mesenchymal cell appearance and become migratory (Weidner, et al. 1990). To establish these changes, a complex program of rearrangements including the modulation of cell-cell and cell-matrix contacts, as well as changes in the actin cytoskeleton must be achieved. Using the ability to scatter as a cellular readout, the influence of FLRT3 on cell-cell adhesion can be tested. Growing MDCK cells on various substrates has been shown to result different scatter responses (Clark 1994). To avoid any influence of the proteins used for coating, MDCK cells were not grown on coated cover slips. This made the tracing of transfected cells using immunofluorescence staining not applicable. Therefore clonal cell lines stably expressing shRNA constructs targeting the endogenous FLRT3 expression were used for scatter assay experiments. Using two different shRNA constructs in four cell lines and three control mock cell lines, no conclusive effect of FLRT3 knockdown could be observed using scatter assays. Several possibilities may account for this. The most obvious explanation would be that the changes of scatter behaviour observed are due to clonal effects based on the derivation of the cell lines from single cells. It is known that variation in cell behaviour of gene expression can occur in cell lines generated by clonal selection (Oh, et al. 2003). Since only a low number of clones was utilized, which were derived from only two shRNA constructs, and a preliminary attempt to rescue the behaviour by overexpression of mouse FL-FLRT3 did not change the scatter behaviour (data not shown), it seems plausible that the observed effects are not due to a specific knock down of FLRT3 protein. Secondly, a variable reduction of FLRT3 protein levels during the culture time was apparent. Keeping cell lines in culture for more than three passages increased the measured protein level substantially (data not shown). Particularly in light of the relatively mild knockdown effect of the constructs used, this could falsify the experimental outcome. It has been reported that using virus mediated shRNA knockdown in MDCK cells can cause them to lose their ability to efficiently downregulate the target genes. This effect seems to be dependent on the respective target gene and a related possible growth disadvantage (Schuck, et al. 2004).

As these experiments can only be considered as pilot experiments, the appropriate controls for gene specific knockdown experiments are missing. Ideally, the use of scrambled oligonucleotide sequences and/or the use of an unrelated target sequence, such as the LacZ or luciferase genes, would be needed as appropriate controls in addition to the mock control. However, even such controls are not a guarantee to exclude so-called off-target effects, as has been shown previously (Mishra, et al. 2008). Furthermore, a rescue experiment would need to done. Finally, using a positive control, such as a cell adhesion molecule, would need to be included into the analysis of MDCK scatter assays as well. Using the strategy chosen for this study, no conclusive information regarding a participation of FLRT3 in cell-cell or cell-matrix events could be obtained.

From data obtained in the early mouse embryo (this study, Egea, et al. 2008) an involvement of FLRT3 in either cell-matrix adhesion of visceral endoderm cells, the maintenance of the BM, cell-cell adhesion of visceral endoderm cells or combination of those seems very likely. Further investigations using different techniques will be needed to answer the question of the cellular function of FLRT3 in this context.

3.10. Outlook

Although in the recent years, understanding of the function of FLRT3 has dramatically increased, many unanswered questions remain. The role of FLRT3 in *Xenopus* development has provided some insight into its involvement in important signalling systems. A biological role of FLRT3 during gastrulation in mouse has been demonstrated. However, the question of how FLRT3 acts at the cellular level still remains unresolved. To address this question, further studies using epithelial cell lines could be undertaken in order to find a possible role for FLRT3 in the establishment and/or maintenance of epithelial sheets. As well as cell-cell adhesion studies, the trans-epithelial resistance (TER) could be analysed in order to gain further information about the influence of FLRT3 on epithelial architecture. Additionally, the use of different cell lines that are better to transfect would be of assistance in these studies. Furthermore, the application of different gene knockdown strategies, either siRNA or viral infection using shRNA constructs, together with available human epithelial cell lines and pre-validated siRNA constructs, would help to answer questions about FLRT3 functions. Together with a redesigned adhesion assay procedure, the use of a shearing assay, where cells are actively removed from a coated surface by shearing forces, may allow the study of possible effects of FLRT3 on ECM interaction.

The possible signalling functions of FLRT3 are a second major question that remains. As yet, no evidence has been found that the interaction of FLRT3 with Rnd1 has functional importance in mouse development. At least for FGFR1, indirect evidence is available through the conditional ablation of FLRT3 in the Isthmus in mouse embryos (Jukkola, et al. 2006). These interactions would need to be verified either in heterologous systems or, ideally, in an *in vivo* situation, in mammalian embryos as well. Nevertheless, further studies are necessary in order to identify potential interaction partners, both extracellular and intracellular. Screening technologies, such as yeast two hybrid or even interaction proteomics screens, could be employed here. Of course, the validation of the potential interactors obtained would be a crucial step. For this, functional cell biological or biochemical assay systems would be necessary that provide a clear readout of FLRT function. Unfortunately these assays need to be further established, but an aggregation assay (Egea, et al. 2008) may prove useful. Also the function of the different domains present in the FLRT3 protein would be an interesting objective for further investigation. It has been shown that the intracellular part is necessary for interaction with Rnd1 and the transduction of FGFR signalling,

while the fibronectin type 3 domain (FN3) establishes the interaction with FGFR1. Nevertheless, the biological role remains unclear. Using different mutant versions of FLRT3, such as a deletion of the entire intracellular domain (deltaC) or a deletion of the FN3 domain (delta FN3), could provide interesting results about the cell biological role of FLRT3. Maybe even the use of different mutant FLRT3 knock in mouse lines could give important insights into the developmental function of FLRT3 *in vivo*.

In addition, the developmental roles of FLRT3 are probably not fully understood. The expression pattern of FLRT3 during and after organogenesis may suggest additional functions, for example in somite formation, neural crest cell production or nervous system development. The early lethality in these mice would need to be overcome using, for instance, conditional gene knockout strategies in combination with the appropriate cre recombinase expressing mouse lines.

In this context, the analysis of FLRT1 and FLRT2 could give important insights into the function of this LRR protein family. Although during early post implantation development, FLRT3 seems to be the most important member of this family, this does not exclude important functions for FLRT1 and FLRT2. Especially because of the observation that FLRT proteins can bind in a homotypic fashion and the comparably high degree of sequence similarity, a possible compensatory mechanism after the loss of one FLRT protein needs to be considered. Therefore a combination of different loss of function alleles might be required.

Research concerning FLRT family proteins opens a wide field for possible functions and importance in several biological processes. This may aid in the understanding of developmental processes in more detail. But so far, we are only at the beginning.

4. Material and Methods

4.1. Material

4.1.1. Chemical, enzymes and commercial kits

All chemicals used were purchased from Sigma, Merck, Fulka, Serva, Roth and Roche unless specified elswhere in the methods section. All water used to prepare buffers and solutions was filtered through a Milli-Q-Water System (Millipore). Restriction enzymes were purchased from New England Biolabs (NEB). Plasmid mini- and maxi-preparations were done using the QIAGEN QIAprep Spin Miniprep or the Plasmid Maxi kits, respectively. QIAquick PCR purification and Gel extraction kits were used for cloning procedures when necessary.

4.1.2. Mouse lines

FLRT3^{-} mouse line was generated by Joaquim Egea (Egea, et al. 2008) and maintained in a mixed Sv129xCD1 or Sv129xC57Bl/6 background (referred to as CD1 or C57xC57Bl/6, respectively). For experiments, the offspring of heterozygous intercrosses was used.

4.1.3. Bacteria

DH5α (Invitrogen)
TOP10 (Invitrogen)

4.1.4. Plasmids

Backbone/insert	Comments	Reference
Mammalian expression		
pcDNA3.1 FLAG		
JEN055	mouse FLRT3 FL (entire CDS)	J. Egea
cfFLRT3long	dog FLRT3 FL (entire CDS + 3'UTR + flag)	J. Egea
cfFLRT3short	dog FLRT3 FL (entire CDS w/o 3'UTR)	C. Erlacher
FLRT3ΔC GFP	mouse FLRT3 c-terminus replaced with GFP	J. Egea
pSUPER shRNA		
pSUPER	pSUPER retro puro	OligoEngine
RNAi11	sequence: `CTACAGAGACAGTGGTATT`	C. Erlacher
RNAi14	sequence: `GGTCAATGTACGTGGGCTT`	C. Erlacher
Riboprobes (ISH)		
Bra/T	for AS: digested BamHI; transcribed T7	B. Herrmann
Eomes	for AS: digested EcoRI; transcribed T7	H. Lickert
FGF8	for AS: digested PstI; transcribed T7	R. Dono
FGFR1	for AS: digested XbaI; transcribed T3	J. Partanen
FGFR2	for AS: digested XbaI; transcribed T3	J. Partanen
FLRT1	for AS: digested HindIII; transcribed SP6	J. Egea
FLRT2	for AS: digested EcoRI; transcribed SP6	J. Egea
FLRT3	for AS: digested BamHI, transcribed SP6	J. Egea
Foxa2	for AS: digested XbaI; transcribed SP6	K. Kaestner
Hoxb1	for AS: digested EcoRI; transcribed T3	R. Krumlauf
Krox20	for AS: digested BamHI; transcribed T3	P. Charnay
Lefty1/2	for AS: digested NdeI; transcribed T7	H. Lickert
Lim1/Lhx1	for AS: digested EcoRI; transcribed T7	T. Fujii
Meox1	for AS: digested XhoI ; transcribed SP6	Candia et al. 1996
Nodal	for AS: digested BamHI; transcribed T7	H. Lickert
Otx2	for AS: digested EcoRI; trnascribed SP6	E. Bonicelli
Snai1	for AS: digested XbaI; transcribed T3	A. Nieto
Shh	for AS: digested Xho; transcribed T3	T. Mäkinen
Sox10	for AS: digested BamHI; transcribed T7	R. Krumlauf
Wnt3	for AS: digested EcoRI; transcribed T3	H. Lickert

4.1.5. Antibodies

Primary antibodies

Antibodies	Species	Company	Application	Dilution
Anti-FLRT1 (#1160)	Rabbit polyclonal	Home made	WB	1:1000
Anti-FLRT2	Goat polyclonal	R&D	WB	1:1000
Anti-FLRT3 (#1134)	Rabbit polyclonal	Home made	WB	1:2000
Anti-FLRT3	Goat polyclonal	R&D	WB, IF	1:2000, 1:200
Anti-PHH3	Rabbit polyclonal	Upstate	IF, IHC	1:500
Anti-cleaved-caspase 3	Rabbit polyclonal	Cell signaling	IF, IHC	1:500
Anti-Tubulin	Mouse monoclonal	SIGMA	WB	1:10000
Anti-E-Cadherin	Mouse monoclonal	R&D	WB	1:2000
Anti-GATA4	Goat polyclonal	Santa Cruz	IHC	1:1000

Secondary Antiboidies

Antibody		Species	Company	Application	dilution
Anti mouse	HRP	Sheep polyclonal	Amersham	WB	1:5000
	Cy2	donkey	(GE)	IF	1:300
	Cy3	donkey	Jackson	IF	1:300
			Jackson		
Anti-rabbit	HRP	Goat polyclonal	Amersham	WB	1:2000
	Cy2	donkey	(GE)	IF	1:300
	Cy3	donkey	Jackson	IF	1:300
	biotin	Sheep	Jackson	IHC	1:1000
			Vector		
Anti-goat	HRP	Rabbit polyclonal	DAKO	WB	1:2000
	Cy2	donkey	Jackson	IF	1:300
	Cy3	donkey	Jackson	IF	1:300
	biotin	horse	Vector	IHC	1:1000

4.1.6. Gene names and symbols

MGI – Mouse Genome Informatics (http://www.informatics.jax.org/)

4.1.7. Buffers and solutions

4.1.7.1. Buffers and solutions for cell transfection

2 M $CaCl_2$ $CaCl_2 \cdot 2H_2O$ 5.88 g
H_2O to 20 ml added.
filter sterilized through 0.22 µm membrane, stored as 5 ml aliquots at -20 °C

2x BES-buffered saline (2xBBS) pH 6.96

50 mM BES	1.07 g
280 mM NaCl	1.60 g
1.5 mM $Na_2HPO_4 \cdot 2H_2O$	0.027 g

100 ml H_2O added, pH of solution adjusted to pH 6.96
aliquots of 40 ml stored at -20°C

4.1.7.2. Solutions for agarose gel electrophoresis

50x TAE
2 M Tris acetate
50 mM EDTA

Gel loading buffer

50% Glycerol	25 ml 100% Glycerol
1x TAE	1 ml 50x TAE
Orange G	0.1 g
H_2O	24 ml

4.1.7.3. Solutions and buffers for western blot analysis

Lysis buffer 2x

40 mM Tris/HCl pH 7.5	20 ml 1 M Tris/HCl pH 7.5
240 mM NaCl	24 ml 5 M NaCl
20% Glycerol	100 ml Glycerol
2% Triton X100	10 ml Triton X100

H_2O to 500 ml added, stored at 4 °C

Supplemented lysis buffer

1x lysis buffer	15 ml 2x lysis buffer
25 mM NaF	3 ml 250 mM NaF (0.55 g in 50 ml H_2O)
20 mM NaPP	3 ml 200 mM NaPP (4.461 g in 50 ml H_2O)
1 mM Na_3VO_4	300 µl 100 mM Na_3VO_4
Protease inhibitor cocktail tablet (Complete, Roche)	1 tablet
H_2O to 30 ml added	

SDS PAGE separating gel 7.5% (10 ml)

H2O	4.85 ml
1.5M Tris pH 8.8, 0.4% SDS	2.6 ml
30% w/v Acrylamid/Bisacrylamid	2.5 ml
10% APS	50 µl
TEMED	5 µl

SDS PAGE stacking gel 4% (5 ml)

H2O	3.05 ml
1.5M Tris pH 6.8, 0.4% SDS	1.30 ml
30% w/v Acrylamid/Bisacrylamid	0.65 ml
10% APS	50 µl
TEMED	5 µl

6x Sample buffer for reducing conditions

12% SDS	3.6 g SDS
300 mM Tris-HCl pH 6.8	6 ml 1.5 M Tris-HCL pH 6.8
600 mM DTT	2.77 g DTT
0.6% BPB	0.18 g BPB
60% Glycerol	18 ml Glycerol
H_2O to 30 ml added, stored as 500 µl aliquots at -20°C	

5x Electrophoresis buffer

Tris base	154.5 g
Glycine	721 g
SDS	50 g
H_2O to 10 l added, stored at RT	

Protein transfer buffer

Tris base	3.03 g
Glycine	14.40 g
MetOH	200 ml
H_2O to 1 l added	

Tris buffered saline (TBS)

120 mM NaCl	24 ml 5 M NaCl
20 mM Tris pH 7.5	20 ml 1 M Tris-HCl pH 7.5
H_2O to 1 l added	

TBST

120 mM NaCl	24 ml 5 M NaCl
20 mM Tris pH 7.5	20 ml 1 M Tris-HCl pH 7.5
0.1 % Tween20	1 ml Tween20
H_2O to 1 l added	

Blocking solution

5% skim milk	2.5 g skim milk powder
50 ml TBST added	

Stripping buffer

5 mM Na_2HPO_4	1.25 ml 1 M Na_2HPO_4
2% SDS	25 ml 20% SDS
0.02% ß-Mercapto Ethanol	50 µl ß-ME added
H_2O to 250 ml added	

4.1.7.4. Solutions for in situ hybridization

Proteinase K 20 mg/ml (w/v)

100 mg Proteinase K

H_2O to 5 ml added, stored as 50 µl aliquots at -20 °C

Formamide, deionized

50 g Resin AG 501-X8 (BIO-RAD)

1 l Formamide

stirred for 40 min, filtered and stored as 45 ml aliquots at -20 °C

Heparin

50 mg/ml (w/v)	500 mg Heparin
H_2O to 10 ml added	

4 M $LiCl_2$ 16.96 g $LiCl_2$
H_2O to 100 ml added

5% CHAPS (w/v) 2.5 g CHAPS
H_2O to 50 ml added

0.5 M EDTA, pH 8.0 1 8.61 g $Na_2EDTA{\cdot}2H_2O$
H_2O to 100 ml added, adjusted to pH 8.0 using 5 M NaOH

20x SSC
69.2 g Sodium Citrate
13.7 g Citric acid
175 g NaCl
H_2O to 1 l added, adjusted to pH 4.5, autoclave and store at RT

5x Maleic Acid Buffer (MAB)
58 g Maleic acid
44 g NaCl
30 g NaOH pellets
H_2O to 1 l added
adjusted to pH 7.5 using 5 M NaOH, stored at 4 °C

MABT 1x MAB
50 ml 5x MAB
0.1% Tween20 2.5 ml 20% Tween20
H_2O to 500 ml added

Prehybridisation Solution

50% deionized Formamide	10 ml deionized Formamide
5x SSC	5 ml 20x SSC
0.2% Tween20	200 µl 20% Tween 20
0.5% CHAPS	2 ml 5% CHAPS
5 mM EDTA pH 8.0	200 µl 0.5 M EDTA pH 8.0
50 µg/ml Heparin	20 µl 50 mg/ml Heparin
50 µg/ml tRNA	100 µl 10 mg/ml yeast tRNA (SIGMA)
0.2% Blocking Reagent	0.4 g Blocking Reagent (Roche)

RNase free H_2O to 20 ml added, dissolved at 70 °C

Solution I

50% deionized Formamide	20 ml deionized Formamide
5x SSC	10 ml 20x SSC pH 4.5
0.2% Tween20	400 µl 20% Tween20
0.5% CHAPS	4 ml 5% CHAPS
H_2O to 40 ml added	

Solution II

50% deionized Formamide	20 ml deionized Formamide
2x SSC	4 ml 20x SSC
0.2% Tween20	400 µl 20% Tween20
0.1% CHAPS	800 µl 5% CHAPS
H_2O to 40 ml added	

Solution III

2x SSC	4 ml 20x SSC
0.2% Tween20	400 µl 20% Tween20
0.1% CHAPS	800 µl 5% CHAPS
H_2O to 40 ml added	

Blocking Solution

1x MAB	4 ml 5x MAB
0.2% Blocking Reagent	0.4 g Blocking Reagent (Roche)
20% Lamb serum	4 ml Lamb serum
0.1% Tween20	100 µl Tween20

H_2O to 20 ml added. Blocking reagent dissolved in H_2O and MAB at 70 °C before adding serum and Tween20.

NTMT

0.1 M NaCl	0.4 ml 5 M NaCl
0.1 M Tris pH 9.5	2 ml 1 M Tris pH 9.5
0.05 M $MgCl_2$	1 ml 1 M $MgCl_2$
0.1% Tween20	100 µl 20% Tween20
H_2O to 20 ml added	

Developing Solution

105 µg/ml NBT	14 µl 75 mg/ml NBT (in 70% DMF)
55 µg/ml BCIP	11 µl 50 µg/ml BCIP (in 100% DMF)
10 ml NTMT added	

Paraformaldehyde 4%

40 g Paraformaldehyde
add H_2O to 900 ml heated to 70 °C
200 µl 5 M NaOH
stirred until dissolved
100 ml 10x PBS
stored as aliquots of 50 ml at -20 °C

4.1.7.5. Solutions for Immunostaining

0.1 M Citrate buffer

0.1 M Citric acid	21 g citric acid monohydrate
0.1 M Na_3Citrate	29.4 g Na_3Citrate

H_2O to 1 l added, adjusted to pH 6.0

4.1.8. Media

4.1.8.1. Media and Antibiotics for bacterial culture

LB (Luria-Bertani) media

10 g Bacto-Trypton
5 g Yeast extract
5 g NaCl
H_2O to 1 l added, adjusted to pH 7.5

SOC

10 g Bacto-Tryptone
2.5 g Bacto-Yeast extract
0.25 g NaCl
5 ml 250 mM KCl
2.5 ml 2 M $MgCl_2$
H_2O to 500 ml added, adjusted to pH 7.0. 10 ml 1 M sterile Glucose solution added.

LB plates LB media supplemented with 15g/l agar

Antibiotics diluted 1:1000 from stock solutions

Ampicillin	100 mg/ml in H_2O
Kanamycin	50 mg/ml in H_2O

4.1.8.2. Mammalian cell culture media, reagents and growth factors

HeLa cells	DMEM (high glucose), 10% FBS, 1% Glutamine, 1% Penicillin/ Streptomycin
MDCK cells	MEM with Earle's salt and Non Essential Amino Acids (NEAA), 10% FBS, 1% Glutamine, 1% Penicillin/Streptomycin
Stable MDCK cells	MEM with Earle's salt and Non Essential Amino Acids (NEAA), 10% FBS, 1% Glutamine, 1% Penicillin/Streptomycin, 4 µg/ml Puromycin

4.1.9. Oligonucleotides

All oligonucleotides were purchased from Eurofins MWG/operon (formerly MWG-Biotech, Germany; http://www.eurofinsdna.com) and purified with HPSF

Genotyping

JEF11	5'GCTTATACTACAAGGGTCTCATGTGAAGCG3'
JER12	5'GGCTGCAGGAATTCGATATCAAGCTTATCG3'
JER19	5'CCGGTACTAAGAAAGACAACTCCATCCTGG3'

shRNA

F3RNA_fwd11	5'GATCCCCCTACAGAGACAGTGGTATTTTCAAGAGAAATACCACTGT CTCTGTAGTTTTTA3'
F3RNA_rev11	5'AGCTTAAAAACTACAGAGACAGTGGTATTTCTCTTGAAAATACCAC TGTCTCTGTAGGGG3'
F3RNA_fwd14	5'GATCCCCGGTCAATGTACGTGGGCTTTTCAAGAGAAAGCCCACGTA CATTGACCTTTTTA3'
F3RNA_rev14	5'AGCTTAAAAAGGTCAATGTACGTGGGCTTTCTCTTGAAAAGCCCAC GTACATTGACCGGG3'

Cloning

Rv_Tag	5'CTCCACTCGAGTGAGTGCGAGTGATCTGAGTCTGG3'
BH_I_FW_CF	5'CGACGGATCCGTGTACAAAGACCTTAACACTGC3'
Rv_notag	5'GTCTGCCTCGAGGCCTCCAGCATCATGAGTGC3'

4.2. Methods

4.2.1. Animal handling and experiments

Mice were handled an dissected as described previously (Hogan, 1994. Manipulating the Mouse Embryo: A Laboratory Manual). Embryos were staged according to Downs and Davies 1993.

4.2.1.1. Dissections

E6.5-E7.5 embryos

Pregnant female mice were sacrificed by cervical dislocation 6 or 7 days after a clearly visible plug was detected. Entire uteri were dissected out and transferred to ice cold PBS (RNAse free for whole mount *in situ* hybridization). The mesometrium was removed using fine tip forceps (Fine Science Tools FST) and the containing decidual tissue was dissected out. The This tissue was cut in the distal third using fine tip forceps. Distal to proximal cuts were performed in such a way that the embryo contained in Reichert's membrane, and attached to the ectoplacental cone, could be removed from the surrounding decidual tissue. Reichert's membrane was carefully removed using the forceps to allow later genotyping. Embryos were then transferred into a glass vial and fixed with 4% PFA O/N at 4 °C

E8.5-E10.5 embryos

After sacrificing the pregnant female, the entire uterus was taken out and kept in ice cold PBS (RNAse free for whole mount *in situ* hybridization) for further dissection. The mesometrium was carefully removed and the contained uterus/decidua carefully opened using fine tip forceps (FST). The visceral yolk sack and amnion were removed from the embryo. The yolk sack was washed twice with cold PBS and collected for genotyping purposes. Embryos were collected individually in 24 well plates and fixed over night at 4 °C with 4% PFA.

4.2.1.2. Genotyping

To determine the genotype of mice and embryos, a PCR based strategy was applied. Tail biopsies of weaned mice were taken and lysed by boiling three times for 15 min at 95 °C in

100 µl 50 mM NaOH with vigorous vortexing in between the boiling steps until the tissue has dissolved. Lysates were neutralized using a 1/10 volume of 1.5 M Tris/HCl pH 8.8 and served as templates for the PCR reaction. Similarly, entire embryos (E6.5), extraembryonic tissue (E7.5) or visceral yolk sacks (E8.5-E10.5), were lysed in 50 mM NaOH to obtain template DNA for the PCR reaction. The total volume of NaOH used, was adjusted according to the tissue size (10-20 µl for E6.5-E7.5 embryos and 30-50 µl for E8.5-E10.5 visceral yolk sacks). Lysates were used immediately for PCR reaction or stored at -20 °C. PCR reactions were performed in a total volume of 50 µl and contained 2.5 mM dNTPs, 50 mM forward (JEF11) and mutant reverse primer (JER19), and 10 mM wildtype reverse primer (JER12), in order to amplify specific DNA sequences in the genome; 1x PCR buffer (NEB), 2 µl Taq DNA polymerase (non commercial) and 2-5 µl of template DNA (depending on the starting material).

To determine the genotype of embryos contained in the deciduum, an immunofluorescence approach was used. While cryosectioning, the collection of every 5th-10th section of the respective embryo created a "genotyping slide". This slide was used to perform immunofluorescence staining using the α-FLRT3 antibody (R&D) and a donkey α-goat secondary antibody conjugated with Cy2. This was combined with phalloidin and DAPI staining to get additional information about the embryonic morphology. All embryos, where FLRT3 staining was clearly absent were considered *FLRT3*$^{-/-}$ embryos whereas embryos showing FLRT3 staining were considered control embryos. Using this method, it is virtually impossible to distinguish between *FLRT3*$^{+/+}$ and *FLRT3*$^{+/-}$ embryos.

4.2.1.3. Processing of embryos.

For immunohistochemistry, ES-LS embryos (E6-E7) were kept within the deciduas for further cryosectioning. Deciduas containing the embryos were fixed in 4% PFA for up to 2 hrs at 4 °C, washed three times with cold PBS and transferred to 20% Sucrose in PBS for cryoprotection over night at 4 °C.

For whole mount in situ hybridization, embryos were dissected out of their deciduas and fixed O/N at 4 °C in 4% PFA. After fixation, embryos were washed three times using cold PBS and then dehydrated using a graded series of methanol (25%, 50%, 75% and 100%) diluted in PBS.

4.2.2. Histology

4.2.2.1. Cryosectioning

Fixed embryos or deciduas were cryoprotected by an overnight incubation with 20% sucrose in PBS at 4 °C. Prior to embedding, embryos were incubated in a mixture of

20% sucrose solution and Tissue-Tek OCT (Sakura; 1:1 ratio) for 1.5 hrs with gentle rotation. For embedding, embryos were transferred to OCT and kept in a mold on ice. Specimens were oriented under a stereomicroscope and frozen in Tissue-Tek OCT on dry-ice. Frozen blocks were stored at -80 °C. Cryosectioning was performed using a Leica CM3050 S cryostat at temperatures of -22 °C to -25 °C. Usually, sections with 7 to 10 µm thickness were cut and collected individually on SuperFrost Plus slides (Menzel-Glaeser). Slides were stored at -20 °C.

4.2.2.2. Paraffin sectioning

After fixation, embryos were washed with PBS and dehydrated through a graded series of ethanol ranging from 0 – 70% ethanol in PBS. Embryos can bewere stored in 70% ethanol for several days up to weeks. Dehydration was completed by two 30 min washing steps with 96% Ethanol and two 30 min washing steps with 100% ethanol. For better visualization a few drops of eosin (Accustain, Sigma) were added to the last ethanol washing step. Embryos were briefly rinsed with 100% ethanol to remove Eosin remains, followed by two xylol-Ersatz (Vogel) incubation steps of up to 15 min, depending on the size of embryo. Embryos were transferred into prewarmed (65 °C) liquid Paraplast (Sherwood Medical/Sigma) for at least 2 hrs, which was changed three times. Embryos were oriented using prewarmed forceps in the liquid paraplast. Paraffin blocks were stored at ambient temperature. 5 to 10 µm thick sections were cut on a Jung Supercut 2065 microtome and collected as ribbons. Ribbons were transferred to SuperFrost Plus slides (Menzel-Glaeser) moistened with 20% ethanol and dried on a warm plate at 45 °C. Slides were stored at ambient temperature.

4.2.2.3. H&E staining

Paraffin sections were dewaxed in xylol-ersatz (Vogel) for two times 10 min, followed by rehydration steps through a graded series of ethanol, namely specifically once 5 min and once 3 min 100% ethanol, once 3 min 96% ethanol and once 70% ethanol. Two 3 min washing steps with demineralized water were followed by a 5 min incubation with haematoxilin (Accustain; Sigma). The slides were washed in running tap water for 5 min, submerged for 10 sec in 1% HCl in 70% ethanol, rinsed with tap water and incubated for 10 sec with 0.1% $LiCO_3$. Before incubating the slides for 5 min with eosin (Accustain; Sigma), slides were washed with tap water. To finish the staining procedure, sections were dehydrated through a series of ethanol steps starting with 70% ethanol for 5 min, 96% ethanol for 3 min, 100% ethanol for 3 min and a second time 100% ethanol for 5 min. Finally slides were incubated two times for 10 min in xylol-ersatz and mounted with a non-aqueous mounting media.

4.2.3. Molecular Biology

4.2.3.1. Preparation of plasmid DNA

Plasmid DNA was purified in a small scale (minipreparation, 4 ml) or in a large scale (maxipreparation, 100 ml) from bacterial cultures. Cultures in LB media, containing 100 µg/ml ampicillin or kanamycin, were inoculated using a single colony of transformed bacteria and grown at 37 °C overnight. Harvesting and further processing of the bacterial cultures for preparation was done according to the manufacturer's protocol. DNA concentration was determined using a spectrophotometer, measuring the absorbance at a wavelength of 260 nm.

4.2.3.2. Generation and labeling of riboprobes for *in situ* hybridization

Digoxigenin-labeled riboprobes were generated using plasmid DNA, containing the respective cDNA flanked by RNA polymerase promoter-sites at the 5' and 3' ends. Sense riboprobes were generated by linearizing the plasmid at the 3' end and using the RNA-polymerase site located at the 5' end of the cDNA. Likewise, AS riboprobes were generated by linearizing the plasmid at the 5' end and using the 3' RNA polymerase site. Linearization of 5µg plasmid DNA was followed by a phenol/chloroform extraction step to purify the linearized DNA. To check the quality and efficiency of the linearization and purification, agarose gel electrophoresis was performed. Linearized DNA was stored as 4 µl aliquots at -20 °C.

For in vitro transcription of RNA, 4 µl of linearized plasmid DNA was used in 20 µl transcription reactions together with 2 µl dig-RNA labeling Mix (Roche), 2 µl transcription buffer (Roche), 2 µl DTT 0.1 M, 1 µl RNAse Inhibitor (Roche), 1 µl RNA Polymerase (T3, T7 or SP6; Roche) and 8 µl RNAse free H_2O. After 3-4 hrs incubation at 37 °C, the transcription efficiency was assessed using agarose gel electrophoresis. RNA was precipitated by centrifugation at 4 °C using 100 µl TE buffer, 10 µl LiCl 4 M and 300 µl EtOH 100%. The pellet was washed twice using 70% EtOH and dried on ice afterwards. After resuspending the pellet in 100 µl TE, the riboprobes were stored as 25 µl aliquots at -80 °C

4.2.3.3. Whole mount *in situ* hybridization

Embryos stored at -20 °C in 100% methanol were rehydrated through serial methanol steps, starting with 6% H_2O_2 in 80% methanol for 1 h at RT, followed by 50% and 25% methanol in PBS for 5 min each. After three washes with PBT, embryos were treated with proteinase K at RT (digestion time dependent on size/stage of the embryos used – see table below). Embryos were rinsed twice with PBT and postfixed for 40 min using 4% PFA + 0.2% glutaraldehyde in PBS (freshly prepared) on ice. Prehybridization in prehyb-solution was carried out at 70 °C for 1 h after rinsing the embryos twice with PBT at RT. Riboprobes were diluted in prehyb-solution (hybridization-solution)

and embryos were incubated O/N with hybridization-solution at 70 °C with gentle rocking, unless otherwise indicated. On the second day, four washing steps of 20 min with solution I, four washing steps of 20 min with solution II and four washing steps of 20 min with solution III were carried out at 70 °C with gentle agitation. For some riboprobes, an RNase A digestion was carried out for 1 h at 37 °C using 20 µg RNase A diluted in solution III. In these cases, the fourth wash with solution III was omitted. After two 5 min washing steps with MABT at RT, two additional washing steps at 37 °C for 30 min using MABT were performed. Embryos were blocked in blocking solution at RT for 90 min and incubated with anti dig-FAB, conjugated with alkaline phosphatase (Roche), and diluted 1:2000 in blocking solution O/N at 4 °C. On the third day, the embryos were washed 9 times 30 min with MABT at RT, followed by two times 15 min washing steps using NTMT to equilibrate embryos to pH 9.5. NBT/BCIP (Roche) diluted in NTMT or BMPurple (Roche) were used as substrates for the alkaline phosphatase. The developing reaction was carried out at RT during the day or at 4 °C O/N until strong specific staining and no or low background was detected. The staining reaction was stopped by washing the embryos three times 5 min at RT and embryos were subsequently postfixed with 4% PFA O/N at 4 °C. The embryos were stored in PBS for future imaging or further processing.

Embryonic stage	Digestion time
E6.5	3 min
E7.5	4 min
E8.5	8 min
E9.5	15 min

4.2.3.4. Further processing of embryos stained by WISH

After postfixation, some embryos underwent a clearing procedure to diminish background staining. Embryos were washed 3 times for 5 min with PBT, followed by a 1 h wash with 50% ethanol in PBST, and an overnight incubation in 100% ethanol at 4 °C. The following day, embryos were rehydrated using 50% ethanol in PBT for 1 h and washed 3 times for 5 min with PBT. A 20 min wash with 25% glycerol in PBT was followed by incubation with 50% glycerol in PBT for up to 3 days at 4 °C. Embryos were returned to PBS via a 20 min washing step using 25% glycerol in PBT. Images of whole mount embryos were taken prior to genotyping and/or cryosectioning.

4.2.4. Cell culture

Cell lines used in this study were standard HeLa and MDCK cells. Cells were grown on Falcon plastic tissue culture dishes in high glucose DMEM or MEM + Earles salt and NEAA for HeLa and MDCK, respectively. Cells were passaged every 3 to 4 days by washing twice with PBS containing no Ca^{2+}/Mg^{2+}, detaching cells using trypsin/EDTA, pelleting by gentle centrifugation and resuspending in fresh growth medium. Cells were usually reseeded in a 1:10 ratio. MDCK cells were frozen in 25% FCS and 10% DMSO in MEM. Cells were kept for 24 hrs at -80 °C in designated freezing containers and then transferred to liquid nitrogen for longer term storage.

4.2.4.1. Adhesion Assays

Non tissue culture grade 96 well microtiter plates were coated with different extracellular matrix proteins at various concentrations by diluting them in PBS containing Ca^{2+} and Mg^{2+}. For coating, 50 µl of the respective dilutions were dispensed into each well and plates were kept overnight at 37 °C in an incubator. Plates were washed twice with PBS containing Mg^{2+} and Ca^{2+} and then blocked for 2 hrs using 1% BSA in PBS. Before seeding the cells, blocking solution was exchanged for 50 µl 1% BSA in culture medium. Cells were detached from the culture plate using PBS without Ca^{2+} and Mg^{2+} containing 5 mM EDTA and resuspended in culture media at a concentration of $2x10^5$ cells/ml. Using a multichannel pipette, cells were seeded on the plate and allowed to settle for 30 min. Plates were washed three times with PBS using a multichannel pipette and fixed for 30 min at RT with 4% PFA. After two washes using PBS, cells were stained for 20 min with 5% crystal violet in 20% methanol. Plates were washed extensively using tap water, dried overnight and the dye solubilized using 100 µl 100 mM acetic acid for photometric analysis. The relative number of adhered cells was determined by measuring the absorbance at 570 nm using a multiplate photometer (Genios; TECAN) and compared to an internal control (no cells seeded). The remaining cells after seeding were used for expression level analysis by western blotting. All conditions were done at least in triplicate. If not indicated otherwise, data represents the average of at least three experiments. Statistical significance was tested using the Student's *t-test*.

4.2.4.2. MDCK Scatter Assay

60-72 hrs prior to the experiment, $2x10^2$ cells were seeded in a 60 mm culture dish and allowed to grow as colonies of 3-6 cells. Growth medium was replaced with MEM containing 5% FBS and 20 ng/ml recombinant HGF (R&D). 12-24 hrs later, cells were washed twice using PBS, fixed for 10 min at RT using 100% methanol and stained for 1 h with 10% Giemsa-solution . After extensive washing, plates were dried overnight and stored at RT for further analysis.

The plates were counted blind to the respective conditions. The number of "scattered" colonies was compared to the total number of colonies present. A single colony was counted as "scattered" if more than 60% of the cells have lost cell-cell contacts, gained fibroblast like morphology and begun to migrate. Each condition in a single experiment was done at least in triplicate. Data shown represents a mean of at least three independent experiments, if not indicated otherwise. Statistical significance was tested using the Student's *t-test*.

4.2.4.3. Knockdown experiments in MDCK cells

For RNAi-mediated gene knockdown, the vector based pSUPER short hairpin RNA (shRNA) system (OligoEngine) was chosen. For the design of the antisense RNA oligonucleotides, the Dharmacon siDESIGN Center web-based algorithm (http://www.dharmacon.com/DesignCenter/DesignCenterPage.aspx) was used. Short hairpin oligonucleotides were ordered and cloned into the pSUPER retro-puro vector according to manufacturer's instructions. To test the knock down efficiency of each individual shRNA vector, co-transfection experiments with the target gene and the shRNA vectors were performed in HeLa cells and protein levels analyzed by western blotting.

4.2.4.4. Establishment of stable cell lines

To generate clonal cell lines stably expressing shRNA constructs targeting the FLRT3 expression, MDCK cells were transfected with the respective shRNA vectors using LF2000 (Invitrogen) according to the manufacturer's instructions. Two days after transfection, cells were split and reseeded into selection media, containing 4 µg/ml puromycin in 10 cm tissue culture dishes. Cells were selected for puromycin resistance for 8 to 10 days, until individual cell colonies of a size of about 100 cells could be identified. Cells were detached using PBS without Ca^{2+} and Mg^{2+} and a pipette tip. These colonies were transferred individually into 96 well plates, trypsinized and fed with fresh selection media. Cells were further passaged through 48 well and 24 well plates, until the cells could be transferred to 60 mm cell culture dishes. From the 60 mm dishes, cells were frozen down for storage in liquid nitrogen (as described previously). Cells were grown continuously in selection media. To test the expression of FLRT3 in the individual cell lines, samples were taken and analyzed by western blot. For shRNA construct RNAi11 and RNAi14, a total of 13 and 11 cell-lines were established, respectively.

4.2.4.5. Transfection

$CaPO_4$

The day before transfection, cells were passaged to reach the desired density. For transfection of HeLa cells, the desired amount of vector DNA was mixed with sterile H_2O and 125 mM $CaCl_2$ (final concentration), ½ volume 2x BBS (pH 6.96) was added and gently vortexed immediately. Transfection mix was incubated at RT for 20 min to allow complex formation and was added slowly to the cells. Expression was analysed 24 – 48 hrs after transfection

Lipofectamine 2000

Transfection using Lipofectamine 2000 (Invitrogen) was mainly used for the epithelial MDCK cell line. Cells were grown to 70-90% confluence. Transfection was done according to manufacturer's instructions. Briefly, Lipofectamine 2000 was used in a ratio of 1:2.5 relating to DNA (µg) and Lipofectamin2000 (µl). Lipofectamine 2000 and DNA were diluted in different vials using OptiMEM1+Glutamax and kept separate for 5 min at RT. Afterwards, both solutions were mixed and allowed to stand at RT for 20 min before the application to cells. Culture medium was exchanged 5 hrs after transfection. The next morning, cells were washed with PBS and new culture media was added. Usually cells were processed or analyzed 24-72 hrs after transfection.

4.2.5. Biochemistry

4.2.5.1. Cell lysis

Cultured cells were placed on ice, washed twice with ice-cold PBS and incubated for 10 min on ice with supplemented lysis buffer and gentle agitation (for amounts of lysis buffer see table below). Cell lysates were collected with a pipette tip, transferred to clean reaction tubes and further incubated for 20 min at 4 °C on a rotating wheel. Cell debris was pelleted by centrifugation for 10 min at 16,000g and 4 °C. The cleared lysates were transferred to clean reaction tubes, used immediately or frozen in liquid nitrogen and stored at -80 °C. Protein concentration was determined using the DC Protein Assay (BioRad) according to manufacturer's instructions.

Plate size	**Volume lysis buffer**	
	HeLa cells	MDCK cells
30 mm dish		200 µl
60 mm dish		500 µl
100 mm dish	300 µl	1000 µl

4.2.5.2. Lectin pull down

To enrich glycoproteins, wheat germ agglutinin (lectin) coupled agarose beads were incubated with similar amounts of protein from different TCL for 4 hrs at 4 °C. After incubation, beads were washed three times with supplemented lysis buffer. Finally, lysis buffer was removed, 6x loading buffer (LB) added and samples were boiled for 5 min at 95 °C. After a final centrifugation step, the agarose bead free supernatant was used for further analysis.

4.2.5.3. Western blotting

Protein lysates (TCL) or samples obtained from lectin pull down experiments were resolved by SDS PAGE according to standard procedures and transferred to nitrocellulose membranes (Protran, Schleicher&Schuell) by semi-dry blotting at 1 mA/cm2 of membrane surface for 30-90 min. Protein transfer was confirmed by a brief incubation with PonceauS (Serva). Membranes were blocked at RT for 1 h with 5% skim milk in TBST, followed by primary antibody incubation for 1 h at RT or overnight at 4 °C. Membranes were washed three times for 15 min with TBST before the secondary antibody, coupled to HRP was applied at RT for 1 h. Subsequently, membranes were washed three times with TBST for 15 min before incubation with ECL solution (GE healthcare /Santa Cruz) for 1 min and exposing to X-ray films (Kodak, GE healthcare). Membranes were reprobed for several antibodies without prior stripping if the primary antibodies were raised in different species. If necessary, membranes were stripped in stripping buffer for 30 min at 65 °C. After stripping, membranes were blocked again and treated as described above.

4.2.6. Microscopy

4.2.6.1. Stereomicroscopy and Epifluorescence Microscopy

To image embryos stained by whole mount in situ hybridization, whole mount antibody staining or unstained whole mount embryos, a Leica MZFLIII stereomicroscope connected to a Leica DC500 digital camera was used. Histological sections of whole mount in situ hybridizations where analyzed using a Zeiss Axioplan2 upright microscope connected to a SPOT RT slider color digital camera using bright field or DIC illumination for a better spatial impression. Immunofluorescence images were also acquired using a Zeiss Axioplan2 upright microscope connected to a SPOT RT monochrome digital camera. Images were acquired using MetaMorph software (Universal Imaging; Version 7 and earlier versions). For Image processing MetaMorph, ImageJ and Adobe Photoshop (CS2 and earlier versions) were used.

4.2.6.2. SEM

For SEM examination, embryos at different stages, ranging from E7.5 to E10.5, were dissected and genotyped as described elsewhere. In order to identify the embryos at later stages of the analysis, bright field images were taken using a stereomicroscope. Embryos were fixed over night, using 4% glutaraldehyde in PBS at 4 °C and subsequently dehydrated, using a graded series of ethanol. Embryos were stored in 70% ethanol. Final dehydration was carried out just before further processing the embryos using 96% ethanol and 100% ethanol dried with $CaCl_2$. For dehydration of older embryos, acetone was used instead of ethanol. Embryos were critical point dried using a Polaron E300 CP drier from CO_2 and carefully mounted on aluminum stubs covered with adhesive carbon foil. Before imaging using a Leo 1430VP scanning electron microscope, embryos were coated with a thin layer of gold using a Biorad SEM coating system (2.4 kV, 20 mA, 120 sec). Digital SEM images taken at 10-30 kV were stored as tiff files.

4.2.6.3. Immunofluorescence

Tissue-sections

Cryosections used for immunofluorescence staining were equilibrated to RT for 30 min, washed 3 times 5 min with PBS to remove the remaining Tissue Tek OCT (Sakkura) and blocked using 5% (donkey-) serum in PBS containing 0.1% triton X100 (PBST 0.1%). Antibody incubation was usually performed overnight at 4 °C with primary antibodies diluted in blocking solution (dilution dependent on AB used – refer to table). Slides were washed 3 times 10 min with PBST 0.1%. Fluorophore conjugated secondary antibodies were diluted in blocking solution (dilution dependent on AB – see table) and applied at RT for 2 hrs. Slides were washed for 10 min with PBST 0.1%, counterstained

with DAPI, diluted 1:10,000 in PBST 0.1% for 10 min and washed for 10 min with PBST 0.1%. Before mounting with Gelmount (Biomeda) or "Antifade Prolong" mounting media (Invitrogen), slides were briefly rinsed in water. Slides were dried overnight and kept at 4 °C in the dark.

Cells

Cells grown on coverslips were removed from the incubator and stored on ice, rinsed twice with cold PBS and fixed on ice with 4% PFA and 8% sucrose for 30 min. After two 10 minute washing steps with PBS, cells were treated with 50 mM NH_4Cl in PBS for 10 min on ice. To permeabilize cells, incubation with PBSTx 0.1% for 5 min was followed by a final 10 min wash with PBS. Cells were stored in PBS at 4 °C until further use.
Coverslips carrying fixed cells were transferred to a humidified chamber and blocked using 10% donkey serum in PBS at RT for 30 min. Primary antibody incubation was performed at RT for 2 hrs with antibodies diluted in blocking solution followed by three washing steps with PBS for 5 min at RT. Fluorophore conjugated secondary antibodies diluted in blocking solution were applied for 1 h at RT. Two 5 min washing steps with PBS were followed by application of DAPI diluted 1:10,000 in PBS. Prior to mounting with Gelmount (Biomeda) or "Antifade Prolong" mounting media (Invitrogen), coverslips were washed once with PBS for 5 min and briefly rinsed with H_2O. Coverslips were dried overnight and stored at 4 °C in the dark.

4.2.6.4. Immunohistochemistry (sections and whole mount)

Paraffin Sections

7 µm thick paraffin sections were dewaxed twice for 5 min in xylol-Ersatz (Vogel) and rehydrated through a graded series of ethanol steps ranging from 100% to 30% ethanol, ending in tap water. Antigen retrieval was performed by boiling slides for 5 min in 10 mM sodium citrate buffer pH 6.0 in a microwave at 900 W. Slides were cooled in H_2O for 30 min at RT before blocking with 3% milk in PBS for 1 h at RT. Incubation with primary antibodies was performed overnight at 4 °C. Three washing steps with PBS were followed by incubation with a biotin conjugated secondary antibody, diluted in blocking solution. While washing the slides 3 times with PBS, the ABC staining solution (VECTASTAIN; Vector Laboratories) was prepared according to the manufacturer's instructions. ABC staining solution conjugated with AP was applied for 30 min to 1 h at RT. Slides were washed three times using PBS. For AP conjugated ABC solution, sections were preincubated with NTMT prior to the application of the substrate for the AP enzyme, NBT/BCIP diluted in NTMT. Reactions were stopped by washing with PBS. If a nuclear counterstain was necessary, nuclear fast red was used. Slides were mounted using Gelmount mounting media (Biomeda).

Cryosections

Slides with 10 µm thick cryosections were dried at RT and remaining OCT was removed with three washes of PBS. To inactivate endogenous peroxidase, sections were dehydrated through a graded series of methanol and incubated for 20 min with 6% H2O2 in 80% methanol. After rehydration, slides were washed three times with PBSTx (0.1% triton X100) and blocked for 1 h with 1.5% milk in PBSTx at RT. Primary antibody incubation was carried out overnight at 4 °C. Antibodies were washed out with three PBST washing steps, followed by the application of a biotinylated secondary antibody for 2 hrs at RT. While sections were washed, the ABC solution conjugated to HRP (VECTASTAIN; Vector Laboratories) was prepared according to manufacturer's instructions. ABC solution was applied for 1 h and excess solution removed by three washes with PBSTx. Slides were incubated with diaminobenzidine (DAB; Sigma) as a chromogenic substrate. Sections were counterstained using nuclear fast red (Sigma) and mounted with Gelmount mounting media (Biomeda).

4.2.6.5. Quantification

To assess the levels of proliferation in the embryos, PHH3 stained embryo sections were used. The mitotic index for each germ layer was determined by building the ratio of PHH3 positive cells (antibody staining) and total number of cells (nuclear counterstain). Total number of cells was ascertained by counting the number of nuclei per germ layer visualized using either DAPI or nuclear FASTred (Sigma) as a counterstain. For E6.5 and E7.5 embryos, all sections of the embryonic region were quantified and data for all sections of a single embryo were pooled to determine the overall mitotic indices of a particular embryo. For statistical analysis the data of individual embryos (at least 3 per genotype) were pooled and compared using the Student's T test.

Similarly, to assess cell death, immunoflourescence staining for activated caspase-3 was performed on cryosectioned embryos. The death rate of cells for each germ layer was theoretically determined by comparing the number of active caspase-3 positive cells with the total number of cells visualized by the nuclear counterstain DAPI. Since the number of cleaved caspase-3 positive cells was very low, no apoptotic indices were determined.

5. Bibliography

Acampora, D., Mazan, S., Lallemand, Y., Avantaggiato, V., Maury, M., Simeone, A., and Brûlet, P. 1995. Forebrain and midbrain regions are deleted in Otx2-/- mutants due to a defective anterior neuroectoderm specification during gastrulation. Development 121(10): 3279-3290.

Al-Awqati, Q., Vijayakumar, S., and Takito, J. 2003. Terminal differentiation of epithelia from trophectoderm to the intercalated cell: the role of hensin. J Am Soc Nephrol 14 Suppl 1: S16-21.

Ang, S.L., Jin, O., Rhinn, M., Daigle, N., Stevenson, L., and Rossant, J. 1996. A targeted mouse Otx2 mutation leads to severe defects in gastrulation and formation of axial mesoderm and to deletion of rostral brain. Development 122(1): 243-252.

Ang, S.L., Wierda, A., Wong, D., Stevens, K.A., Cascio, S., Rossant, J., and Zaret, K.S. 1993. The formation and maintenance of the definitive endoderm lineage in the mouse: involvement of HNF3/forkhead proteins. Development 119(4): 1301-1315.

Arnold, S.J., Hofmann, U.K., Bikoff, E., and Robertson, E. 2008. Pivotal roles for eomesodermin during axis formation, epithelium-to-mesenchyme transition and endoderm specification in the mouse. Development 135(3): 501-511.

Arnold, S.J. and Robertson, E.J. 2009. Making a commitment: cell lineage allocation and axis patterning in the early mouse embryo. Nat Rev Mol Cell Biol.

Arnold, S.J., Stappert, J., Bauer, A., Kispert, A., Herrmann, B.G., and Kemler, R. 2000. Brachyury is a target gene of the Wnt/beta-catenin signaling pathway. Mechanisms of Development 91(1-2): 249-258.

Aumailley, M., Bruckner-Tuderman, L., Carter, W.G., Deutzmann, R., Edgar, D., Ekblom, P., Engel, J., Engvall, E., Hohenester, E., Jones, J.C., Kleinman, H.K., Marinkovich, M.P., Martin, G.R., Mayer, U., Meneguzzi, G., Miner, J., Miyazaki, K., Patarroyo, M., Paulsson, M., Quaranta, V., Sanes, J.R., Sasaki, T., Sekiguchi, K., Sorokin, L.M., Talts, J.F., Tryggvason, K., Uitto, J., Virtanen, I., von der Mark, K., Wewer, U.M., Yamada, Y., and Yurchenco, P.D. 2005. A simplified laminin nomenclature. Matrix Biol 24(5): 326-332.

Aumailley, M., Pesch, M., Tunggal, L., Gaill, F., and Fässler, R. 2000. Altered synthesis of laminin 1 and absence of basement membrane component deposition in (beta)1 integrin-deficient embryoid bodies. Journal of Cell Science 113 Pt 2: 259-268.

Beddington, R.S. 1994. Induction of a second neural axis by the mouse node. Development 120(3): 613-620.

Bellomo, D., Lander, A., Harragan, I., and Brown, N.A. 1996. Cell proliferation in mammalian gastrulation: the ventral node and notochord are relatively quiescent. Dev Dyn 205(4): 471-485.

Belo, J.A., Bouwmeester, T., Leyns, L., Kertesz, N., Gallo, M., Follettie, M., and De Robertis, E.M. 1997. Cerberus-like is a secreted factor with neutralizing activity expressed in the anterior primitive endoderm of the mouse gastrula. Mechanisms of Development 68(1-2): 45-57.

Ben-Haim, N., Lu, C., Guzman-Ayala, M., Pescatore, L., Mesnard, D., Bischofberger, M., Naef, F., Robertson, E., and Constam, D.B. 2006. The nodal precursor acting via activin receptors induces mesoderm by maintaining a source of its convertases and BMP4. Developmental Cell 11(3): 313-323.

Biben, C., Stanley, E., Fabri, L., Kotecha, S., Rhinn, M., Drinkwater, C., Lah, M., Wang, C.C., Nash, A., Hilton, D., Ang, S.L., Mohun, T., and Harvey, R.P. 1998. Murine cerberus homologue mCer-1: a candidate anterior patterning molecule. Developmental Biology 194(2): 135-151.

Böttcher, R. and Niehrs, C. 2005. Fibroblast growth factor signaling during early vertebrate development. Endocrine Reviews 26(1): 63-77.

Böttcher, R., Pollet, N., Delius, H., and Niehrs, C. 2004. The transmembrane protein XFLRT3 forms a complex with FGF receptors and promotes FGF signalling. Nat Cell Biol 6(1): 38-44.

Candia, A.F., Hu, J., Crosby, J., Lalley, P.A., Noden, D., Nadeau, J.H., and Wright, C.V. 1992. Mox-1 and Mox-2 define a novel homeobox gene subfamily and are differentially expressed during early mesodermal patterning in mouse embryos. Development 116(4): 1123-1136.

Carver, E.A., Jiang, R., Lan, Y., Oram, K.F., and Gridley, T. 2001. The mouse snail gene encodes a key regulator of the epithelial-mesenchymal transition. Mol Cell Biol 21(23): 8184-8188.

Chen, C. and Shen, M.M. 2004. Two modes by which Lefty proteins inhibit nodal signaling. Curr Biol 14(7): 618-624.

Chen, Y., Aulia, S., Li, L., and Tang, B.L. 2006. AMIGO and friends: an emerging family of brain-enriched, neuronal growth modulating, type I transmembrane proteins with leucine-rich repeats (LRR) and cell adhesion molecule motifs. Brain Research Reviews 51(2): 265-274.

Ciruna, B. and Rossant, J. 2001. FGF signaling regulates mesoderm cell fate specification and morphogenetic movement at the primitive streak. Developmental Cell 1(1): 37-49.

Ciruna, B.G. and Rossant, J. 1999. Expression of the T-box gene Eomesodermin during early mouse development. Mechanisms of Development 81(1-2): 199-203.

Clark, P. 1994. Modulation of scatter factor/hepatocyte growth factor activity by cell-substratum adhesion. J Cell Sci 107 (Pt 5): 1265-1275.

Colognato, H. and Yurchenco, P.D. 2000. Form and function: the laminin family of heterotrimers. Dev Dyn 218(2): 213-234.

Constam, D.B. and Robertson, E.J. 2000a. SPC4/PACE4 regulates a TGFbeta signaling network during axis formation. Genes & Development 14(9): 1146-1155.

Constam, D.B. and Robertson, E.J.. 2000b. Tissue-specific requirements for the proprotein convertase furin/SPC1 during embryonic turning and heart looping. Development 127(2): 245-254.

Corson, L.B., Yamanaka, Y., Lai, K.M., and Rossant, J. 2003. Spatial and temporal patterns of ERK signaling during mouse embryogenesis. Development 130(19): 4527-4537.

Coucouvanis, E. and Martin, G.R. 1999. BMP signaling plays a role in visceral endoderm differentiation and cavitation in the early mouse embryo. Development 126(3): 535-546.

Crossley, P.H. and Martin, G.R. 1995. The mouse Fgf8 gene encodes a family of polypeptides and is expressed in regions that direct outgrowth and patterning in the developing embryo. Development 121(2): 439-451.

Ding, J., Yang, L., Yan, Y.T., Chen, A., Desai, N., Wynshaw-Boris, A., and Shen, M.M. 1998. Cripto is required for correct orientation of the anterior-posterior axis in the mouse embryo. Nature 395(6703): 702-707.

Downs, K.M. and Davies, T. 1993. Staging of gastrulating mouse embryos by morphological landmarks in the dissecting microscope. Development 118(4): 1255-1266.

Dunn, N.R., Vincent, S.D., Oxburgh, L., Robertson, E., and Bikoff, E. 2004. Combinatorial activities of Smad2 and Smad3 regulate mesoderm formation and patterning in the mouse embryo. Development 131(8): 1717-1728.

Eakin, G. and Behringer, R. 2004. Diversity of germ layer and axis formation among mammals. Seminars in Cell & Developmental Biology 15(5): 619-629.

Eakin, G., Hadjantonakis, A., Papaioannou, V.E., and Behringer, R. 2005. Developmental potential and behavior of tetraploid cells in the mouse embryo. Dev Biol 288(1): 150-159.

Egea, J., Erlacher, C., Montanez, E., Burtscher, I., Yamagishi, S., Heß, M., Hampel, F., Sanchez, R., Rodriguez-Manzaneque, M.T., Bösl, M.R., Fässler, R., Lickert, H., and Klein, R. 2008. Genetic ablation of FLRT3 reveals a novel morphogenetic function for the anterior visceral endoderm in suppressing mesoderm differentiation. Genes & Development 22(23): 3349-3362.

Eswarakumar, V.P., Lax, I., and Schlessinger, J. 2005. Cellular signaling by fibroblast growth factor receptors. Cytokine & Growth Factor Reviews 16(2): 139-149.

Fässler, R., Pfaff, M., Murphy, J., Noegel, A.A., Johansson, S., Timpl, R., and Albrecht, R. 1995. Lack of beta 1 integrin gene in embryonic stem cells affects morphology, adhesion, and migration but not integration into the inner cell mass of blastocysts. J Cell Biol 128(5): 979-988.

Fujiwara, H., Hayashi, Y., Sanzen, N., Kobayashi, R., Weber, C.N., Emoto, T., Futaki, S., Niwa, H., Murray, P., Edgar, D., and Sekiguchi, K. 2007. Regulation of mesodermal differentiation of mouse embryonic stem cells by basement membranes. J Biol Chem 282(40): 29701-29711.

García-Castro, M. and Bronner-Fraser, M. 1999. Induction and differentiation of the neural crest. Current Opinion in Cell Biology 11(6): 695-698.

Gladdy, R.A., Nutter, L.M., Kunath, T., Danska, J.S., and Guidos, C.J. 2006. p53-Independent apoptosis disrupts early organogenesis in embryos lacking both ataxia-telangiectasia mutated and Prkdc. Mol Cancer Res 4(5): 311-318.

Glinka, A., Wu, W., Delius, H., Monaghan, A.P., Blumenstock, C., and Niehrs, C. 1998. Dickkopf-1 is a member of a new family of secreted proteins and functions in head induction. Nature 391(6665): 357-362.

Gotoh, N., Manova, K., Tanaka, S., Murohashi, M., Hadari, Y., Lee, A., Hamada, Y., Hiroe, T., Ito, M., Kurihara, T., Nakazato, H., Shibuya, M., Lax, I., Lacy, E., and Schlessinger, J. 2005. The docking protein FRS2alpha is an essential component of multiple fibroblast growth factor responses during early mouse development. Mol Cell Biol 25(10): 4105-4116.

Hackett, B.P. 2002. Formation and malformation of the vertebrate left-right axis. Curr Mol Med 2(1): 39-66.

Haines, B.P., Wheldon, L.M., Summerbell, D., Heath, J.K., and Rigby, P.W. 2006. Regulated expression of FLRT genes implies a functional role in the regulation of FGF signalling during mouse development. Dev Biol 297(1): 14-25.

Hakem, R., de la Pompa, J.L., Sirard, C., Mo, R., Woo, M., Hakem, A., Wakeham, A., Potter, J., Reitmair, A., Billia, F., Firpo, E., Hui, C.C., Roberts, J., Rossant, J., and Mak, T.W. 1996. The tumor suppressor gene Brca1 is required for embryonic cellular proliferation in the mouse. Cell 85(7): 1009-1023.

Hall, J.G., Friedman, J.M., Kenna, B.A., Popkin, J., Jawanda, M., and Arnold, W. 1988. Clinical, genetic, and epidemiological factors in neural tube defects. Am J Hum Genet 43(6): 827-837.

Hamada, H., Meno, C., Watanabe, D., and Saijoh, Y. 2002. Establishment of vertebrate left-right asymmetry. Nat Rev Genet 3(2): 103-113.

Handler, M., Yurchenco, P.D., and Iozzo, R.V. 1997. Developmental expression of perlecan during murine embryogenesis. Dev Dyn 210(2): 130-145.

Harris, M.J. and Juriloff, D.M. 2007. Mouse mutants with neural tube closure defects and their role in understanding human neural tube defects. Birth Defects Res Part A Clin Mol Teratol 79(3): 187-210.

Hashimoto, K. and Nakatsuji, N. 1989. Formation of the Primitive Streak and Mesoderm Cells in Mouse Embryos - Detailed Scanning Electron Microscopical Study. Dev Growth Differ 31(3): 209-218.

Hobmayer, B., Rentzsch, F., Kuhn, K., Happel, C.M., von Laue, C.C., Snyder, P., Rothbächer, U., and Holstein, T.W. 2000. WNT signalling molecules act in axis formation in the diploblastic metazoan Hydra. Nature 407(6801): 186-189.

Hogan, B., Beddington, R., Costantini, F., Lacey, E., 1994. Manipulating the mouse embryo: A Laboratory Manual. CSHL Press.

Hoodless, P.A., Pye, M., Chazaud, C., Labbé, E., Attisano, L., Rossant, J., and Wrana, J.L. 2001. FoxH1 (Fast) functions to specify the anterior primitive streak in the mouse. Genes & Development 15(10): 1257-1271.

Hunter, A.G. 1984. Neural tube defects in Eastern Ontario and Western Quebec: demography and family data. Am J Med Genet 19(1): 45-63.

Isaacs, H.V., Pownall, M.E., and Slack, J.M. 1994. eFGF regulates Xbra expression during Xenopus gastrulation. EMBO J 13(19): 4469-4481.

Isaacs, H.V., Pownall, M.E., and Slack, J.M.. 1995. eFGF is expressed in the dorsal midline of Xenopus laevis. Int J Dev Biol 39(4): 575-579.

Jin, O., Harpal, K., Ang, S.L., and Rossant, J. 2001. Otx2 and HNF3beta genetically interact in anterior patterning. Int J Dev Biol 45(1): 357-365.

Jukkola, T., Lahti, L., Naserke, T., Wurst, W., and Partanen, J. 2006. FGF regulated gene-expression and neuronal differentiation in the developing midbrain–hindbrain region. Developmental Biology 297(1): 141-157.

Kaufman, M.H. 1992. The Atlas of Mouse Development. Academic Press, London.

Karaulanov, E., Böttcher, R., and Niehrs, C. 2006. A role for fibronectin-leucine-rich transmembrane cell-surface proteins in homotypic cell adhesion. EMBO Rep 7(3): 283-290.

Kelly, O., Pinson, K.I., and Skarnes, W.C. 2004. The Wnt co-receptors Lrp5 and Lrp6 are essential for gastrulation in mice. Development 131(12): 2803-2815.

Kibar, Z., Capra, V., and Gros, P. 2007. Toward understanding the genetic basis of neural tube defects. Clin Genet 71(4): 295-310.

Kidd, T. 1999. Slit Is the Midline Repellent for the Robo Receptor in Drosophila. Cell 96(6): 785-794.

Kiefer, J.C. 2007. Back to basics: Sox genes. Dev Dyn 236(8): 2356-2366.

Kim, S., Burette, A., Chung, H., Kwon, S., Woo, J., Lee, H., Kim, K., Kim, H., Weinberg, R., and Kim, E. 2006. NGL family PSD-95–interacting adhesion molecules regulate excitatory synapse formation. Nat Neurosci 9(10): 1294-1301.

Kimura, C., Yoshinaga, K., Tian, E., Suzuki, M., Aizawa, S., and Matsuo, I. 2000. Visceral endoderm mediates forebrain development by suppressing posteriorizing signals. Dev Biol 225(2): 304-321.

Kimurayoshida, C., Nakano, H., Okamura, D., Nakao, K., Yonemura, S., Belo, J., Aizawa, S., Matsui, Y., and Matsuo, I. 2005. Canonical Wnt Signaling and Its Antagonist Regulate Anterior-Posterior Axis Polarization by Guiding Cell Migration in Mouse Visceral Endoderm. Developmental Cell 9(5): 639-650.

Kinder, S.J., Tsang, T.E., Quinlan, G.A., Hadjantonakis, A.K., Nagy, A., and Tam, P.P. 1999. The orderly allocation of mesodermal cells to the extraembryonic structures and the anteroposterior axis during gastrulation of the mouse embryo. Development 126(21): 4691-4701.

Kispert, A. and Herrmann, B.G. 1993. The Brachyury gene encodes a novel DNA binding protein. EMBO J 12(8): 3211-3220.

Klingensmith, J., Ang, S.L., Bachiller, D., and Rossant, J. 1999. Neural induction and patterning in the mouse in the absence of the node and its derivatives. Developmental Biology 216(2): 535-549.

Kuja-Panula, J., Kiiltomäki, M., Yamashiro, T., Rouhiainen, A., and Rauvala, H. 2003. AMIGO, a transmembrane protein implicated in axon tract development, defines a novel protein family with leucine-rich repeats. J Cell Biol 160(6): 963-973.

Kwon, G.S., Viotti, M., and Hadjantonakis, A. 2008. The endoderm of the mouse embryo arises by dynamic widespread intercalation of embryonic and extraembryonic lineages. Developmental Cell 15(4): 509-520.

Lacy, S.E., Bönnemann, C.G., Buzney, E.A., and Kunkel, L.M. 1999. Identification of FLRT1, FLRT2, and FLRT3: a novel family of transmembrane leucine-rich repeat proteins. Genomics 62(3): 417-426.

Lee, K.Y. and DeMayo, F.J. 2004. Animal models of implantation. Reproduction 128(6): 679-695.

Li, S., Edgar, D., Fässler, R., Wadsworth, W., and Yurchenco, P.D. 2003. The role of laminin in embryonic cell polarization and tissue organization. Dev Cell 4(5): 613-624.

Li, S., Harrison, D., Carbonetto, S., Fässler, R., Smyth, N., Edgar, D., and Yurchenco, P.D. 2002. Matrix assembly, regulation, and survival functions of laminin and its receptors in embryonic stem cell differentiation. The Journal of Cell Biology 157(7): 1279-1290.

Lickert, H., Kutsch, S., Kanzler, B., Tamai, Y., Taketo, M.M., and Kemler, R. 2002. Formation of multiple hearts in mice following deletion of beta-catenin in the embryonic endoderm. Developmental Cell 3(2): 171-181.

Lin, J., Ho, W., Gurney, A., and Rosenthal, A. 2003. The netrin-G1 ligand NGL-1 promotes the outgrowth of thalamocortical axons. Nat Neurosci 6(12): 1270-1276.

Liu, P., Wakamiya, M., Shea, M.J., Albrecht, U., Behringer, R.R., and Bradley, A. 1999. Requirement for Wnt3 in vertebrate axis formation. Nat Genet 22(4): 361-365.

Macri, L., Silverstein, D., and Clark, R.A. 2007. Growth factor binding to the pericellular matrix and its importance in tissue engineering. Advanced Drug Delivery Reviews 59(13): 1366-1381.

Maretto, S., Müller, P.S., Aricescu, A.R., Cho, K.W., Bikoff, E., and Robertson, E. 2008. Ventral closure, headfold fusion and definitive endoderm migration defects in mouse embryos lacking the fibronectin leucine-rich transmembrane protein FLRT3. Dev Biol 318(1): 184-193.

Matsushima, N., Tachi, N., Kuroki, Y., Enkhbayar, P., Osaki, M., Kamiya, M., and Kretsinger, R.H. 2005. Structural analysis of leucine-rich-repeat variants in proteins associated with human diseases. Cell Mol Life Sci 62(23): 2771-2791.

Mayor, R., Morgan, R., and Sargent, M.G. 1995. Induction of the prospective neural crest of Xenopus. Development 121(3): 767-777.

Meno, C., Takeuchi, J., Sakuma, R., Koshiba-Takeuchi, K., Ohishi, S., Saijoh, Y., Miyazaki, J., ten Dijke, P., Ogura, T., and Hamada, H. 2001. Diffusion of nodal signaling activity in the absence of the feedback inhibitor Lefty2. Developmental Cell 1(1): 127-138.

Miner, J. 2004. Compositional and structural requirements for laminin and basement membranes during mouse embryo implantation and gastrulation. Development 131(10): 2247-2256.

Miner, J. and Yurchenco, P.D. 2004. Laminin functions in tissue morphogenesis. Annu Rev Cell Dev Biol 20: 255-284.

Mishra, A., Knerr, B., Paixão, S., Kramer, E.R., and Klein, R. 2008. The protein dendrite arborization and synapse maturation 1 (Dasm-1) is dispensable for dendrite arborization. Mol Cell Biol 28(8): 2782-2791.

Mohamed, O., Clarke, H., and Dufort, D. 2004. Beta-catenin signaling marks the prospective site of primitive streak formation in the mouse embryo. Dev Dyn 231(2): 416-424.

Molkentin, J.D., Lin, Q., Duncan, S.A., and Olson, E.N. 1997. Requirement of the transcription factor GATA4 for heart tube formation and ventral morphogenesis. Genes & Development 11(8): 1061-1072.

Mongiat, M., Otto, J., Oldershaw, R., Ferrer, F., Sato, J.D., and Iozzo, R.V. 2001. Fibroblast growth factor-binding protein is a novel partner for perlecan protein core. J Biol Chem 276(13): 10263-10271.

Murshed, M., Smyth, N., Miosge, N., Karolat, J., Krieg, T., Paulsson, M., and Nischt, R. 2000. The absence of nidogen 1 does not affect murine basement membrane formation. Mol Cell Biol 20(18): 7007-7012.

Nakaya, Y., Sukowati, E., Wu, Y., and Sheng, G. 2008. RhoA and microtubule dynamics control cell-basement membrane interaction in EMT during gastrulation. Nat Cell Biol 10(7): 765-775.

Newell, P.C., Telser, A., and Sussman, M. 1969. Alternative developmental pathways determined by environmental conditions in the cellular slime mold Dictyostelium discoideum. J Bacteriol 100(2): 763-768.

Nieto, M.A. 2002. The snail superfamily of zinc-finger transcription factors. Nat Rev Mol Cell Biol 3(3): 155-166.

Nieto, M.A., Bradley, L.C., and Wilkinson, D.G. 1991. Conserved segmental expression of Krox-20 in the vertebrate hindbrain and its relationship to lineage restriction. Development Suppl 2: 59-62.

Niswander, L. and Martin, G.R. 1992. Fgf-4 expression during gastrulation, myogenesis, limb and tooth development in the mouse. Development 114(3): 755-768.

Nonaka, S., Tanaka, Y., Okada, Y., Takeda, S., Harada, A., Kanai, Y., Kido, M., and Hirokawa, N. 1998. Randomization of left-right asymmetry due to loss of nodal cilia generating leftward flow of extraembryonic fluid in mice lacking KIF3B motor protein. Cell 95(6): 829-837.

Norris, D., Brennan, J., Bikoff, E., and Robertson, E. 2002. The Foxh1-dependent autoregulatory enhancer controls the level of Nodal signals in the mouse embryo. Development 129(14): 3455-3468.

Ogata, S., Morokuma, J., Hayata, T., Kolle, G., Niehrs, C., Ueno, N., and Cho, K.W. 2007. TGF-beta signaling-mediated morphogenesis: modulation of cell adhesion via cadherin endocytosis. Genes Dev 21(14): 1817-1831.

Oh, M., Scoles, D., Haipek, C., Strand, A., Gutmann, D., Olson, J., and Pulst, S. 2003. Genetic heterogeneity of stably transfected cell lines revealed by expression profiling with oligonucleotide microarrays. J Cell Biochem 90(5): 1068-1078.

Parameswaran, M. and Tam, P.P. 1995. Regionalisation of cell fate and morphogenetic movement of the mesoderm during mouse gastrulation. Dev Genet 17(1): 16-28.

Perea-Gomez, A., Camus, A., Moreau, A., Grieve, K., Moneron, G., Dubois, A., Cibert, C., and Collignon, J. 2004. Initiation of gastrulation in the mouse embryo is preceded by an apparent shift in the orientation of the anterior-posterior axis. Curr Biol 14(3): 197-207.

Perea-Gomez, A., Lawson, K.A., Rhinn, M., Zakin, L., Brûlet, P., Mazan, S., and Ang, S.L. 2001. Otx2 is required for visceral endoderm movement and for the restriction of posterior signals in the epiblast of the mouse embryo. Development 128(5): 753-765.

Perea-Gomez, A., Meilhac, S., Piotrowska-Nitsche, K., Gray, D., Collignon, J., and Zernicka-Goetz, M. 2007. Regionalization of the mouse visceral endoderm as the blastocyst transforms into the egg cylinder. BMC Dev Biol 7: 96.

Perea-Gomez, A., Rhinn, M., and Ang, S.L. 2001. Role of the anterior visceral endoderm in restricting posterior signals in the mouse embryo. Int J Dev Biol 45(1): 311-320.

Perea-Gómez, A., Shawlot, W., Sasaki, H., Behringer, R.R., and Ang, S. 1999. HNF3beta and Lim1 interact in the visceral endoderm to regulate primitive streak formation and anterior-posterior polarity in the mouse embryo. Development 126(20): 4499-4511.

Perea-Gomez, A., Vella, F.D., Shawlot, W., Oulad-Abdelghani, M., Chazaud, C., Meno, C., Pfister, V., Chen, L., Robertson, E., Hamada, H., Behringer, R., and Ang, S. 2002. Nodal antagonists in the anterior visceral endoderm prevent the formation of multiple primitive streaks. Developmental Cell 3(5): 745-756.

Pöpperl, H., Bienz, M., Studer, M., Chan, S.K., Aparicio, S., Brenner, S., Mann, R.S., and Krumlauf, R. 1995. Segmental expression of Hoxb-1 is controlled by a highly conserved autoregulatory loop dependent upon exd/pbx. Cell 81(7): 1031-1042.

Pöschl, E., Schlötzer-Schrehardt, U., Brachvogel, B., Saito, K., Ninomiya, Y., and Mayer, U. 2004. Collagen IV is essential for basement membrane stability but dispensable for initiation of its assembly during early development. Development 131(7): 1619-1628.

Rakeman, A.S. and Anderson, K.V. 2006. Axis specification and morphogenesis in the mouse embryo require Nap1, a regulator of WAVE-mediated actin branching. Development 133(16): 3075-3083.

Rivera-Pérez, J.A., Mager, J., and Magnuson, T. 2003. Dynamic morphogenetic events characterize the mouse visceral endoderm. Dev Biol 261(2): 470-487.

Robertson, E., Norris, D., Brennan, J., and Bikoff, E. 2003. Control of early anterior-posterior patterning in the mouse embryo by TGF-beta signalling. Philos Trans R Soc Lond, B, Biol Sci 358(1436): 1351-1357; discussion 1357.

Robinson, M., Parsons Perez, M.C., Tébar, L., Palmer, J., Patel, A., Marks, D., Sheasby, A., De Felipe, C., Coffin, R., Livesey, F.J., and Hunt, S.P. 2004. FLRT3 is expressed in sensory neurons after peripheral nerve injury and regulates neurite outgrowth. Mol Cell Neurosci 27(2): 202-214.

Rodriguez, T., Srinivas, S., Clements, M.P., Smith, J.C., and Beddington, R.S. 2005. Induction and migration of the anterior visceral endoderm is regulated by the extra-embryonic ectoderm. Development 132(11): 2513-2520.

Roebroek, A.J., Umans, L., Pauli, I.G., Robertson, E.J., van Leuven, F., Van de Ven, W.J., and Constam, D.B. 1998. Failure of ventral closure and axial rotation in embryos lacking the proprotein convertase Furin. Development 125(24): 4863-4876.

Rossant, J., Chazaud, C., and Yamanaka, Y. 2003. Lineage allocation and asymmetries in the early mouse embryo. Philos Trans R Soc Lond, B, Biol Sci 358(1436): 1341-1348; discussion 1349.

Rossant, J. and Tam, P.P. 2004. Emerging asymmetry and embryonic patterning in early mouse development. Dev Cell 7(2): 155-164.

Saijoh, Y., Adachi, H., Sakuma, R., Yeo, C.Y., Yashiro, K., Watanabe, M., Hashiguchi, H., Mochida, K., Ohishi, S., Kawabata, M., Miyazono, K., Whitman, M., and Hamada, H. 2000. Left-right asymmetric expression of lefty2 and nodal is induced by a signaling pathway that includes the transcription factor FAST2. Mol Cell 5(1): 35-47.

Sakuma, R., Ohnishi Yi, Y., Meno, C., Fujii, H., Juan, H., Takeuchi, J., Ogura, T., Li, E., Miyazono, K., and Hamada, H. 2002. Inhibition of Nodal signalling by Lefty mediated through interaction with common receptors and efficient diffusion. Genes Cells 7(4): 401-412.

Sasaki, H. and Hogan, B.L. 1993. Differential expression of multiple fork head related genes during gastrulation and axial pattern formation in the mouse embryo. Development 118(1): 47-59.

Schuck, S., Manninen, A., Honsho, M., Füllekrug, J., and Simons, K. 2004. Generation of single and double knockdowns in polarized epithelial cells by retrovirus-mediated RNA interference. Proc Natl Acad Sci USA 101(14): 4912-4917.

Schymeinsky, J., Nedbal, S., Miosge, N., Pöschl, E., Rao, C., Beier, D.R., Skarnes, W.C., Timpl, R., and Bader, B.L. 2002. Gene structure and functional analysis of the mouse nidogen-2 gene: nidogen-2 is not essential for basement membrane formation in mice. Mol Cell Biol 22(19): 6820-6830.

Shawlot, W. and Behringer, R.R. 1995. Requirement for Lim1 in head-organizer function. Nature 374(6521): 425-430.

Shawlot, W., Wakamiya, M., Kwan, K.M., Kania, A., Jessell, T.M., and Behringer, R.R. 1999. Lim1 is required in both primitive streak-derived tissues and visceral endoderm for head formation in the mouse. Development 126(22): 4925-4932.

Shook, D. and Keller, R. 2003. Mechanisms, mechanics and function of epithelial-mesenchymal transitions in early development. Mechanisms of Development 120(11): 1351-1383.

Sirard, C., de la Pompa, J.L., Elia, A., Itie, A., Mirtsos, C., Cheung, A., Hahn, S., Wakeham, A., Schwartz, L., Kern, S.E., Rossant, J., and Mak, T.W. 1998. The tumor suppressor gene Smad4/Dpc4 is required for gastrulation and later for anterior development of the mouse embryo. Genes & Development 12(1): 107-119.

Smyth, N., Vatansever, H.S., Meyer, M., Frie, C., Paulsson, M., and Edgar, D. 1998. The targeted deletion of the LAMC1 gene. Ann N Y Acad Sci 857: 283-286.

Soares, M.L., Haraguchi, S., Torres-Padilla, M., Kalmar, T., Carpenter, L., Bell, G., Morrison, A., Ring, C.J., Clarke, N.J., Glover, D.M., and Zernicka-Goetz, M. 2005. Functional studies of signaling pathways in peri-implantation development of the mouse embryo by RNAi. BMC Dev Biol 5: 28.

Spemann, H. and Mangold, H. 2001. Induction of embryonic primordia by implantation of organizers from a different species. 1923. Int J Dev Biol 45(1): 13-38.

Srinivas, S. 2006. The anterior visceral endoderm-turning heads. genesis 44(11): 565-572.

Srinivas, S., Rodriguez, T., Clements, M., Smith, J.C., and Beddington, R.S. 2004. Active cell migration drives the unilateral movements of the anterior visceral endoderm. Development 131(5): 1157-1164.

Steele, R.E. 2002. Developmental signaling in Hydra: what does it take to build a "simple" animal? Dev Biol 248(2): 199-219.

Stern, C.D. 2001. Initial patterning of the central nervous system: how many organizers? Nat Rev Neurosci 2(2): 92-98.

Sun, X., Meyers, E.N., Lewandoski, M., and Martin, G.R. 1999. Targeted disruption of Fgf8 causes failure of cell migration in the gastrulating mouse embryo. Genes & Development 13(14): 1834-1846.

Takaoka, K., Yamamoto, M., Shiratori, H., Meno, C., Rossant, J., Saijoh, Y., and Hamada, H. 2006. The mouse embryo autonomously acquires anterior-posterior polarity at implantation. Developmental Cell 10(4): 451-459.

Takito, J. and Al-Awqati, Q. 2004. Conversion of ES cells to columnar epithelia by hensin and to squamous epithelia by laminin. J Cell Biol 166(7): 1093-1102.

Tam, P.P., Kanai-Azuma, M., and Kanai, Y. 2003. Early endoderm development in vertebrates: lineage differentiation and morphogenetic function. Curr Opin Genet Dev 13(4): 393-400.

Tam, P.P., Khoo, P.L., Lewis, S.L., Bildsoe, H., Wong, N., Tsang, T.E., Gad, J.M., and Robb, L. 2007. Sequential allocation and global pattern of movement of the definitive endoderm in the mouse embryo during gastrulation. Development 134(2): 251-260.

Tam, P.P. and Loebel, D.A. 2007. Gene function in mouse embryogenesis: get set for gastrulation. Nat Rev Genet 8(5): 368-381.

Tam, P.P. and Rossant, J. 2003. Mouse embryonic chimeras: tools for studying mammalian development. Development 130(25): 6155-6163.

Tam, P.P. and Steiner, K.A. 1999. Anterior patterning by synergistic activity of the early gastrula organizer and the anterior germ layer tissues of the mouse embryo. Development 126(22): 5171-5179.

Tanabe, K., Bonilla, I., Winkles, J.A., and Strittmatter, S.M. 2003. Fibroblast growth factor-inducible-14 is induced in axotomized neurons and promotes neurite outgrowth. J Neurosci 23(29): 9675-9686.

Technau, U. 2001. Brachyury, the blastopore and the evolution of the mesoderm. Bioessays 23(9): 788-794.

Technau, U. and Scholz, C.B. 2003. Origin and evolution of endoderm and mesoderm. Int J Dev Biol 47(7-8): 531-539.

Thomas, P. and Beddington, R. 1996. Anterior primitive endoderm may be responsible for patterning the anterior neural plate in the mouse embryo. Curr Biol 6(11): 1487-1496.

Thomas, P.Q., Brown, A., and Beddington, R.S. 1998. Hex: a homeobox gene revealing peri-implantation asymmetry in the mouse embryo and an early transient marker of endothelial cell precursors. Development 125(1): 85-94.

Trainor, P.A. 2005. Specification of neural crest cell formation and migration in mouse embryos. Seminars in Cell & Developmental Biology 16(6): 683-693.

Tsuji, L., Yamashita, T., Kubo, T., Madura, T., Tanaka, H., Hosokawa, K., and Tohyama, M. 2004. FLRT3, a cell surface molecule containing LRR repeats and a FNIII domain, promotes neurite outgrowth. Biochemical and Biophysical Research Communications 313(4): 1086-1091.

Weidner, K.M., Behrens, J., Vandekerckhove, J., and Birchmeier, W. 1990. Scatter factor: molecular characteristics and effect on the invasiveness of epithelial cells. J Cell Biol 111(5 Pt 1): 2097-2108.

Whitman, M. 2001. Nodal signaling in early vertebrate embryos: themes and variations. Developmental Cell 1(5): 605-617.

Wilkinson, D.G., Bhatt, S., and Herrmann, B.G. 1990. Expression pattern of the mouse T gene and its role in mesoderm formation. Nature 343(6259): 657-659.

Wilkinson, D.G., 1992. In situ hybridization: A practical approach. Oxford University Press

Williamson, R.A., Henry, M.D., Daniels, K.J., Hrstka, R.F., Lee, J.C., Sunada, Y., Ibraghimov-Beskrovnaya, O., and Campbell, K.P. 1997. Dystroglycan is essential for early embryonic development: disruption of Reichert's membrane in Dag1-null mice. Hum Mol Genet 6(6): 831-841.

Winnier, G., Blessing, M., Labosky, P.A., and Hogan, B.L. 1995. Bone morphogenetic protein-4 is required for mesoderm formation and patterning in the mouse. Genes & Development 9(17): 2105-2116.

Wood, H.B. and Episkopou, V. 1999. Comparative expression of the mouse Sox1, Sox2 and Sox3 genes from pre-gastrulation to early somite stages. Mechanisms of Development 86(1-2): 197-201.

Yamaguchi, T.P., Bradley, A., McMahon, A.P., and Jones, S. 1999. A Wnt5a pathway underlies outgrowth of multiple structures in the vertebrate embryo. Development 126(6): 1211-1223.

Yamamoto, M., Saijoh, Y., Perea-Gomez, A., Shawlot, W., Behringer, R., Ang, S., Hamada, H., and Meno, C. 2004. Nodal antagonists regulate formation of the anteroposterior axis of the mouse embryo. Nature 428(6981): 387-392.

Yurchenco, P.D., Amenta, P.S., and Patton, B.L. 2004. Basement membrane assembly, stability and activities observed through a developmental lens. Matrix Biol 22(7): 521-538.

Yurchenco, P.D. and Wadsworth, W.G. 2004. Assembly and tissue functions of early embryonic laminins and netrins. Current Opinion in Cell Biology 16(5): 572-579.

Zhang, H., Toyofuku, T., Kamei, J., and Hori, M. 2003. GATA-4 regulates cardiac morphogenesis through transactivation of the N-cadherin gene. Biochemical and Biophysical Research Communications 312(4): 1033-1038.

Acknowledgements

Zu allererst möchte ich meinen Eltern und ganz besonders meiner Mutter für Ihre Unterstützung in allen Lebenslagen danken. Ohne sie wäre all dies nicht möglich gewesen. Mein besonderer Dank gilt auch Michaela für all Ihre Unterstützung und Ihr Verständnis während der letzen Jahre. Auch an Alois, Astrid und Kathrin geht ein großes Dankeschön.

I would like to thank my thesis supervisor Rüdiger Klein, who gave me the opportunity to work in a great scientific environment. I am grateful for his constant support and interest in my project.

I also want to thank Joaquim Egea for his constant support and willingness to share his project with me. He has deepened my interest in developmental biology and taught me many important techniques and useful tricks. I am particularly grateful for numerous scientific discussions at any time of the day.

I thank my thesis committee members, Rüdiger Klein, Joaquim Egea, Magdalena Götz and Heiko Lickert for their interest, critical discussions and suggestions.

A special thanks goes to my collaborator Martin Heß, who provided great help with the SEM analysis and was very interested in my project from the first minute on. Without his expertise, I would not have been able to show any of the beautiful "crater" pictures.

I want to thank the service facilities of the MPI, especially the animal house staff and the EDV for their support. Without you guys, our life would be so much harder. In particular, I enjoyed all the "geeky" conversations with the EDV.

Of course I want to thank all present and past members of the Klein department for a great working atmosphere, critical discussions, help whenever needed and lots of fun at various occasions. My special thanks goes to Taija Mäkinen, Ingvar Ferby, Stefan Weinges, Helge zum Buttel, Satoru Yamagishi, Katrin Deininger, Falko Hampel, Sónia Paixão, Louise Gaitanos, Laura Loschek, Andreas Schaupp and Svetla Dimitrova.

Last but not least a special thanks to Louise Gaitanos, Joaquim Egea, Katrin Deininger and Helge zum Buttel for critically reading this dissertation.